Università degli Studi del Piemonte Orientale
"Amedeo Avogadro"

***Department of Science and Technological Innovation***

Ph.D. Program in "Chemistry & Biology"

XXXIV cycle

2018-2021

# Exploring biological mechanisms and biomarkers through lipidomics

SSD CHIM/01

Candidate: Sara Timo

Tutor: Professor Emilio Marengo

PhD program Coordinator: Professor Gian Cesare Tron

UNIVERSITÀ DEL PIEMONTE ORIENTALE

*Department of Science and Technological Innovation*

Ph.D. Program in "Chemistry & Biology"

XXXIV cycle

2018-2021

# Exploring biological mechanisms and biomarkers through lipidomics

Candidate: Sara Timo

Tutor: Professor Emilio Marengo

UNIVERSITÀ DEL PIEMONTE ORIENTALE
DOTTORATO DI RICERCA
IN CHEMISTRY & BIOLOGY

Via Duomo, 6
13100 – Vercelli (ITALY)

# DECLARATION AND AUTHORIZATION TO ANTIPLAGIARISM DETECTION

The undersigned **SARA TIMO** student of the Chemistry and Biology Ph.D. course (XXXIV cycle)

**declares:**

- to be aware that the University has adopted a web-based service to detect plagiarism through a software system called "Turnit.in",
- his/her Ph.D. thesis was submitted to Turnit.in scan and reasonably it resulted an original document, which correctly cites the literature;

**acknowledges:**

- his/her Ph.D. thesis can be verified by his/her Ph.D. tutor and/or Ph.D. Coordinator in order to confirm its originality.

Date: 03/11/2021 Signature: 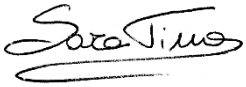

# *Index*

# *Chapter 1: General introduction*

## *Introduction to omics sciences*

The word "omics" refers to a particular field of study in biological disciplines that ends with *-omics*, such as genomics, metabolomics, lipidomics, proteomics, or transcriptomics. The objects of study of these disciplines are described adding the ending –ome to the field of interest. We can thus speak about the genome, metabolome, lipidome, proteome, and transcriptome, respectively.

- Genomics is the study of the complete set of DNA (genome). In the last years, thanks to the new next-generation sequencing technologies, genome-scale data have never been so accessible. This leads to a better understanding of the whole genome, decreasing the gap between genotype and phenotype.
- Transcriptomics is the study of the total RNA (transcriptome). This is another omic science which has benefited from the improvement of sequencing technologies. In fact, these technologies have allowed RNA analysis through cDNA sequencing on a massive scale (RNAseq) [1], eliminating the limited dynamic range of detection. Thanks to transcriptomics it is possible to have a snapshot of cellular metabolism.
- Proteomics is the study of all sets of proteins in a biological matrix (proteome). From a proteomic analysis it is supposed to obtain the protein inventory of a biological sample at a defined time point, in

order to find potential biomarkers, identify possible post-translational modifications, and study protein-protein interactions.

- Metabolomics is based on the global profiling of metabolites in a biological sample (metabolome). Metabolomics focus on the chemical fingerprints that specific cellular processes establish during their activity. This allows outlining a detailed profile about an individual's metabolism, even if this profile can vary over the day.

## *Lipidomics*

Since the 1960s, lipids have constituted a great field of study for the understanding of biological activities. It is only in recent years that lipid research has gained prominence with the emergence of lipidomics [2]. Lipidomics investigates the lipidome: the comprehensive and quantitative description of a set of lipid species constituting a cell, a tissue, or an organ. For many years, lipidomics was not distinct from metabolomics, even if there is a continuum of polarity between lipophilic and hydrophilic metabolites [3]. An individual's phenotype is more similar to the metabolome than the proteome, and even if the number of involved metabolites is smaller, their study is more complex and at the same time more informative about human health.

## *Lipids and lipid classes*

The main challenge in lipidomics is the extremely high diversity of molecular lipid species in biological matrices [4]. This complexity is reflected in the division and nomenclature of lipids.

According to their chemical building blocks, namely ketoacyl groups or isoprene groups [5], lipids are classified into eight main categories: fatty acyls,

glycerolipids, glycerophospholipids, sphingolipids, sterols, prenol lipids, saccharolipids, and polyketides (figure 1).

The considered categories are further subdivided into lipid classes and subclasses. The LIPID MAPS structure database (LMSD) is the most comprehensive database for lipidomics, and provides a total of 43,659 individual lipids, 21,706 curated compounds and 21,953 computationally generated compounds [6]. Nonetheless, the number of naturally occurring lipids is far higher than the reported lipids in this database. It is speculated that the number of lipids ranges at 100,000 or even more species.

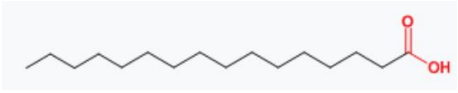

**A** Fatty acyls

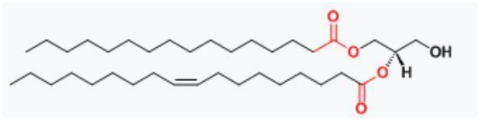

**B** Glycerolipids

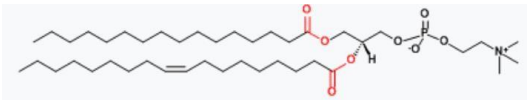

**C** Glycerophospholipids

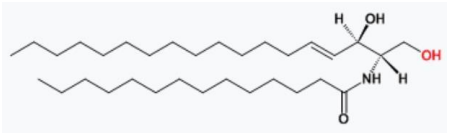

**D** Sphingolipids

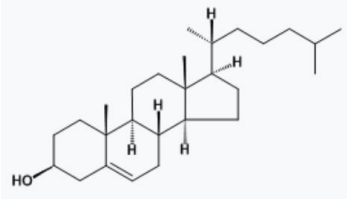

**E** Sterol lipids

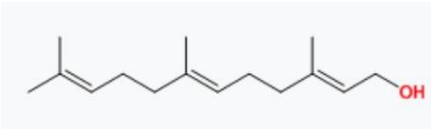

**F** Prenol lipids

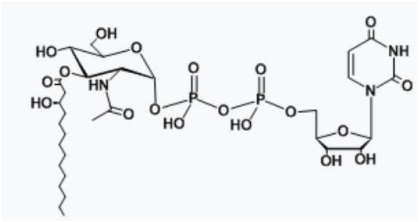

**G** Saccharolipids

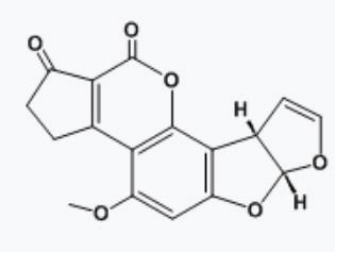

**H** Polyketides

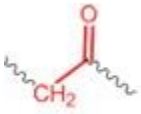

Acetyl

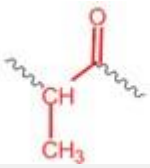

Propionyl

**I** Ketoacyl “building block”

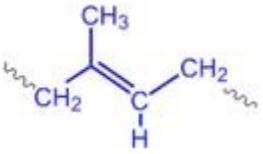

**L** Isoprene “building block”

**Figure 1**: the eight main lipid classes and their building blocks: Fatty acyls (**A**): hexadecanoic acid; Glycerolipids (**B**): 1-hexadecanoyl-2-(9Z-octadecenoyl)-sn-glycerol; Glycerophospholipids (**C**): 1-hexadecanoyl-2-(9Z-octadecenoyl)-sn-glycerol-3-phosphocholine; Sphingolipids (**D**): N-(tetradecanoyl)-sphing-4-enine;

Sterol lipids (**E**): cholest-5-en-3β-ol; Prenol lipids (**F**): 2E,6E-farnesol; Saccharolipids (**G**): UDP-3-O-(3R-hydroxyl-tetradecanoyl)-αD-N-acetylglucosamine; Polyketides (**H**): aflatoxin; Ketoacyl group (**I**); Isoprene group (**L**).

## *Identification of lipids in biological matrices*

It is clear that lipids include a large number of species that can be ubiquitous and that, thanks to their various structures, have numerous biochemical functions [7]. As reported above, it is estimated that over 100,000 possible lipid species exist, without taking into account all of the possible combinations of double bond positions on the carbon chain, backbone substitutions, and stereochemistry [8]. Furthermore, the number of potential lipids increases when all these structural differences are accounted for.

Thus, one major challenge that comes together with lipidomics is the process of identification [9].

Another drawback is that lipidomics is an emerging technique with little community consensus on the software of choice for comprehensive and accurate lipid identification using chromatographic and tandem mass spectrometric data.

Additionally, the limited number of synthesized standards available makes it difficult to cover the large variety of lipid structures for MS/MS spectral matching. This challenge has been partially overcome by the development of *in silico* libraries, such as LipidBlast, released by Kind et al. in 2013 [10].

The accurate annotation of lipids based on the observed fragmentation is also challenging [11]. This annotation is indeed based on structural resolution, which is the amount of structural information derived from experimental data, specifically MS/MS spectra.

Structural resolution for lipids depends on specific known structural characteristics, such as double bond positions, geometric isomerism and the lengths, degrees of unsaturation, and position of fatty acyl constituents in the

more complex lipids. For example, if you observe only the exact mass of the precursor ion and the choline, head group of a phosphatidylcholine, the lipid can only be annotated by total carbons and degrees of unsaturation, like in the following way: PC (32:1). On the contrary, if the precursor mass and fatty acyl fragments are known, the same lipid can be identified by acyl-constituents, even if the exact position of the two acyl chains on the glycerol backbone remains unknown. For this reason, the annotation of the considered lipid should be PC 16:0_18:1, where the underscore denotes the lack of information on the position of the two chains. This kind of annotation is possible only using Ultra-High Liquid Chromatography coupled to High-Resolution Mass Spectrometry (UHPLC-HRMS).

### *Ultra-High Liquid Chromatography coupled to High-Resolution Mass Spectrometry*

For lipidomics, it has been fundamental the development of new analytical techniques allowing the study of lipids in biological matrices and their interaction in biological pathways [12].

As reported previously, UHPLC-HRMS enhances lipid separation and relative detection, identification, and characterization. Lipid separation can be achieved by reversed-phase or HILIC chromatography, on the basis of the composition of their fatty acyl chains or their polar head groups, respectively. High resolution mass spectrometry is able to discriminate various adduct ions and to identify lipids with a precision of 5 decimals. Furthermore, the possibility to perform MS/MS events (like top N analysis) leads to the collection of fragmentation patterns that increase the accuracy of the identification in databases.

Thanks to these technological improvements, lipidomic MS/MS allows determining analyte masses with such high precision and accuracy that lipids can be identified unambiguously in complex mixtures [13].

## *Lipidomic workflow*

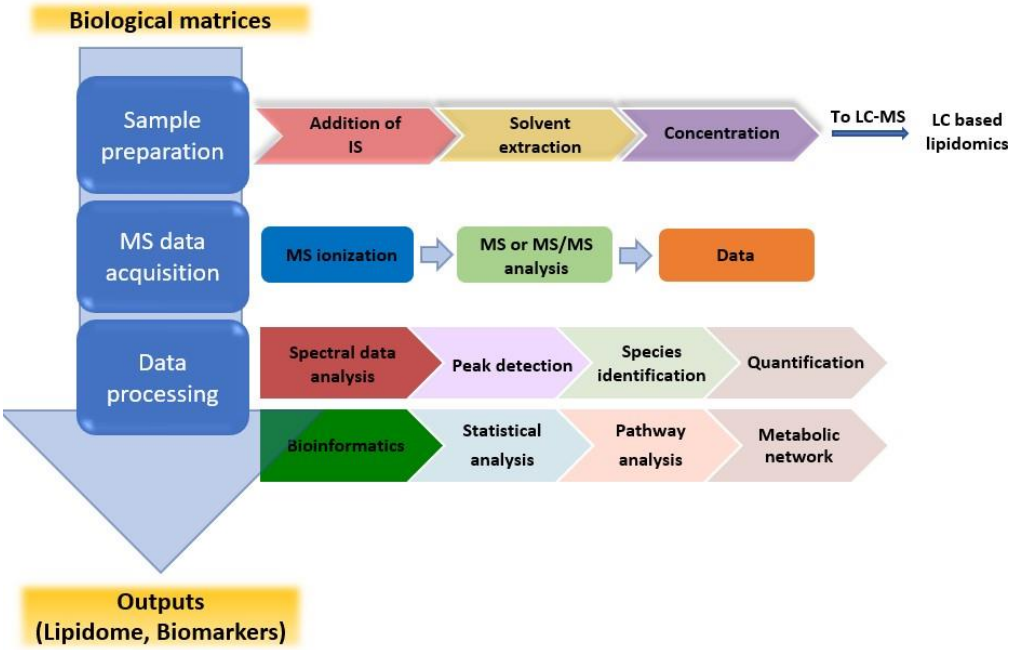


**Figure 2**: typical lipidomic workflow: from preparation of biological samples, mass spectrometry-based analysis and data processing. MS: mass spectrometry; MS/MS: tandem mass spectrometry; LC: liquid chromatography; IS: internal standard. (adapted from [14]).

When lipidomic analysis is performed on biological matrices like plasma, serum, or cells, proper sampling, sample storage, and adequate sample preparation, followed by the most suitable analyses and data processing, are mandatory.

Depending on the type of biological matrix, sample preparation must be the most proper for the selected analytical technique. In figure 2 are summarized the principal steps of the lipidomic workflow (adapted from [14]).

The first step of lipid extraction consists of the addition of appropriate internal standards (IS). In MS, IS help to compensate for possible variations in instrument performance and sample processing (alterations in lipid extraction efficacy, lipid class-dependent losses, matrix effects, and ionization suppression). The addition of IS before lipid extraction is used for quantifying lipids. In lipidomics, it is perhaps impossible to have an internal standard for each lipid species. For this reason, it is common to use a panel of deuterated IS per lipid class, with an MS/MS fragmentation pattern comparable to the corresponding class.

In general, lipid extraction from biological matrices is performed by liquid-liquid extraction; involving solvents with different polarity grades, such as mixtures of methanol, chloroform, [15], isopropanol, and water [16]. In this way, it is possible to isolate lipids with different physicochemical properties. To increase lipid recovery, the extraction solvent can be dried and the sample resuspended in less volume of a different solvent.

At this point, lipid separation is achieved by liquid chromatography or other separation techniques coupled with a mass spectrometer.

The last step is data processing, together with bioinformatic analysis. Raw data from HRMS has to be processed in order to identify and quantify lipid species. MS1 peaks and MS2 fragment ion peaks must be integrated to generate chromatographic peak areas used both for alignment across the samples and for the identification of lipid molecules. There are several available software, such as LipidSearch™ [17], and open-source software like MS-DIAL [18], LipidMatch [19], and LipidDataAnalyzer [20], that automatize the tedious processing of peak picking and alignment. These software assign an annotation for the lipids recognized thanks to the HRMS *m/z* and the fragmentation pattern. Usually, the annotations are possible because the

software has an internal library of masses and fragment ions from fatty acid chains and head groups (*in silico* library).

The peak picking, alignment, and annotation processes are not free from errors, so it is important to manually check the results.

Once the software has completed the processing, the resulting .txt or .excel files are the base to perform additional modifications, such as the normalization of lipids by internal standards and other statistics.

The highly multidimensional MS1 datasets are composed by hundreds of lipids species for each analyzed sample. In order to describe and differentiate between the numerous classes in the analysis, effective methodologies capable of swiftly extracting sample-specific molecular ion patterns are required. To do so, different techniques can be applied: univariate or multivariate statistical analysis. Univariate analysis uses a single variable to describe and summarize patterns in the data (*t*-test and ANOVA), while multivariate analysis uses a group of variables (PCA) [21].

# *Aim of the thesis*

Thanks to the recent technological development, today, the analysis of lipids extracted from different biological matrices can be easily performed in a comprehensive and detailed mode. Moreover, using untargeted methods, the identification and quantification of lipids that characterize specific phenotypes can be performed.

The aim of the present Ph.D. thesis was to use lipidomic analysis to explore biological mechanisms and biomarkers. In particular, we described three different case-studies in which the lipidomic approach allowed the in-depth study of lipid and biological alterations due to infection, environmental condition, and cancer disease.

The first study is focused on the alteration of plasma and cells lipids in patients affected by COVID-19. The lipidomic investigation was carried out on plasma from a large cohort of patients (n = 161), resulting in one of the most complete and representative lipidomics work on the host response to SARS-CoV-2 infection. Our data demonstrated that lipids are involved in the host response, particularly the glycerophospholipids class and fatty acids (arachidonic acid and oleic acid), but also in membrane remodeling and prostaglandins production. Notably, some lipid species resulted suitable to be used as possible biomarkers. The lipidomic analysis was also performed on peripheral blood mononuclear cells of the same cohort of samples. From this pilot study, that enrolled only a small number of patients (n = 21), confirmed the role of lipids in the immune response against SARS-CoV-2 infection.

The second part of the research focused on the study of the lipidome alteration caused by different types of gravity (G) forces *in vitro* and *in vivo*. Lipidomic

analysis was performed to characterize the effects of microgravity on human pancreatic ductal adenocarcinoma (PDCA) cell line (PaCa-44 cells). It was observed that exposure to microgravity for seven days lead to a morphological alteration, towards the acquisition of stemness profile. This finding was supported by increased levels of total fatty acids and increased ratio between long-intermediate-chain acylcarnitines (C16-C20) to short-chain ones (C4) that suggest an impairment of the β-oxidation, tipical of cancer stem cells.

Using a murine model, the investigation of the lipidomic and proteomic profile of plasma from mice kept in a condition of hypergravity (3G) for one month has been performed. Circulating lipids are representative of the host phenotype and they are indicators of possible alteration in biological functions and mechanisms. The lipidomic analysis suggested a stress response of the animal to hypergravity, resulting in decreased levels of most of the lipid classes identified.

The last part of the research study reports an untargeted and targeted UHPLC-HRMS lipidomics analysis on plasma samples belonging to patients affected by prostate cancer and patients affected by chronic prostate inflammation. Both groups presented elevated levels of prostate specific antigen (PSA) and for this reason both groups of patients were subjected to biopsy. The first untargeted analysis was carried out on 30 patients and 5 promising lipid biomarkers were obtained. These biomarkers were then validated on a larger cohort of patients (n = 140).

In this thesis it has been shown how lipidomics can be used to better understand the impairment in biological pathways and mechanisms that occur in the host. Furthermore, it was demonstrated that lipids can be used as a powerful diagnostic tool for some pathologies, avoiding unnecessary and invasive treatments.

## *Bibliography*


1. Voelkerding, K.V.; Dames, S.A.; Durtschi, J.D. Next-Generation Sequencing: From Basic Research to Diagnostics. *Clinical Chemistry* **2009**, *55*, 641–658, doi:10.1373/clinchem.2008.112789.
2. Seppänen-Laakso, T.; Orešič, M. How to Study Lipidomes. *Journal of Molecular Endocrinology* **2009**, *42*, 185–190, doi:10.1677/JME-08-0150.
3. Monnerie, S.; Comte, B.; Ziegler, D.; Morais, J.A.; Pujos-Guillot, E.; Gaudreau, P. Metabolomic and Lipidomic Signatures of Metabolic Syndrome and Its Physiological Components in Adults: A Systematic Review. *Sci Rep* **2020**, *10*, 669, doi:10.1038/s41598-019-56909-7.
4. Züllig, T.; Köfeler, H.C. HIGH RESOLUTION MASS SPECTROMETRY IN LIPIDOMICS. *Mass Spec Rev* **2021**, *40*, 162–176, doi:10.1002/mas.21627.
5. Fahy, E.; Cotter, D.; Sud, M.; Subramaniam, S. Lipid Classification, Structures and Tools. *Biochimica et Biophysica Acta (BBA) - Molecular and Cell Biology of Lipids* **2011**, *1811*, 637–647, doi:10.1016/j.bbalip.2011.06.009.
6. Sud, M.; Fahy, E.; Cotter, D.; Brown, A.; Dennis, E.A.; Glass, C.K.; Merrill, A.H.; Murphy, R.C.; Raetz, C.R.H.; Russell, D.W.; et al. LMSD: LIPID MAPS Structure Database. *Nucleic Acids Research* **2007**, *35*, D527–D532, doi:10.1093/nar/gkl838.
7. Dowhan, W. MOLECULAR BASIS FOR MEMBRANE PHOSPHOLIPID DIVERSITY:Why Are There So Many Lipids? *Annu. Rev. Biochem.* **1997**, *66*, 199–232, doi:10.1146/annurev.biochem.66.1.199.
8. Yetukuri, L.; Ekroos, K.; Vidal-Puig, A.; Orešič, M. Informatics and Computational Strategies for the Study of Lipids. *Mol. BioSyst.* **2008**, *4*, 121–127, doi:10.1039/B715468B.
9. Lintonen, T.P.I.; Baker, P.R.S.; Suoniemi, M.; Ubhi, B.K.; Koistinen, K.M.; Duchoslav, E.; Campbell, J.L.; Ekroos, K. Differential Mobility Spectrometry-Driven Shotgun Lipidomics. *Anal. Chem.* **2014**, *86*, 9662–9669, doi:10.1021/ac5021744.
10. Kind, T.; Liu, K.-H.; Lee, D.Y.; DeFelice, B.; Meissen, J.K.; Fiehn, O. LipidBlast in Silico Tandem Mass Spectrometry Database for Lipid

Identification. *Nat Methods* **2013**, *10*, 755–758, doi:10.1038/nmeth.2551.

11. Liebisch, G.; Vizcaíno, J.A.; Köfeler, H.; Trötzmüller, M.; Griffiths, W.J.; Schmitz, G.; Spener, F.; Wakelam, M.J.O. Shorthand Notation for Lipid Structures Derived from Mass Spectrometry. *Journal of Lipid Research* **2013**, *54*, 1523–1530, doi:10.1194/jlr.M033506.
12. Zehethofer, N.; Pinto, D.M. Recent Developments in Tandem Mass Spectrometry for Lipidomic Analysis. *Analytica Chimica Acta* **2008**, *627*, 62–70, doi:10.1016/j.aca.2008.06.045.
13. Gerszten, R.E.; Wang, T.J. The Search for New Cardiovascular Biomarkers. *Nature* **2008**, *451*, 949–952, doi:10.1038/nature06802.
14. Yang, K.; Han, X. Lipidomics: Techniques, Applications, and Outcomes Related to Biomedical Sciences. *Trends in Biochemical Sciences* **2016**, *41*, 954–969, doi:10.1016/j.tibs.2016.08.010.
15. Folch, Jordi.; Ascoli, I.; Lees, M.; Meath, J.A.; LeBaron, F.N. PREPARATION OF LIPIDE EXTRACTS FROM BRAIN TISSUE. *Journal of Biological Chemistry* **1951**, *191*, 833–841, doi:10.1016/S0021-9258(18)55987-1.
16. Matyash, V.; Liebisch, G.; Kurzchalia, T.V.; Shevchenko, A.; Schwudke, D. Lipid Extraction by Methyl-Tert-Butyl Ether for High-Throughput Lipidomics. *Journal of Lipid Research* **2008**, *49*, 1137–1146, doi:10.1194/jlr.D700041-JLR200.
17. Breitkopf, S.B.; Ricoult, S.J.H.; Yuan, M.; Xu, Y.; Peake, D.A.; Manning, B.D.; Asara, J.M. A Relative Quantitative Positive/Negative Ion Switching Method for Untargeted Lipidomics via High Resolution LC-MS/MS from Any Biological Source. *Metabolomics* **2017**, *13*, 30, doi:10.1007/s11306-016-1157-8.
18. Tsugawa, H.; Cajka, T.; Kind, T.; Ma, Y.; Higgins, B.; Ikeda, K.; Kanazawa, M.; VanderGheynst, J.; Fiehn, O.; Arita, M. MS-DIAL: Data-Independent MS/MS Deconvolution for Comprehensive Metabolome Analysis. *Nat Methods* **2015**, *12*, 523–526, doi:10.1038/nmeth.3393.
19. Koelmel, J.P.; Kroeger, N.M.; Ulmer, C.Z.; Bowden, J.A.; Patterson, R.E.; Cochran, J.A.; Beecher, C.W.W.; Garrett, T.J.; Yost, R.A. LipidMatch: An Automated Workflow for Rule-Based Lipid Identification Using Untargeted High-Resolution Tandem Mass

Spectrometry Data. *BMC Bioinformatics* **2017**, *18*, 331, doi:10.1186/s12859-017-1744-3.

20. Hartler, J.; Triebl, A.; Ziegl, A.; Trötzmüller, M.; Rechberger, G.N.; Zeleznik, O.A.; Zierler, K.A.; Torta, F.; Cazenave-Gassiot, A.; Wenk, M.R.; et al. Deciphering Lipid Structures Based on Platform-Independent Decision Rules. *Nat Methods* **2017**, *14*, 1171–1174, doi:10.1038/nmeth.4470.
21. Sen, P.K.; Anderson, T.W.; Arnold, S.F.; Eaton, M.L.; Giri, N.C.; Gnanadesikan, R.; Kendall, M.G.; Kshirsagar, A.M.; Mardia, K.V.; Kent, J.T.; et al. Contemporary Textbooks on Multivariate Statistical Analysis: A Panoramic Appraisal and Critique. *Journal of the American Statistical Association* **1986**, *81*, 560, doi:10.2307/2289251.

# *Chapter 2: Lipidomic studies of the host response after SARS-CoV-2 infection*

## *General introduction to the chapter*

In the present chapter are reported the main results and findings on lipid alterations that occur during the infection of SARS-CoV-2 in human patients. Plasma and peripheral blood mononuclear cells (PBMCs) from different patients were investigated (figure 1).

The study on plasma involved a large cohort of COVID-19 patients and controls: 103 and 58 respectively, resulting in the first large-scale untargeted metabolomic and lipidomic investigation of plasma from COVID-19 patients and controls. The samples were collected in northern Italy, the pandemic's epicenter in this country. Findings reveal a number of processes and pathways involved in the host response to SARS-CoV-2, as well as several promising lipid biomarkers and therapeutic targets.

Regarding cells investigation, 21 PBMCs samples were analyzed: 14 from patients with positive nucleic acid test results to COVID-19 and 7 from healthy subjects. This is a preliminary study, for this reason a small number of samples is involved.

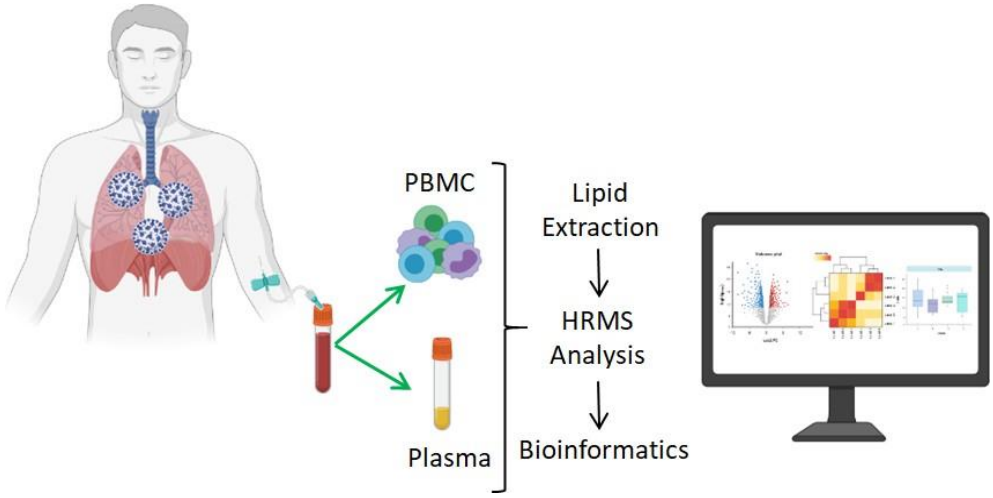


**Figure 1:** workflow of the two studies investigating the host response to SARS-CoV-2 infection in the lipidome of plasma and cells (peripheral blood mononuclear cells, PBMCs).

## *Introduction to the topic*

In December 2019 the novel coronavirus (SARS-CoV-2) caused the spread of a viral pneumonia from Wuhan, China, all over the world. The number of cases continues to rise, with over 1,250,000 deaths recorded worldwide. The most common symptoms are cough, fever, muscle ache, shortness of breath, disorientation, headache, sore throat, rhinorrhea, whole body ache, diarrhea and nausea [1,2].

The low respiratory tract is the principal organ attacked by SARS-CoV-2, and some patients develop a life-threatening acute respiratory distress syndrome, while immediate myocardial injury and persistent cardiovascular damage have also been discovered [3]. Although more than 80% of COVID-19 patients experience only mild symptoms, conditions can rapidly progress from mild to severe, particularly if no adequate targeted medical intervention is programmed.

Up to now, researchers mainly focused on the epidemiological and clinical characteristics associated with the virus SARS-CoV-2 [4,5]. The physiological changes related to SARS-CoV-2 have not been understood yet, even if some studies have found a deep impact on the immune function [6].

Since molecules such as lipids, metabolites, and proteins play crucial roles in pathogenesis and in numerous cell activities, profiling the human biofluids, lipidome, metabolome, and proteome provides insight into critical conditions and diseased states. Longitudinal analysis of molecular components can be employed for precision health treatment and for the improvement of disease knowledge as well. Such approach lead to the discovery of changes in the metabolome and lipidome in human plasma of patients affected by Ebola virus or H1N1 influenza pneumonia [7–9], and to the identification of lipid

metabolism abnormalities in recovered severe acute respiratory syndrome (SARS) patients after 12 years of infection [10].

A targeted metabolomic and lipidomic method revealed changes in energy metabolism and hepatic dysfunction in COVID-19 patients. Despite these findings, the study involved only 34 Chinese patients and did not perform untargeted profiling of the molecules present in plasma [11].

Another study [12] discovered molecular alterations in COVID-19 patients' sera, linking macrophage dysregulation, platelet degranulation, complement system pathways, and severe metabolic suppression to the disease. Even in this case, the research was limited to a circumscribed number of Chinese patients (n = 46).

Other studies have found interesting links between the SARS-CoV-2 infection and metabolic dysregulation such as monosialodihexosyl gangliosides (GM3s)-enriched exosomes [13] and alterations of kynurenine pathway and fatty acids metabolism [14]; however, these two works involved a small cohort of COVID-19 patients: 50 and 33 respectively.

Our knowledge of the effects of SARS-CoV-2 on host targets remains largely limited. In particular, there has not been a large-scale, untargeted metabolomic and lipidomic investigation of European COVID-19 patients. Furthermore, the small numbers of patients in the previously mentioned studies highlight the need for a bigger and more representative research study.

The first study reported in this chapter, which is part of the newly formed COVID-19 mass spectrometry coalition (www.covid19-msc.org) [15], was the first large-scale untargeted metabolomics and lipidomics investigation of plasma from COVID-19 patients and controls. The plasma samples were collected in northern Italy, the pandemic's epicenter in this country. Italy was the first country in Western Europe to be infected with COVID-19. Our findings reveal a number of processes and pathways involved in the host

response to SARS-CoV-2, as well as several promising biomarkers and therapeutic targets.

The deep investigation of the lipidome of plasma from patients infected with SARS-CoV-2 virus has shown an alteration in lipid levels and has highlighted the possibility to use lipidomics as a tool to better understand the host response to virus infection.

These observations led us to interrogate if the alteration of lipidome also involves cellular levels, particularly regarding the immune system.

PBMCs consist of lymphocytes (T cells, B cells, NK cells) and monocytes, whereas erythrocytes and platelets have no nuclei, and granulocytes (neutrophils, basophils, and eosinophils) have multi-lobed nuclei. In humans, lymphocytes make up the majority of the PBMC population, followed by monocytes, and only a small percentage of dendritic cells.

A recent *in vitro* and *in vivo* study of SARS-CoV-2 infection of human PBMCs pointed out that *in vitro* infection of cells from healthy donors produced viral offspring, revealing that monocytes, as well B and T cells, are vulnerable to SARS-CoV-2 active infection. SARS-CoV-2 was also frequently found in monocytes and B lymphocytes from COVID-19 patients, although less commonly in CD4+ T cells, according to flow cytometry and immunofluorescence studies [45].

To date in literature, no studies focusing on the lipidome of PBMCs from the blood of infected patients exist.

To complete our understanding about the host response after virus infection, a lipidomic investigation on PBMCs from patients infected with SARS-CoV-2 is reported.

In the following sections, lipidomic results and findings of both studies were critically discussed.

### *Overview of the studies and patients involved*

The workflow of the study is reported in figure 2. In the first study a total of 161 plasma samples were collected, 103 of whom from patients infected with SARS-CoV-2 (COVID-19 group), while 58 were from subjects with negative nucleic acid test results (non-COVID-19 group). In table 1 the details of the patients are reported. All of the patients were admitted to the Novara University Hospital (Piedmont, North Italy), the Italian epicenter of the pandemic, for pneumonia and/or respiratory failure.

Both the two main groups (COVID-19 and non-COVID-19 groups) were subdivided into critical and non-critical patients. Out of the 103 individuals from the COVID-19 group, 19 were critical and 84 non-critical, while out of 32 subjects from non-COVID-19 groups 20 were non-critical and 12 critical. Critical patients were those admitted to the intensive care unit (ICU COVID-19 group) with respiratory failure, requiring mechanical ventilation, while non-critical patients characterized by mild or severe respiratory failure, with no require for mechanical or invasive ventilation.

Furthermore, we enrolled 26 healthy subjects as controls (healthy group).

As regards cells samples: 14 patients positive to the SARS-CoV-2 test (COVID-19 group) and 7 healthy subjects as control group (healthy group) were enrolled.

Lipidomic analysis was carried out by ultra-performance liquid chromatography/tandem mass spectrometry (UHPLC-MS/MS) using an untargeted approach, in both positive and negative ionization modes. The acquired raw data were processed using the MS-DIAL software in order to automate mass spectral deconvolution of high-resolution MS data [16].

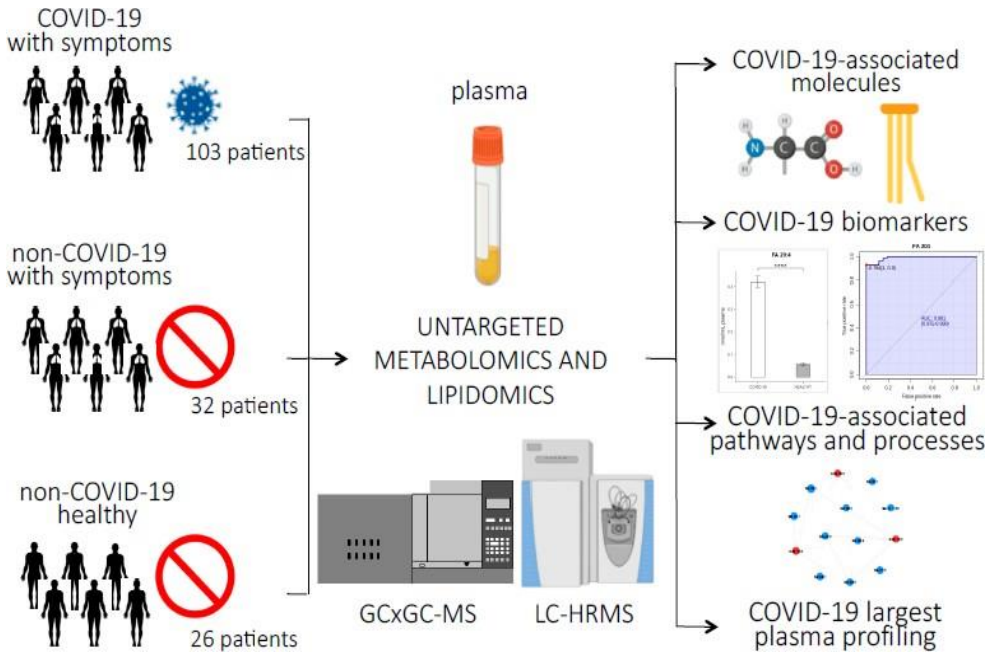


**Figure 2**: experimental design of the study: untargeted lipidomic and metabolomic analyses were performed on plasma samples from 103 patients infected with SARS-CoV-2, 84 of whom had non-critical COVID-19, while 19 had critical COVID-19 and recovered in the ICU; 20 non-COVID-19 patients with similar clinical symptoms as the COVID-19 patients; 26 healthy subjects; and 12 ICU patients who tested negative for COVID-19. The abundance of small molecules and lipids were used to identify COVID-19-associated biomarkers, pathways, and processes related to the host response to the virus. ($p$-value < 0.0001 = ****).

**Table 1:** Characteristics of the patients included in the plasma study**.**

| Variable | Non-COVID-19 patients | | | | COVID-19 patients | | |
|---|---|---|---|---|---|---|---|
| | Total (58) | Healthy Control (N=26) | Non-critical (N=20) | Critical (N=12) | Total (N=103) | Non-critical (N=84) | Critical (N=19) |
| **Sex (no.)** | | | | | | | |
| Male | 23 | 11 | 9 | 6 | 61 | 48 | 13 |
| Female | 29 | 15 | 11 | 6 | 42 | 36 | 6 |
| **Age (year)** | | | | | | | |
| Mean ± SD | 61.8 ± 15.4 | 50.1 ± 5.3 | 68.6 ± 8.9 | 67.4 ± 17.3 | 67.3 ± 18.0 | 59.7 ± 13.0 | 69.0 ± 18.5 |
| Range | 38.0 - 96.0 | 42.0 - 56.0 | 56.0 - 82.0 | 38.0 - 96.0 | 21.0 - 107.0 | 21.0 - 76.0 | 29.0 - 107.0 |
| **Time from onset to admission (days)** | | | | | | | |
| Mean ± SD | | | 5.7 ± 10.0 | 7.7 ± 6.5 | 5.8 ± 7.2 | 5.8 ± 7.6 | 5.5 ± 5.0 |
| Range | | | 1.0 - 45.0 | 1.0 - 12.0 | 1.0 - 32.0 | 1.0 - 32.0 | 1.0 - 19.0 |
| **Time from admission to severe (days)** | | | | | | | |
| Mean ± SD | | | | 1.8 ± 4.9 | | | 6.5 ± 7.3 |
| Range | | | | 1.0 - 13.0 | | | 1.0 - 28.0 |
| **Symptoms (n°)** | | | | | | | |
| Fever | | | 9 | 0 | 52 | 40 | 12 |
| Cough | | | 5 | 0 | 34 | 25 | 13 |
| Headache | | | 0 | 0 | 1 | 1 | 0 |
| Fatigue | | | 1 | 1 | 8 | 8 | 0 |
| Dyspnea | | | 4 | 0 | 27 | 23 | 4 |
| Diarrhea | | | 2 | 1 | 13 | 9 | 4 |
| Chest pain | | | 3 | 0 | 5 | 5 | 0 |
| Abdominal pain | | | 4 | 0 | 5 | 4 | 1 |
| Vomiting | | | 6 | 0 | 3 | 3 | 0 |
| **Comorbidity (n°)** | | | | | | | |
| Hypertension | | | 0 | 2 | 38 | 29 | 9 |
| Diabetes | | | 0 | 1 | 17 | 12 | 5 |
| Respiratory system | | | 1 | 0 | 6 | 6 | 0 |
| Cardiovascular system | | | 4 | 1 | 38 | 34 | 4 |
| Other endocrine system | | | 0 | 0 | 12 | 9 | 3 |
| Chronic kidney | | | 1 | 0 | 9 | 7 | 2 |
| Digestive system | | | 2 | 0 | 16 | 15 | 1 |

| **Oxygen saturation index (%)** | | | | | | | |
|---|---|---|---|---|---|---|---|
| Mean ± SD | | | 85.5 ± 6.3 | 94.3 ± 3.8 | 90.7 ± 6.7 | 90.8 ± 6.4 | 90.3 ± 8.2 |
| Range | | | 81.0 - 90.0 | 87.0 - 99.0 | 71.0 - 99.0 | 71.0 - 99.0 | 71.0 - 98.0 |

## *Materials and Methods*

Materials and methods of these studies are grouped at the end of Chapter 2, in the section "Materials and Methods", where are reported in details reagents, sample preparation, lipidomic analysis, quality controls, data processing, and bioinformatic analysis.

## *Plasma investigation results*

2075 and 1108 detected lipid species were found in positive and negative modes, respectively, while the total numbers of identified lipids were 467 and 89, respectively.

In order to have a preliminary understanding of the results after data processing, multivariate analysis was performed. The groups of non-critical positive COVID-19 and healthy individuals were inspected using PCA score plot (figure 3A and B). A significant separation of the two groups according to the diagnosis had been highlighted by the PCA score. Partial least square discriminant analysis (PLS-DA) was also performed (figure 4A and B), confirming the PCA results. Together with PLS-DA the VIP (variable of importance in projection) score of the most predictive or discriminative lipids (figure 4C and D) was as well calculated. The differences between the two groups were mostly due to lipid species such as PCs, PEs, LPCs, and TGs, and fatty acids (FAs).

Through MetaboAnalyst software we performed a univariate analysis of quantified lipids.

265 lipids were modulated in COVID-19 patients compared to healthy group ($p$-value ≤ 0.05, fold change > 1.5). The volcano plots in figure 5A and 5C showed the most significant differences among the lipids and the positive or negative fold changes in the comparison. In figure 5B and 5D are reported the hierarchical heatmaps highlighting the two clusters of samples. The complete list of modulated lipids is reported in table 2, in the section "Materials and methods", at the end of the chapter.

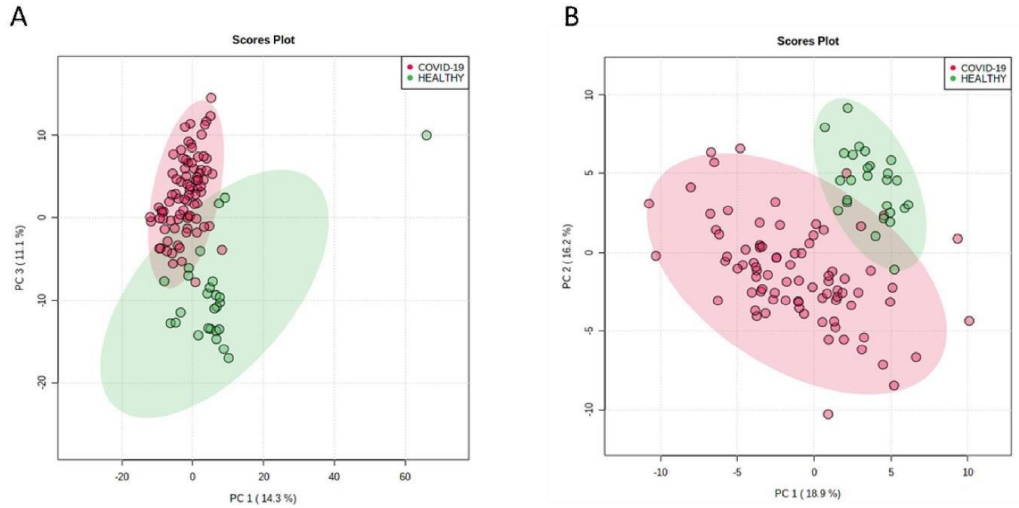


**Figure 3**: lipidomic score plot of COVID-19 and healthy groups. PCA positive (**A**) and negative (**B**).

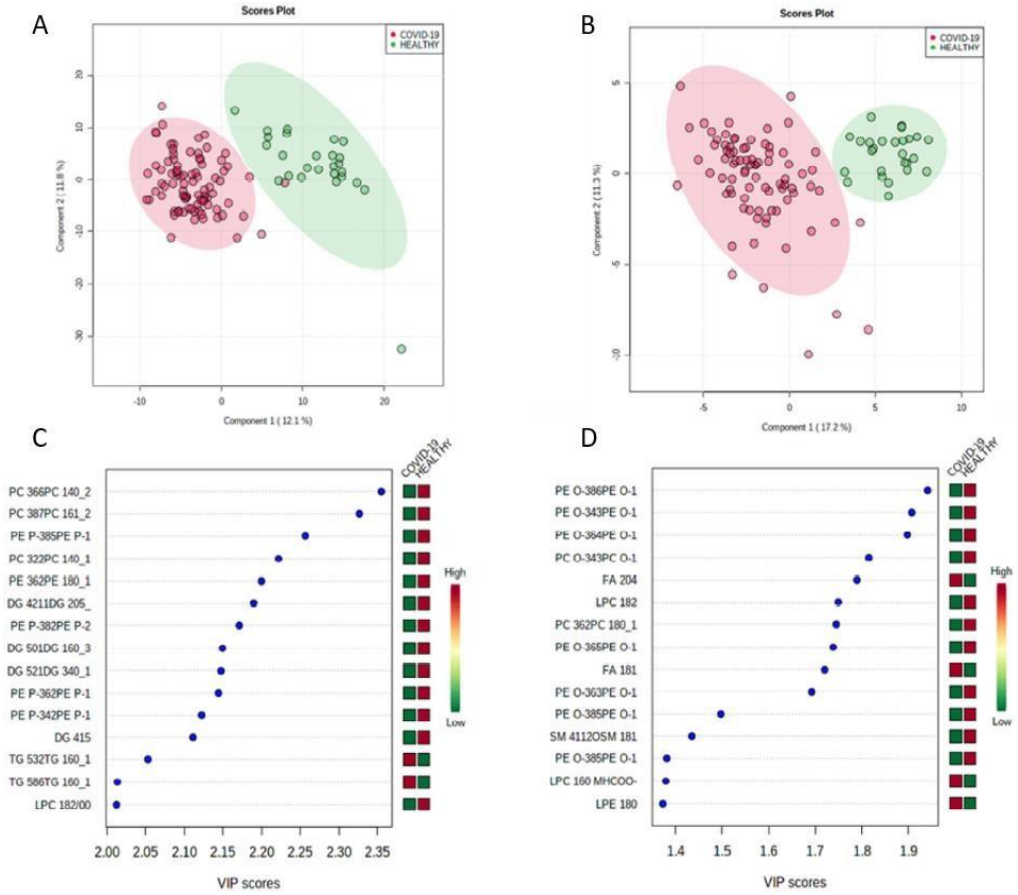


**Figure 4**: lipidomic score plot of COVID-19 and healthy groups. PLS-DA for positive (**A**) and negative (**B**) mode, VIP score for positive (**C**) and negative (**D**) mode.

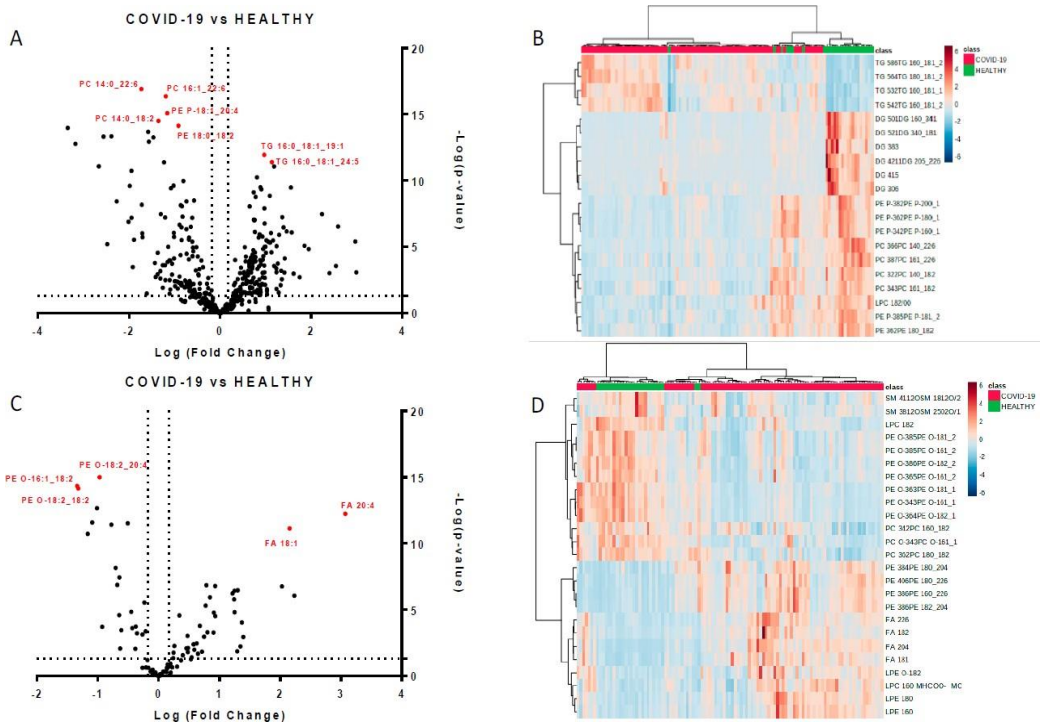


**Figure 5**: modulated lipids in SARS-CoV-2 infection. Volcano plots of quantified lipids in positive (**A**) and negative (**C**) modes. A total of 265 lipids were modulated with a *p*-value ≤ 0.05 and a fold change > 1.5. Hierarchical heat maps of quantified lipids in positive (**B**) and negative (**D**) modes, highlighting the two clusters of samples, with COVID-19 patients in red and healthy subjects in green.

## *Lipids are strongly involved in the host response to SARS-CoV-2*

The study of plasma metabolic alterations could reveal new or previously unknown pathways related to the host response to SARS-CoV-2 infection. Through bioinformatic analysis, we sought to gain a better understanding of how metabolic changes found in blood samples could be related to the overall response and to aid in the identification of potential biochemical linkages between SARS-CoV-2 infection and blood metabolic abnormalities.

We discovered that CAR, DG, FA, LPC, LPE, PC, PE, SM and TG were the most modulated lipid classes by comparing COVID-19 patients to healthy

individuals (figure 6). As a consequence of the infection, PCs were significantly down-regulated. PC 14:0_22:6, PC 16:1_22:6, PC 14:0_18:2, and PC O-16:1_18:2 were the most decreased in COVID-19 group, with fold changes of 0.305, 0.443, 0.395, and 0.495, respectively. Another down-modulated class was the PE class, while several free fatty acids (FA 18:1, FA 18:2, FA 22:6, FA 44:5, and FA 20:4) were up-regulated.

In general, a great heterogeneity between the modulated lipids has been observed, as shown in the MetaMapp visualization in figure 7. Red nodes represent lipids with higher concentrations, while blue nodes indicate lipids with lower concentrations in the COVID-19 group.

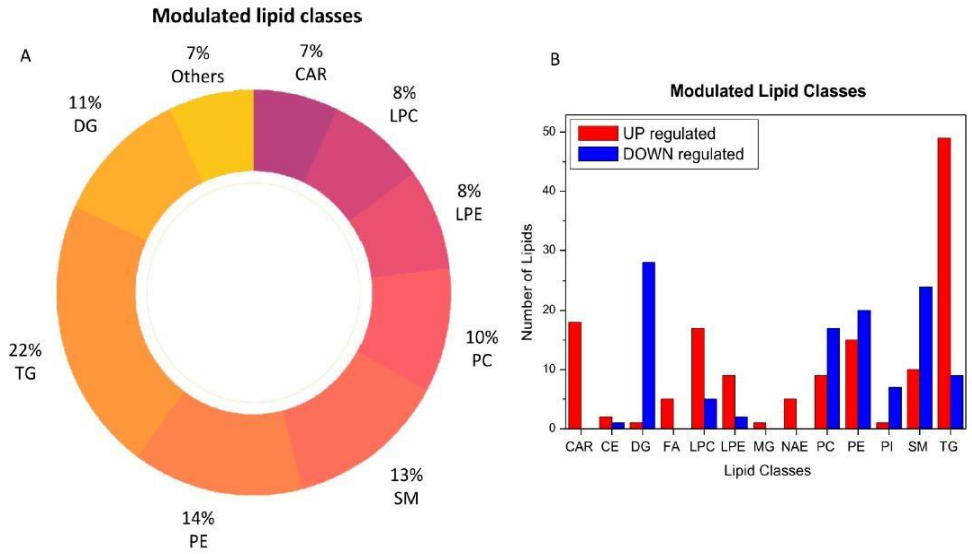


**Figure 6**: modulated lipid classes after SARS-CoV-2 infection (**A**) and number of modulated lipids within each single class (**B**); red up-regulated and blue down-regulated.

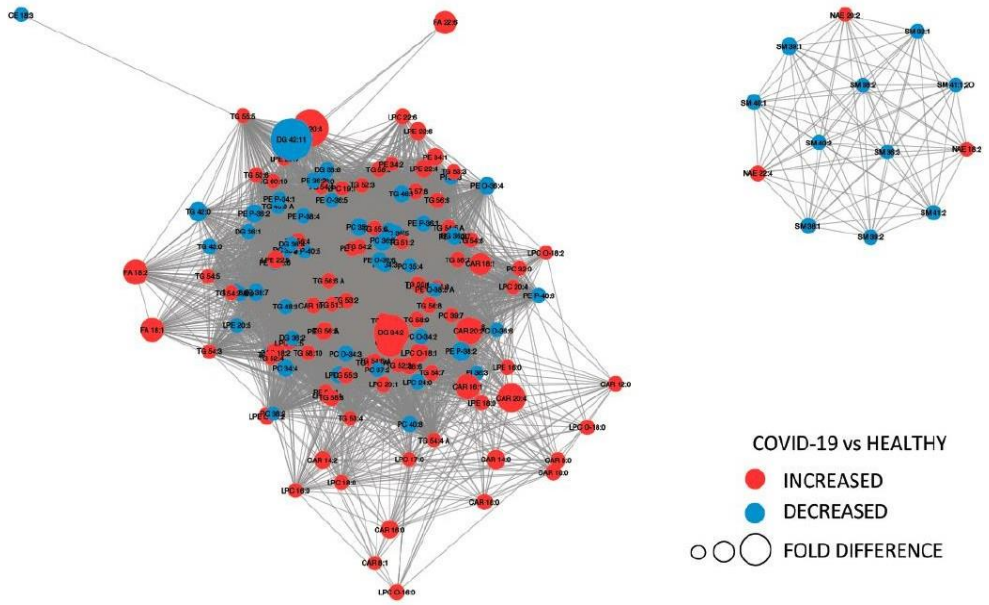


**Figure 7**: MetaMapp visualization of lipidomic changes in COVID-19 patients. Lipids with increased concentration are depicted using red nodes, while lipids with decreased concentration are represented by blue nodes. The lipids grouped on the right are sphingomyelins and N-acylethanolamine, while on the left are reported glycerolipids.

Notably, an increase in LPC and LPE classes was found in COVID-19 patients. This variation could be associated with viral replication in infected cells, considering that the alteration in the lipid homeostasis of host cells is a viral strategy for generating a suitable environment for replication [17]. In the COVID-19 group, all of the 18 CARs identified were increased. CAR are acyl esters of carnitine and are essential compounds for fatty acids oxidation and organic acid metabolism [18]. Furthermore, the modulated lipids were inspected with a KEGG functional enrichment analysis using LIPEA web tool (2018), which suggested two significant pathways with a Benjamini and Bonferroni corrected $p$-values $< 0.05$: fat digestion and adsorption and glycerophospholipid metabolism.

*Lipidomics alterations in critical COVID-19 Patients*

Our data confirmed that lipidomics is able to reveal perturbations in the levels of different lipid species due to the infection of SARS-CoV-2. For this reason, we decided to investigate the lipid profile of plasma samples from critical COVID-19 patients who were admitted to the intensive care unit (ICU COVID-19). Comparing 19 ICU COVID-19 patients to 12 ICU non-COVID-19, we identified 77 modulated lipids.

Even in this comparison, the two groups were well separated by PCA score plot and heatmap, as reported in figure 8, showing only the results in the positive mode.

TGs were the most increased lipids in the critical class ICU COVID-19 (figure 9): TG 16:1_16:1_18:2, TG 16:0_18:1_24:1, and TG 24:0_18:1_18:1 were the most expressed with fold changes of 14.9, 4.30, and 4.20, respectively.

These results were also confirmed by the comparison between the non-critical COVID-19 group and the critical COVID-19 group. The higher levels of TGs in critical group suggested a link between adipose tissue lipolysis and the physiological response to critical illness. Worth note were the levels of FA 18:1 and FA 20:4, oleic acid, and arachidonic acid respectively, which directly correlated to the severity of the disease (figure 10), with higher levels in ICU COVID-19 patients.

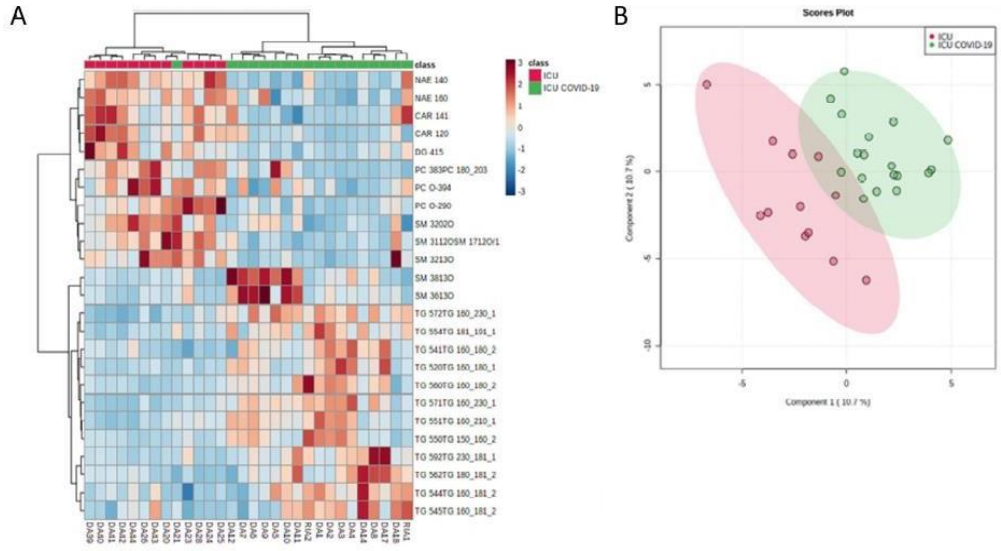


**Figure 8**: hierarchical heatmap of ICU and ICU-COVID-19 groups (**A**) and PCA score plot (**B**) in positive mode.

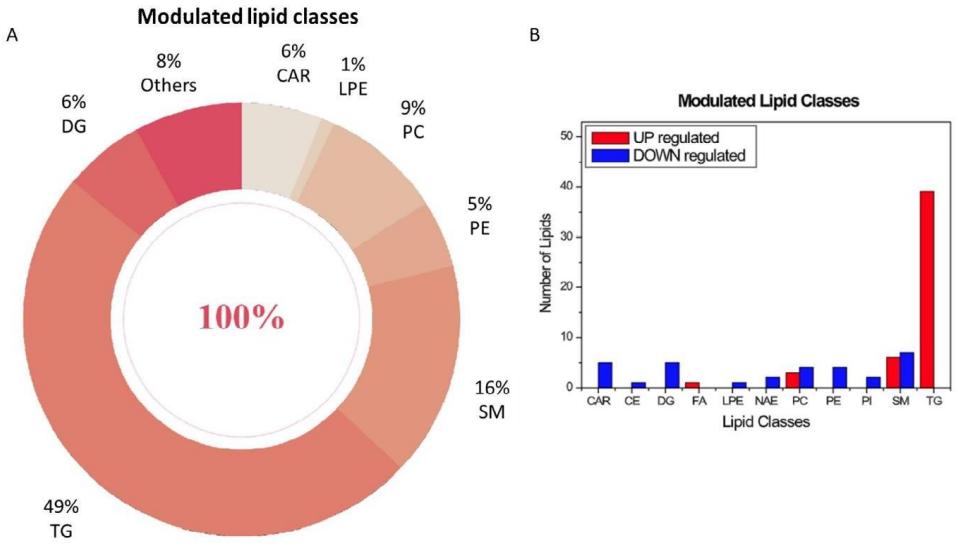


**Figure 9**: modulated lipid classes (**A**) and number of up-regulated and down-regulated lipids (**B**) in ICU COVID-19 vs ICU groups.

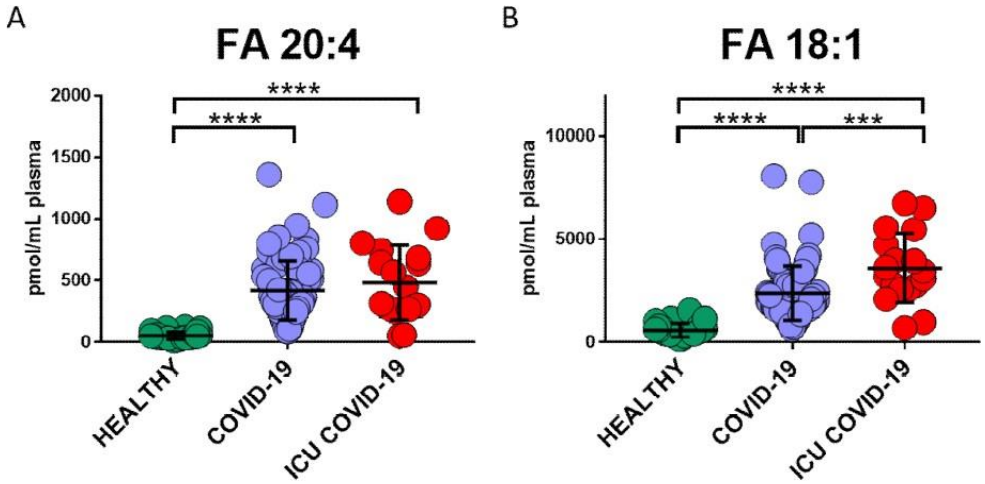


**Figure 10**: bar plots (average ± SD) of FA 20:4 (**A**) and FA 18:1 (**B**) in healthy subjects (healthy), non-critical (COVID-19) and critical COVID-19 patients (ICU COVID-19).
*p*-value < 0.001 = ***; *p*-value < 0.0001 = ****.

## *Potential Biomarkers of COVID-19*

Investigation of modulated lipids and the use of ROC (Receiver Operating Characteristic) curves lead us to explore potential lipid biomarkers.

The analysis showed the presence of seven lipids potentially able to discriminate COVID-19 patients from healthy subjects. As regard the positive mode, PC 14:0_22:6, PC 16:1_22:6, and PE 18:1_20:4 showed an area under the curve (AUC) values of 0.96 (sensitivity (SE): 93%, specificity (SP): 89%), 0.97 (SE: 90%, SP: 96%), and 0.94 (SE: 86%, SP: 96%), respectively, while their combined ROC reported an AUC of 0.97 (figure 11A, B, C, and H). In the negative mode, FA 20:4 (arachidonic acid), FA 18:1 (oleic acid), PE O-18:2_20:4, and PE O-16:1_18:2 showed an AUC values of 0.99 (SE: 93%, SP: 100%), 0.98 (SE: 96%, SP: 88%), 0.92 (SE: 89%, SP: 86%), and 0.92 (SE: 96%, SP: 82%), respectively, while their combined ROC reported an AUC of 1 (figure 11D, E, F, G and I).

Gender is often ignored when evaluating biomarkers for human disease; nonetheless, it is now obvious that the severity of SARS-CoV-2 infection is

linked to gender. In order to investigate this aspect, we explored the PCA score plot (figure 12A and B) of the female and male infected patients. It is evident the heterogeneity in the distribution of samples and that there are no clusters related to the gender. Importantly, no gender differences were found in the main circulating biomarkers (figure 12C and D).

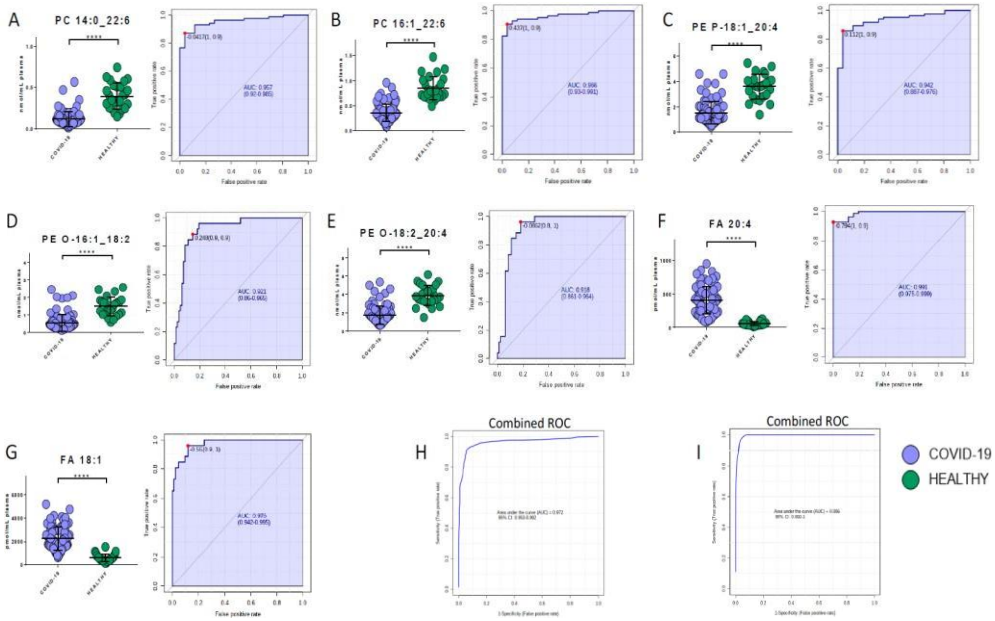


**Figure 11**: bar plots (average ± SD) with relative statistical significance (*p*-value < 0.0001 = ****) and ROC curves with the optimal cutoff calculated for each ROC analysis (red dot) are reported in order to show the best potential biomarkers identified using lipidomics analysis. PC 14:0_22:6 (**A**), PC 16:1_22:6 (**B**), PE 18:1_20:4 (**C**), FA 20:4 (**D**), FA 18:1 (**E**), PE (O-18:2_20:4) (**F**), and PE (O-16:1_18:2) (**G**). Combined ROCs (**H**, **I**) are also shown.

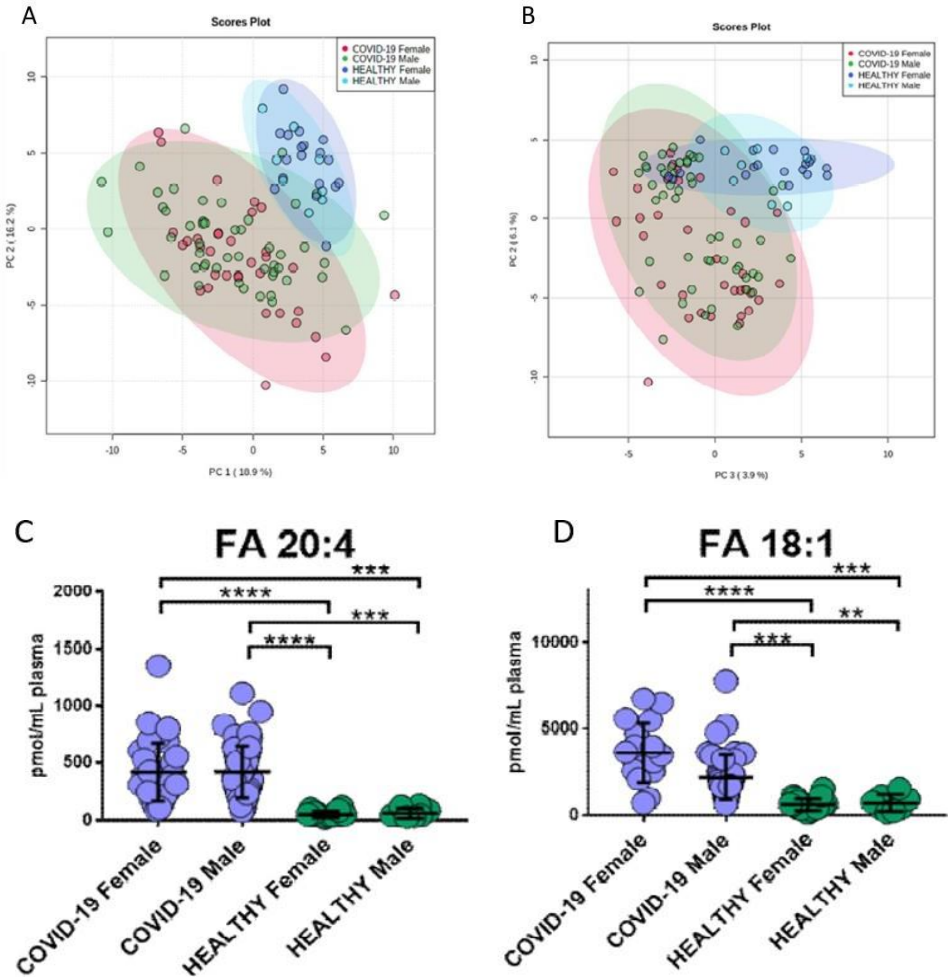


**Figure 12**: score plots from PCA indicating COVID-19 female patients (red dots), COVID-19 male patients (green dots), healthy female subjects (violet dots) and healthy male patients (blue dots). Lipidomic PCA was performed in positive (**A**) and negative (**B**) mode. Box-plots (average ± SD) of main circulating biomarkers FA 20:4 (**C**), FA 18:1 (**D**) with COVID-19 patients and healthy subjects divided for gender. *p*-value < 0.01 = **; *p*-value < 0.001 = ***; *p*-value < 0.0001 = ****

In the end, we wanted to investigate and validate the diagnostic performance of our lipid biomarkers by analyzing patients resulted negative to COVID-19 test, but with symptoms correlated to the SARS-CoV-2 infection (healthy + non-COVID-19 group).

The analysis confirmed the previous selected lipid biomarkers in detecting COVID-19 infection. PC 14:0_22:6, PC 16:1_22:6, and PE 18:1_20:4 showed AUC values of 0.89 (SE: 83%, SP: 84%), 0.89 (SE: 88%, SP: 80%), and 0.87 (SE: 83%, SP: 86%), respectively. The ROC curves for FA 20:4, FA 18:1, PE (O-18:2_20:4), and PE (O-16:1_18:2) were characterized by AUC values of 0.84 (SE: 74%, SP: 88%), 0.87 (SE: 81%, SP: 86%), 0.85 (SE: 83%, SP: 80%), and 0.82 (SE: 76%, SP: 81%), respectively (figure 13).

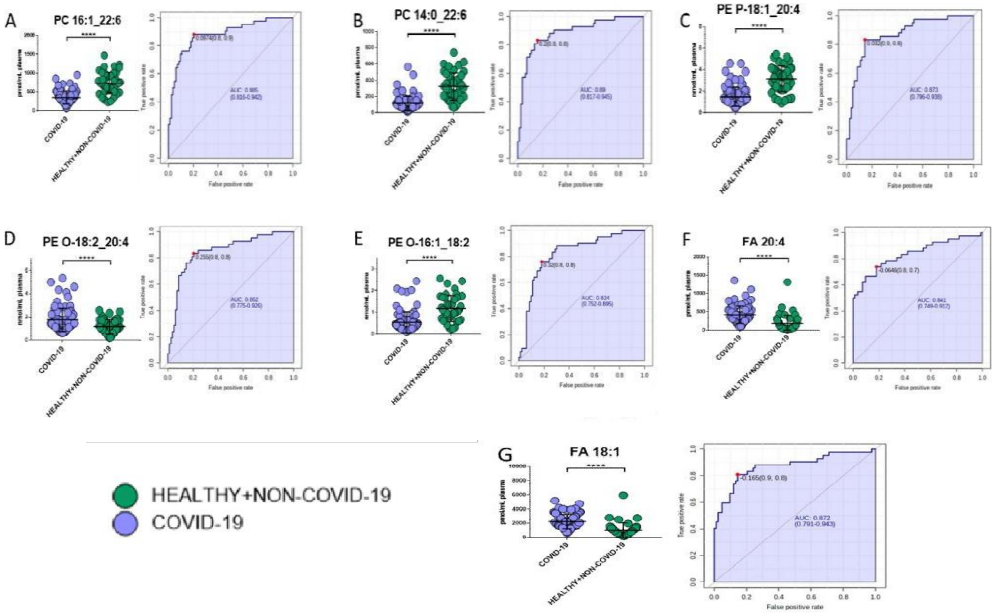


**Figure 13**: validation of selected potential lipid biomarkers including non-COVID-19 patients with similar symptoms as those with the COVID-19 infection. The figure reports the box-plots (average ± SD) and ROCs of PC 14:0_22:6 (**A**), PC 16:1_22:6 (**B**), PE 18:1_20:4 (**C**), PE (O-18:2_20:4) (**D**), PE (O-16:1_18:2) (**E**), FA 20:4 (**F**) and FA 18:1 (**G**).

## *PBMCs investigation results*

In order to understand the possible effects of SARS-CoV-2 infection on the immune system, we performed an untargeted lipidomic analysis of PBMCs isolated from plasma of COVID-19 patients and healthy subjects. From the untargeted analysis carried out both in positive and negative ionization, 251 lipids, belonging to 17 different lipid classes, were detected and putatively identified by the *in silico* library LipidBlast [46]. The most abundant detected class was PE with 43 lipids, representing 17% of total lipids, followed by TG, with 41 lipids (16%), and PC with 26 species (10%). The other classes (DG, NAE, Cer, FA, LPE, and PI) had a percentage of less than 10%. The classes with a percentage ≤ 5% were grouped under the name of OTHER and comprised CAR; CE; MG; LPC; LPI; SM; HexCer, and PS (figure 14). The untargeted analysis revealed for the very first time a heterogeneous profile of the lipid composition of the PBMCs.

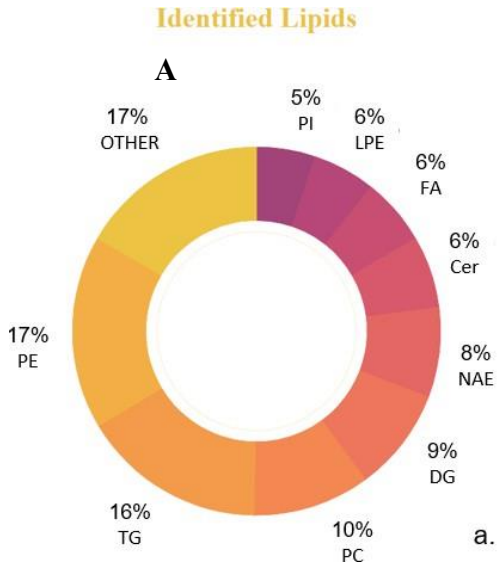


B

| Class | n° of lipids |
|---|---|
| CAR | 7 |
| CE | 1 |
| Cer | 16 |
| DG | 23 |
| FA | 15 |
| HexCer | 11 |
| LPC | 6 |
| LPE | 14 |
| LPI | 1 |
| MG | 3 |
| NAE | 20 |
| PC | 26 |
| PE | 43 |
| PI | 13 |
| PS | 1 |
| SM | 10 |
| | 41 |

b.

**Figure 14:** percentage of identified lipids per class (**A**); details of the number of lipids identified (**B**).
Legend: CAR acylcarnitine; CE cholesteryl ester; Cer ceramide; DG diacylglycerol; FA free fatty acids; HexCer glycosylceramides; LPC lysophophatidylcholine; LPE

lysophosphatidylethanolamine; LPI lysophosphatidylinositol; MG monoacylglycerol; NAE N-acyl ethanolamines; PC phosphatidylcholine; PE phosphatidylethanolamine; PI phosphatidylinositol; PS phosphatidylserine; SM sphingomyelin; TG triacylglycerol; OTHER: CAR; CE; MG; LPC; LPI; SM; HexCer; PS.

We used a mix of internal standards to correct the area under the peak of the chromatogram and to estimate the concentration of all lipids (expressed as μg/mL). The quality of the analysis was assessed by calculating the relative standard deviations (RSDs) of the standards spiked in the QC samples. For all of the standards a RSDs ≤ 20% was found (see table 3 in the "Materials and Methods" section at the end of chapter 2).

We then performed statistical analysis on MetaboAnalyst software comparing the healthy group with the COVID-19 group. The volcano plot in figure 18A highlighted the most relevant modulated lipids, while the PLS-DA score plot and the hierarchical heatmap showed a clear separation between the two groups (figure 15D and E).

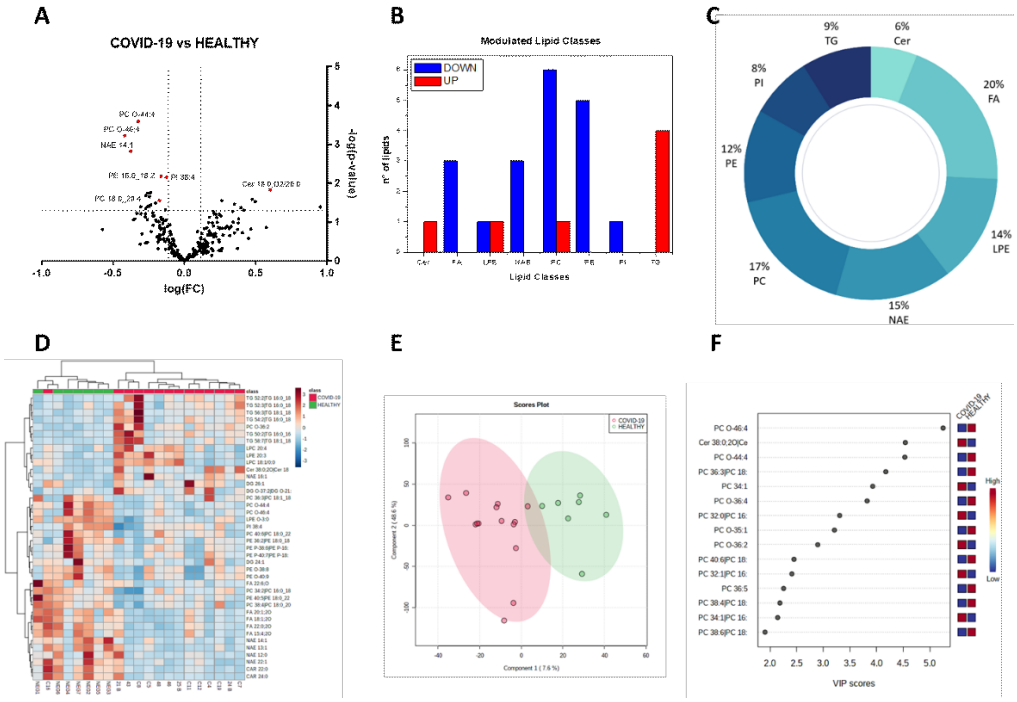


**Figure 15:** volcano plot (**A)**; histograms with number of modulated lipids per class (blue down and red up modulated) (**B**); percentage of modulated lipids per class (**C)**; hierarchical heatmap (**D**); PLS-DA (**E**) and VIP score (**F**). FC > 1.3, *p*-value ≤ 0.05

The comparison between the COVID-19 and the healthy groups showed a total of 27 modulated lipids, 19 decreased and 8 increased in the infected case, belonging to 8 different lipid classes: Cer, FA, LPE, NAE, PC, PE, PI, and TG. A complete list of the modulated lipids with related fold changes and *p*-values is reported in table 4 and in the "Materials and Methods" section. Interestingly, we found a down-modulation of glycerophospholipids (PCs, PEs and PIs) in the COVID-19 group (figure 18B.); other classes down-modulated were FA and NAE. The FA class had also the higher percentage of modulated lipids per class (20%) with FA 18:1;2O; FA 20:1;2O and FA 22:0;2O, followed by PC (17%), NAE (15%), LPE (14%) and PE (12%) (figure 18C.).

These findings suggested that SARS-CoV-2 infection may have a greater impact on fatty acid and glycerophospholipid classes. In detail, regarding glycerophospholipids, PC, PE, and PI, were characterized by a high number of carbon atoms, from 34 to 40, and all the modulated phospholipids presented from 2 to 9 unsaturations. For the ones annotated with acyl chain information, we can observe from 16 to 22 carbon atoms with 2, 1, or no unsaturation. Interestingly, some acyl chains were composed by C18:0, C18:1, C18:2 and C20:4, like PC 18:0_20:4, PC 16:0_18:2, PC 18:1_18:2 and PE 18:0_18:2 with a fold change of 0.667, 0.735, 0.553 and 0.687, respectively. The PI class had only one down-modulated lipid, namely PI 38:4, without information about the acyl chain and a FC of 0.747.

The only up-modulated lipids were Cers and TGs. Cer class was represented by only one lipid (Cer 18:0;2O/20:0, FC = 4.0) and constituted the 6% of the total lipids, while the TG class had 4 species, characterized by a high number of carbon atoms, 50 to 58, with a number of unsaturations variable from 2 to 7. Cer and TG classes were also the less modulated, together with PI, 6%, 9%, and 8%, respectively.

All these findings suggest that the virus infection impacts in different ways the lipidome of the PBMCs, affecting several lipid classes. In particular, the observed down-modulation of glycerophospholipids and the increase in the TG levels are consistent with the findings from the previous section *("SARS-CoV-2 infection impacts on the plasma lipidome of the host"*).

### *Plasma investigation discussion*

This work reports for the first time a complete profile of human plasma lipidome in a large cohort of COVID-19 patients and control group: a total of 161 Italian patients hospitalized in the Novara University Hospital, in northern Italy, the epicenter of COVID-19 spread, were enrolled for the study and subdivided in critical and non-critical COVID-19 (n = 103), critical and non-critical patients admitted to the intensive care unit with negative COVID-19 test (n = 32) and healthy subjects (n = 26).

Even if other studies already characterized the metabolomic profile of COVID-19 patients [11–13,19], the cohort enrolled was limited, without gender-specific analyses, and, in one case, a control group was composed by young people [11,13,19]. Furthermore the mean age of COVID-19 groups was 43 [13], 48 [12] and 56 [19] years, despite it is well know that elderly individuals have higher mortality rate [20].

Our study involved the largest cohort of patients infected with SARS-CoV-2 virus, with a mean age of 67 in the frailest group.

Our results highlighted an impairment in the lipidome of patients as a response to the infection. There were some differences in the lipid modulation compared to the mentioned studies, probably connected with the larger number of individuals involved, the higher average age and the patients' various geographical origins.

We have found that the virus directly or indirectly impacts on several host responses and plasma lipidome is one of them.

CARs, DGs, FAs, PCs, PEs, SMs and TGs were the most modulated lipids in non-critical COVID-19 patients. A general decrease of glycerophospholipids, that together with fatty acids such as arachidonic acid, have a significant role in HCoV-229E-infected cells, as shown in [21], was observed. Fatty acids were up-modulated in patients infected by the virus. This may be a

consequence of the defense mechanism of the host, but, at the same time, the higher levels of FAs may also cause inflammation. The inflammation caused by the infection of SARS-CoV-2 in the severe cases, lead indeed to a "cytokine storm", induced by arachidonic acid that modulates the cytokine production [22,23].

However, cytokines have also an active role in the defense mechanism against microorganisms responsible for respiratory diseases, inducing the release of unsaturated FAs [24].

Glycerophospholipids, particularly PCs, showed decreased levels in COVID-19 patients. A down-regulation of PCs linked to hepatic alterations in COVID-19 infection was already reported by previous studies [11,13]. Furthermore a down-modulation of PCs in human plasma has been also reported in sepsis, cancer and Dengue virus infection [25].

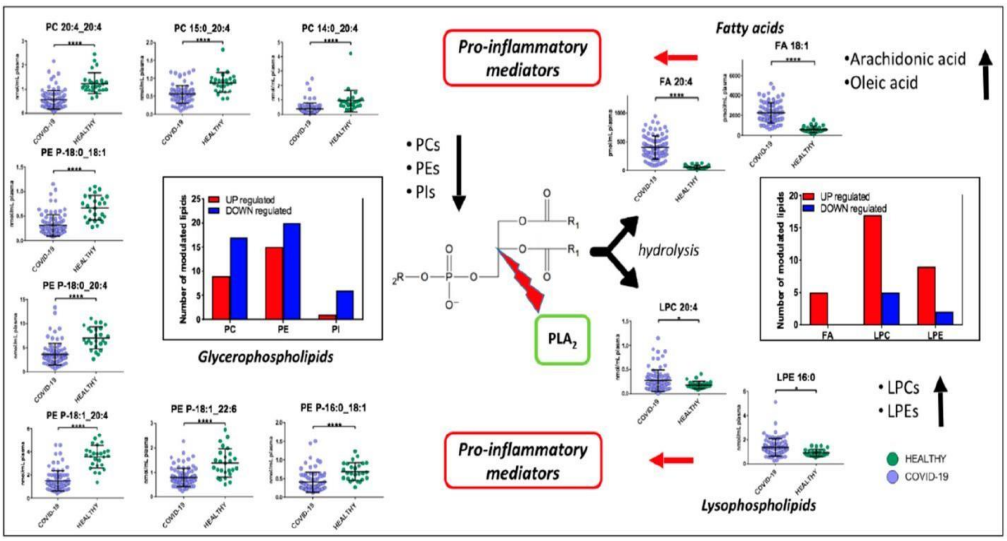


**Figure 16**: proposed mechanism involved in COVID-19 pathogenesis. PLA2 hydrolyze phospholipids to yield fatty acids and lysophospholipids. We found a down-regulation of glycerophospholipids (PCs, PEs and PIs) and up-regulation of lysophospholipids (LPCs and LPEs), arachidonic acid, and oleic acid. Fatty acids and lysophospholipids are pro-inflammatory mediators. ($p$-value < 0.05 = *; $p$-value < 0.0001 = ****).

In figure 16 it is possible to observe the detail of acyl chains of some of the modulated glycerophospholipids: PC 20:4_20:4, PC P-15:0_20:4, PC P-14:0_20:4, PE P-16:0_18:1, PE P-18:1_20:4, PE P-18:0_20:4, PE P-18:1_22:6, and PE P-18:0_18:1. These lipids are characterized by one acyl chain constituted by C20:4 or C18:1, arachidonic acid and oleic acid structure, respectively, which can generate prostaglandins, important in the inflammatory response [26]. It has been reported that some lipid mediators, like oleic acid, can be associated with the antiviral response in mouse models of influenza virus infection [27].

Other interesting glycerophospholipid classes in the context of inflammation are LPC and LPE classes.

An increase of these two classes can be associated with Dengue virus and COVID-19 infection [13,25]. LPCs in plasma are the product of the action of phospholipases A2 (PLA2), which remove one fatty acid from a PC [28]. Additionally, the increased levels of LPCs may be linked to their pro-inflammatory role in certain inflammatory states: in fact, LPCs are known to play a role in all stages of vascular inflammation as key homeostatic mediators.

LPC class is able to reduce the production of nitric oxide (NO) acting on the endothelium-dependent vasomotor regulation [29]. Furthermore, through boosting the expression of adhesion molecules such as intercellular adhesion molecule 1, vascular cell adhesion protein 1, and P-selectin, LPCs may directly contribute to immune cell infiltration during vascular inflammation [30], thanks to the production of monocyte chemoattractant protein, IL-8 and Chemokine ligand 5. Interestingly, LPC was found to act as a chemoattractant for previously mentioned molecules: monocytes [31]; T cells [32] and natural killer cells [33].

It was shown that LPCs can enhance T lymphocytes activation while having little effect on resting cells [34]. High levels of LPCs directly correlate with ROS production and chemokine receptor expression in human T cells [35]. Moreover, this lipid class seems to enhance IFN-secretion and gene expression in CD4+ and CD8+ [36].

In conclusion, research on monocytes and macrophages has shown that LPCs can activate macrophages, increase their phagocytic activity in the presence of T lymphocytes [37] and increase neutrophil oxidative burst and reactive oxygen generation [38].

Taken together the decrease of PCs, PEs and PIs and the increase of LPCs, LPE, FA 20:4 and FA 18:1, point out the role of PLA2 in the pathogenesis and progression of COVID-19 (figure 15). PLA2 catalyzes the hydrolysis of the sn-2 position of membrane glycerophospholipids in order to release FA 20:4 and, consequently, produce lysophospholipids. This is the rate-limiting step of arachidonate metabolism that brings as final products bioactive molecules such as prostaglandins and lysophospholipids [39]. It seems that PLA2 is strongly involved in the replication of coronavirus, by producing lysophospholipids, required to form the specialized membrane compartments in which viral RNA synthesis takes place [40].

Our study provides further evidence for considering PLA2 activation as a potential key factor in the pathogenesis of COVID-19 and a potential therapeutic target.

In infected patients higher levels of CARs have been found; these lipids are secreted by mitochondria, and it has already been observed that CARs characterized by long-chain can accumulate at the air-fluid interface when metabolism is inhibited. This accumulation can represent a risk factor for patients with dysfunctional FAO [41]. Furthermore, viruses that impact on the respiratory system, like the influenza one, can aggravate CAR accumulation.

For this reason, we suppose that the higher levels of acylcarnitines in plasma samples from COVID-19 patients may be linked to this mechanism.

An accumulation of amphiphilic long-chain CARs can lead to a toxicity condition, by inhibition of ion channels, disruption of calcium signaling and an alteration of ATP [42].

Other up-modulated lipids in the COVID-19 group were the TGs. Higher levels of these neutral lipids may suggest an increase in adipose tissue lipolysis in patients infected by the virus, confirmed also by the higher levels of free fatty acids, indicating a role of adipose tissue in the circulating lipid profile [18]. Modulated TGs were characterized by long fatty acid chains, composed of an average of 54 carbons, with an average of 5 unsaturations. Thanks to pathway analysis we confirmed a modulation of the glycerophospholipid metabolism pathway in patients affected by SARS-CoV-2 infection, also found by Wu et al [11].

In the same way, our results showed an increase of FA 18:1 and FA 18:2 in the COVID-19 group and it was already observed that an increase of free fatty acids with 18 carbons in serum was associated with the development of acute respiratory distress syndrome [43].

The up-modulation of TGs was maintained also in the critical group (ICU COVID-19) when compared to the non-critical one and showed a direct correlation between TG levels and severity of the disease. Glycerophosphocholines down-regulation was also confirmed.

We found decreased levels of SMs in critical patients, as already shown in COVID-19 patients [13]. This lipid class, together with glycerophospholipids, constitutes membrane cells and can modulate some processes, like growth regulation and inflammatory responses [10]. Virus entry and infection seem to be hindered by low levels of SMs [44] and for this reason SM metabolism

could be a promising target for therapeutic intervention against COVID-19 infection.

As the last step of our work, we investigated some modulated lipids in order to find possible biomarkers for COVID-19 infection. The lipids with the best AUC values were FA 20:4 and FA 18:1, with 0.99 and 0.98 respectively, in the comparison between healthy subjects and COVID-19patients. Unfortunately, by adding non-COVID-19 patients to the healthy group the AUC decreased: 0.87 and 0.84 respectively.

Even if the AUC values are such promising, and these two fatty acids seem to directly correlate to the severity of the disease (figure 17), fatty acids cannot be considered as good biomarkers because an increase of these lipids has already been reported in several studies [15]. Also, FA 18:1 and FA 20:4 are not able to discriminate between COVID-19 and ICU non-COVID-19 patients.

Analyzing non-COVID-19 patients with similar symptoms to COVID-19 patients confirmed the previously lipid biomarkers found, suggesting that our lipid candidates are directly linked to the host response to the virus.

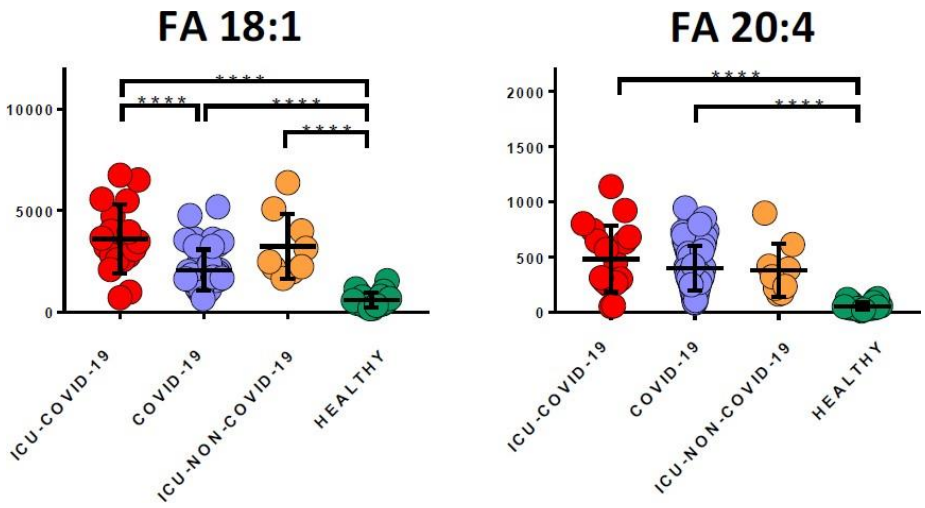


**Figure 17**: bar plots (average ± SD) of FA 18:1 (left) and FA 20:4 (right) in healthy subjects, non-critical and severe COVID-19 patients and in critical non-COVID-19 patients.

The best lipid candidates are following reported: PC 14:0_22:6 (AUC = 0.96), PC 16:1_22:6 (AUC = 0.97), and PE 18:1_20:4 (AUC = 0.94). Our study demonstrated that COVID-19 infection heavily impacts on plasma lipids.

The main results from our findings highlights the involvement of PLA2 in the SARS-CoV-2 pathogenesis, which can be used as a possible candidate for antiviral drug development. Further studies should be carried out in order to focus on the levels and activity of PLA2.

Mostly, in this work we present the first lipidomic study that aims to elucidate the SARS-CoV-2 impact on metabolism. Furthermore, this is the largest untargeted LC-MS/MS study in literature involving COVID-19 patients with a mean age higher than the control groups.

### *PBMCs investigation discussion*

To date, a global lipidomic study on peripheral blood mononuclear cells is still missing. Indeed, a previous work [45] already focused on SARS-CoV-2 infection of PBMCs both *in vivo* and *in vitro*, but without bringing attention to the lipids involved in the replication of the virus.

Thus, in this preliminary study, we aimed to understand the influence of SARS-CoV-2 virus infection on the lipidome of peripheral blood mononuclear cells of hospitalized patients with a positive SARS-CoV-2 test. For the first time, an in-deep investigation of the changes of lipids belonging to different classes in PBMCs after virus infection was performed.

The down-regulation of glycerophospholipids (PCs, PEs, and PIs) in the COVID-19 group suggests that the SARS-CoV-2 may have a great impact on the composition of membrane lipids. Furthermore, these results are in line with the decreased levels of glycerophospholipids already observed in the plasma of patients affected by the virus and reported in the previous section. Currently, in literature no studies about the effect of SARS-CoV-2 on the lipid composition of PBMCs exist, so we hypothesized that viral infection could modulate the membrane structure of the host cells.

It is known that PCs and PEs are important lipids for the structure of the cell membrane and constitute the most abundant lipids in the outer and in the inner leaflet respectively [47].

Alterations of the membrane composition and fluidity were described as the main biological processes responsible for microdomain generation, able to affect the dynamic roles of the membrane, as signal transduction and immune activation processes. PCs also prevent membrane leakage to abolish hepatocyte injury and, subsequently, lobular inflammation and liver fibrosis [48].

Even if only one ceramide (Cer 18:0;2O/20:0) was modulated, it is interesting to note the accumulation of this lipid in the infected patients since that the accumulation of ceramides with long chains has been previously associated with deleterious outcomes [49]. Ceramides are membrane lipids with a cone-shaped conformation that is the result of their small hydroxyl head groups. The hexagonal structure adopted by these lipids promotes the aggregation and fusion of the ceramides present in the lipid rafts. Thanks to these domains, a negative curvature of the membrane is favored [50,51].

It is well known that lipid rafts are relevant for facilitating the entry of numerous viruses, including SARS-CoV-2, into host cells [52]. Ceramides belong to the sphingolipid family, known as essential constituents of organelle and cell membranes that play an additional role in signal transductions of crucial physiological processes such as growth, differentiation, proliferation, migration, apoptosis, and cell death.

Finally, an increase in ceramide levels leads to an activation of sPLA2, enzyme for which a potential role in the pathogenesis of COVID-19 had already been assessed in plasma samples, as reported in the previous section. In one study [53] it has been in fact demonstrated that adding ceramides to the cellular substrate provokes an increase in the activity of the sPLA2.

Another interesting class is the PI. Accordingly to researchers [54], PIs seem to be able to neutralize respiratory syncytial virus (RSV). One proposed mechanism by which PIs disrupt RSV-elicited proinflammatory signaling is by direct interaction with the virus. PIs bind to RSV with high affinity in a concentration-dependent and saturable reaction. The high-affinity interaction of phosphoinositols with the virus blocks the attachment of the second one to the epithelial cell plasma membrane preventing infection. In our case, a down-regulation of PI 38:4, the only one modulated PI, may suggest the absence of this preventing action, thus leading to SARS-CoV-2 infection.

These preliminary findings suggest that the viral infection of PBMCs leads to an alteration of the lipid profile, even if not so well marked as the modulation observed in plasma samples of COVID-19 patients. Moreover, we found similitudes with the results discussed in the previous section, like the decrease of some species of PCs and PEs and the involvement of sPLA2 activity in COVI-19 pathogenesis

## *Conclusion of chapter 2*

In this chapter, two case studies in which lipidomics has been applied to the study of the host response to viral infection were reported. This kind of investigation became necessary due to the spread in December 2019 of SARS-CoV-2, which effects on host lipidome remain largely unclear.

The first study focused on the analysis of plasma samples from a large cohort of patients, composed by 161 subjects, subdivided in COVID-19 ($n$ = 103) and non-COVID-19 ($n$ = 58) groups. The main findings revealed a number of processes and pathways involved in the host response to SARS-CoV-2, as well as several promising biomarkers and therapeutic targets. Furthermore, it was observed an increase of fatty acids in patients infected by the virus. This finding may be a consequence of the defense mechanism of the host, but, at the same time, the higher levels of FAs may also cause inflammation. In addition, it was highlighted that gender has no influence on the disease severity: no gender differences were found in the main circulating biomarkers.

The large untargeted lipidomic analysis of plasma highlighted the involvement of the immune system. In order to deepen our knowledge about SARS-CoV-2 infection, a global lipidomic study on peripheral blood mononuclear cells was performed. Even if this research was just a preliminary study, with a limited number of samples (14 patients in COVID-19 group, and 7 healthy subjects), lipidomics performed on PBMCs samples of COVID-19 patients interestingly pointed out some similarities with the study of plasma lipidome, like the decreased levels of some glycerophospholipids species (PCs, PEs, and PIs).

At the cellular level, we found a significant modulation of lipids involved in membrane structure and all our findings suggest a membrane remodeling,

favored by some lipid classes such as ceramides, enhancing the entry of the virus into host cells.

It will be interesting to perform a large scale lipidomic analysis also on PBMCs in order to have a representative vision of the host response to viral infection from SARS-CoV-2 at the cellular level.

# *Materials and Methods*

## *Reagents*

For the analysis LC-MS-grade solvents and reagents were used. Formic acid, ammonium formate, tert-Butyl methyl ether (MTBE) and toluene were from Merck (Darmstad, Germany), water ($H_2O$) and acetonitrile (ACN) were from VWR (Milano, Italy) and methanol (MeOH) and isopropanol (IPA) were from Scharlab (Barcelona, Spain). As internal standards for lipidomics analysis we employed the SPLASH Lipidomix® [PC 15:0-18:1(d7); PE 15:0-18:1(d7); PS 15:0-18:1(d7); PG 15:0-18:1(d7); PG 15:0-18:1(d7); PA 15:0-18:1(d7); LysoPC 18:1(d7); LysoPE 18:1(d7); Chol Ester 18:1 (d7); 18:1(d7) MG; DG 15:0-18:1(d7); TG 15:0-18:1(d7)-15:0; SM 18:1(d9); Cholesterol (d7)] and 12-[[(cyclohexylamino)carbonyl]amino]-dodecanoic acid (CUDA) (Cayman Chemicals, Ann Arbor, Michigan, USA).

## *PBMC cells preparation for Lipidomic analysis*

Cells were extracted using a solution 75:15 IPA/$H_2O$, after the addition of 100 µL of MeOH 5% deuterated standard (Splash Lipidomix®). Then the samples were vortexed for 30 s, sonicated for 2 min and vortexed again for 30s and then they were incubated for 30 min at 4 °C, under a gently, constant shaking. Another 30 minutes were used to keep the sample rest in ice. To remove debris and other impurities, the samples were centrifuged for 10 min at3500 g at 4 °C. 1 mL of surnatant was collected and dried usind a SpeedVac. The dried samples were reconstituted in 100 µL of MeOH containing the internal standard CUDA (12.5 ng/mL).

## *Plasma preparation for Lipidomic analysis*

Lipids extraction from plasma samples was carried out using a biphasic method (modified Matyash, [55]). In detail: 30 µL of plasma were placed in a

1.5 Eppendorf tube and extracted with 225 µL of cold MeOH, containing a mixture of deuterated standard (Splash Lipidomix®) at the concentration provided by the manufacturer. The solution was vortexed for 10 s, and 750 µL of cold MTBE was added, then vortexed for another 10 s. The Eppendorf tube is then placed in a thermomixer (Eppendorf ThermoMixer® C) at 4°C and letting shaking for 6 min at 2000 rpm.

188 µL of water was added in order to enhance phase separation, then the samples is centrifuged for 2 min at 14000 rpm at 4 °C. 300 µL of surnatant was collected and evaporated using a SpeedVac (ScanVaccoolsafeLaboGene®). The dried sample was preserved at -80 °C until the analysis. 50 µL of a solution MeOH/tol 9:1 containing the internal standard CUDA (12.5 ng/mL) was use to reconstitute the sample.

### *LC-MS/MS analysis lipids*

For the analysis of the reconstituted lipids a UHPLC Vanquish system (Thermo Scientific, Rodano, Italy) coupled with an Orbitrap Q-Exactive Plus (Thermo Scientific, Rodano, Italy) was used. A reverse phase column was used for the separation of lipids (Accucore™ RP-MS 100 x 2.1 mm, particle size 2.6 µm), the column was maintained at 45 °C at a flow rate of 0.260 mL/min. The analysis were performed both in positive and in negative mode and the same mobile phases were used with the exception for the modifiers: mobile phase A consisted of acetonitrile/water 60:40 (v/v) while B was isopropanol/acetonitrile 90:10 (v/v) both modified with ammonium formate (10 mM) and 0.1% formic acid for positive mode, while in the negative ESI mode ammonium formate was replaced with ammonium acetate (10 mM). Following the details of the chromatographic run: 0–2 min from 30% to 43% B, 2–2.1 min from 43% to 55% B, 2.1–12 min from 55% to 65% B, 12–18

min from 65% to 85% B, 18–20 min from 85% to 100% B; 20-25 min 100% B was kept, then the gradient return to the initial proportions until 30 minutes. The HESI source voltage was maintained at 3.5 kV in the positive ion mode and 2.8 kV in the negative one. All other interface settings were identical for the two types of analysis. Capillary temperature: 320 °C, sheath gas flow 40 arb, auxiliary gas flow 3 arb, and S-lens:50 rf. A data-dependent (ddMS2) top 10 scan mode was used for all the acquisition. Survey full-scan MS spectra (mass range m/z 80 to 1200) were acquired with resolution R = 70,000 and AGC target 1x106. MS/MS fragmentation was performed using high-energy c-trap dissociation (HCD) with resolution R = 17,500 and AGC target 1x105. The stepped normalized collision energy (NCE) was set to 15, 30, and 45. The injection volume was 3 µL. Background ions were excluded from the fragmentation events thanks the use of an exclusion list, generated analyzing the same procedural blank sample, both for the positive and negative ESI mode.

## *Lipidomic Data Processing*

The acquired raw data from the ddMS2 analysis were processed using MS-DIAL software (Yokohama City, Kanagawa, Japan), v. 4.24 [17]. Detection of peaks, deconvolution of MS2 data, compound identification, and the alignment of peaks through all the samples was all automatized. For the identification a cut off value of 85% was selected. For the reproducibility evaluation of internal standards all the files were imported in Skyline program. Dataset containing m/z values, retention time, peak area, and annotation from the aligned files were exported as a txt file and manually checked in order to eliminate signals from blanks or wrong records. For quantification purpose, the peak area for different detected molecular species for each particular lipid was combined (e.g., [M + NH4]+& [M + Na]+ for TG) followed by

normalization using the deuterated internal standard for each lipid class or the standard having the closer retention time. In order to obtain an estimated concentration expressed in nmol/mL (plasma) the normalized areas were multiplied by the concentration of the internal standard. An in-house library of standards was also used for lipids identification.

Statistical analysis were performed with MetaboAnalyst 4.0 software (www.metaboanalyst.org).

## *Quality control of lipidomics analysis*

Retention time stability mass accuracy and intensity are key player in LC-MS based lipidomics. Quality control was assured by: analyzing pooled samples at the beginning and at the end of the batch; injecting blanks to check for residual interference; by using internal standards, directly in the plasma samples, that cover a number of analyte classes at appropriate levels for biological matrices (Avanti SPLASH Lipidomix) and an internal standard (CUDA) before the LC-MS analysis, in order to evaluate instrument performances.For PBMCs analysis the pool sample wasobtained by mixing 10 µL of each resuspendedsample. While for plasma analysis the pool sample was obtained by mixing 10 µL of each plasma sample.

Since the analysis were performed over a long time period, the pool samples were made using plasma from subjects not included in this study since we wanted to preserve the quality of patients' samples and avoid unnecessary freeze thaw cycles. Instrument variability was determined by calculating the coefficient of variation percentage (CV%) of internal standards in each sample and in the pooled quality control samples.

## *List of tables*

**Table 2**: list of modulated lipids with fold change and *p*-value of the comparison of COVID-19 group vs healthy subjects in the study of SARS-CoV-2 effects on plasma.

| Name | FC | p-value | | Name | FC | p-value |
|---|---|---|---|---|---|---|
| CAR 10:0 | 2.02E+00 | 1.90E-02 | | DG 52:1 DG 34:0_18:1 | 1.73E-01 | 1.05E-13 |
| CAR 10:1 | 1.91E+00 | 7.80E-03 | | DG 52:2 DG 16:0_36:2 | 3.11E-01 | 1.46E-06 |
| CAR 11:1 | 1.83E+00 | 2.79E-03 | | LPC 16:0/0:0 | 1.67E+00 | 8.38E-06 |
| CAR 12:0 | 1.88E+00 | 7.32E-03 | | LPC 18:0 | 1.80E+00 | 1.29E-02 |
| CAR 14:0 | 3.00E+00 | 5.28E-07 | | LPC 18:2/0:0 | 4.34E-01 | 8.27E-12 |
| CAR 14:1 | 2.68E+00 | 8.09E-04 | | LPC 18:3/0:0 | 2.04E+00 | 2.74E-06 |
| CAR 14:2 | 2.54E+00 | 7.44E-03 | | LPC 19:1/0:0 | 1.66E+00 | 1.99E-03 |
| CAR 16:0 | 2.66E+00 | 1.85E-07 | | LPC 20:1/0:0 | 1.86E+00 | 2.01E-07 |
| CAR 16:1 | 4.77E+00 | 2.25E-08 | | LPC 20:4 | 1.59E+00 | 2.09E-02 |
| CAR 18:0 | 2.11E+00 | 2.13E-06 | | LPC 22:4/0:0 | 1.91E+00 | 4.31E-05 |
| CAR 18:1 | 3.89E+00 | 1.23E-05 | | LPC 22:5/0:0 | 1.60E+00 | 2.24E-03 |
| CAR 18:2 | 3.11E+00 | 8.63E-04 | | LPC 22:6 | 2.03E+00 | 5.16E-03 |
| CAR 20:1 | 6.12E+00 | 1.98E-07 | | LPC 22:6/0:0 | 1.55E+00 | 2.28E-02 |
| CAR 20:2 | 5.38E+00 | 8.16E-04 | | LPC 24:0/0:0 | 5.51E-01 | 3.81E-07 |
| CAR 20:3 | 2.45E+00 | 2.81E-02 | | LPC O-16:0 | 1.97E+00 | 3.72E-06 |
| CAR 20:4 | 5.94E+00 | 2.19E-04 | | LPC O-18:0 | 1.90E+00 | 8.07E-05 |
| CAR 8:0 | 2.01E+00 | 2.82E-02 | | LPC O-18:1 | 3.00E+00 | 3.78E-11 |
| CAR 8:1 | 1.63E+00 | 4.81E-04 | | LPC O-18:2 | 1.51E+00 | 2.99E-03 |
| CE 18:3 | 5.98E-01 | 6.21E-04 | | LPE 16:0 | 1.63E+00 | 1.60E-05 |
| CE 24:6 | 3.43E+00 | 1.44E-03 | | LPE 18:0 | 1.70E+00 | 2.22E-05 |
| CE 26:6 | 2.42E+00 | 1.81E-04 | | LPE 18:2 | 6.23E-01 | 8.83E-03 |
| DG 17:0 | 2.74E-01 | 4.27E-06 | | LPE 20:4 | 1.63E+00 | 2.46E-02 |
| DG 24:3 | 2.55E-01 | 4.39E-10 | | LPE 20:5 | 6.41E-01 | 2.87E-02 |
| DG 25:0 | 5.10E-01 | 1.10E-02 | | LPE 22:4 | 2.09E+00 | 3.22E-02 |
| DG 25:1 | 4.26E-01 | 1.46E-02 | | LPE 22:5 | 2.61E+00 | 2.10E-03 |
| DG 26:1 | 4.79E-01 | 2.00E-02 | | LPE 22:6 | 2.40E+00 | 2.70E-04 |
| DG 30:6 | 2.65E-01 | 3.71E-11 | | LPE O-16:1 | 1.84E+00 | 1.58E-04 |
| DG 31:3 | 4.72E-01 | 4.00E-02 | | LPE O-18:1 | 1.64E+00 | 3.10E-03 |
| DG 34:2 | 7.97E+00 | 2.77E-06 | | LPE O-18:2 | 2.40E+00 | 4.69E-06 |
| DG 36:1 DG 18:0_18:1 | 5.64E-01 | 9.28E-03 | | MG 15:1 | 1.66E+00 | 1.19E-04 |
| DG 36:2 DG 18:1_18:1 | 5.97E-01 | 2.95E-05 | | NAE 18:1 | 1.83E+00 | 1.26E-06 |
| DG 36:3 DG 18:1_18:2 | 5.59E-01 | 5.12E-07 | | NAE 18:2 | 1.57E+00 | 1.34E-04 |
| DG 36:4 DG 18:2_18:2 | 6.23E-01 | 1.35E-02 | | NAE 20:2 | 1.60E+00 | 8.10E-05 |
| DG 38:10 | 3.07E-01 | 1.12E-08 | | NAE 22:4 | 2.02E+00 | 2.41E-05 |
| DG 38:2 | 2.64E-01 | 1.05E-07 | | NAE 22:5 | 2.26E+00 | 2.83E-06 |
| DG 38:3 | 1.61E-01 | 1.61E-11 | | PC 30:0 | 1.89E+00 | 2.21E-02 |
| DG 38:5 DG 18:1_20:4 | 4.95E-01 | 1.09E-06 | | PC 32:0 PC 16:0_16:0 | 1.71E+00 | 6.04E-07 |
| DG 38:6 DG 18:2_20:4 | 5.44E-01 | 2.20E-03 | | PC 32:1 | 2.39E+00 | 6.94E-04 |
| DG 40:2 | 4.39E-01 | 1.03E-07 | | PC 32:2PC 14:0_18:2 | 3.95E-01 | 7.47E-15 |
| DG 40:3 | 2.12E-01 | 6.38E-09 | | PC 34:3 PC 16:1_18:2 | 5.72E-01 | 1.56E-10 |
| DG 40:4 | 2.53E-01 | 2.09E-07 | | PC 34:4 PC 14:0_20:4 | 4.12E-01 | 5.88E-08 |
| DG 40:5 | 1.83E-01 | 8.82E-06 | | PC 35:4 | 2.74E+00 | 1.00E-06 |
| DG 40:6 | 5.52E-01 | 8.45E-03 | | PC 35:4 PC 15:0_20:4 | 6.61E-01 | 1.17E-07 |
| DG 40:6 DG 16:0_24:6 | 4.27E-01 | 2.51E-04 | | PC 36:4 | 1.73E+00 | 3.90E-05 |
| DG 41:5 | 1.12E-01 | 3.35E-13 | | PC 36:5 PC 16:0_20:5 | 5.61E-01 | 4.78E-06 |
| DG 42:11 DG 20:5_22:6 | 9.96E-02 | 2.21E-14 | | PC 36:6 PC 14:0_22:6 | 3.05E-01 | 3.15E-17 |
| DG 44:6 DG 18:0_26:6 | 5.25E-01 | 1.53E-02 | | PC 37:2 PC 19:0_18:2 | 6.45E-01 | 5.15E-07 |
| DG 50:1 DG 16:0_34:1 | 1.94E-01 | 9.96E-14 | | PC 38:2 PC 18:0_20:2 | 6.66E-01 | 1.77E-05 |

| | | | | | | |
|---|---|---|---|---|---|---|
| PC 38:3 PC 18:0_20:3 | 6.62E-01 | 6.86E-06 | | SM 34:0 3O | 3.93E-01 | 4.05E-05 |
| PC 38:7 PC 16:1_22:6 | 4.43E-01 | 1.10E-16 | | SM 34:1 2O | 2.05E+00 | 1.32E-06 |
| PC 39:7 PC 17:1_22:6 | 1.51E+00 | 2.60E-03 | | SM 34:7 3O | 2.60E+00 | 3.57E-08 |
| PC 40:5 | 1.58E+00 | 1.05E-04 | | SM 36:1 3O | 1.88E+00 | 3.46E-02 |
| PC 40:6 | 1.61E+00 | 4.08E-04 | | SM 36:2 2O | 2.72E+00 | 4.46E-05 |
| PC 40:8 PC 20:4_20:4 | 4.82E-01 | 7.22E-10 | | SM 36:3 2O SM 18:1 2O/18:2 | 6.08E-01 | 1.03E-02 |
| PC 42:9 | 5.07E-01 | 3.00E-06 | | SM 37:2 2O SM 18:1 2O/19:1 | 6.59E-01 | 2.44E-02 |
| PC O-34:2 | 5.56E-01 | 1.37E-08 | | SM 38:1 2O SM 16:1 2O/22:0 | 5.09E-01 | 4.94E-03 |
| PC O-36:6 | 6.41E-01 | 7.97E-03 | | SM 38:1 3O | 1.75E+00 | 1.83E-02 |
| PC O-42:10 | 2.57E+00 | 4.95E-04 | | SM 38:2 2O | 1.73E+00 | 3.82E-03 |
| PC O-46:4 | 6.27E-01 | 1.18E-04 | | SM 38:2 2O SM 18:2 2O/20:0 | 6.42E-01 | 1.24E-02 |
| PE 34:1 PE 16:0_18:1 | 1.94E+00 | 3.43E-04 | | SM 39:1 2O SM 17:1 2O/22:0 | 4.09E-01 | 8.87E-04 |
| PE 36:2 PE 18:0_18:2 | 5.33E-01 | 1.68E-14 | | SM 39:2 2O SM 18:2 2O/21:0 | 5.63E-01 | 6.83E-03 |
| PE 36:4 | 2.15E+00 | 1.42E-06 | | SM 40:1 2O SM 18:1 2O/22:0 | 5.12E-01 | 5.10E-03 |
| PE 37:6 | 1.67E+00 | 2.01E-03 | | SM 40:2 2O SM 18:2 2O/22:0 | 5.44E-01 | 6.28E-03 |
| PE 38:5 | 2.15E+00 | 3.28E-05 | | SM 41:1 2O SM 18:1 2O/23:0 | 4.88E-01 | 1.62E-03 |
| PE 38:6 | 2.44E+00 | 2.00E-06 | | SM 41:2 2O SM 17:1 2O/24:1 | 5.59E-01 | 7.89E-03 |
| PE 38:6 PE 16:0_22:6 | 1.91E+00 | 1.17E-04 | | SM 41:2;3O | 4.76E-01 | 1.57E-04 |
| PE 40:6 PE 18:0_22:6 | 1.97E+00 | 1.20E-05 | | SM 41:3;3O | 4.68E-01 | 1.40E-04 |
| PE 40:7 | 3.66E+00 | 6.58E-06 | | SM 41:8;2O | 4.54E-01 | 1.28E-05 |
| PE P-34:1 PE P-16:0_18:1 | 6.27E-01 | 4.54E-06 | | SM 42:4;2O | 2.31E+00 | 1.72E-04 |
| PE P-34:2 PE P-16:0_18:2 | 3.43E-01 | 2.59E-13 | | SM 44:9;3O | 1.62E+00 | 8.66E-03 |
| PE P-36:1 PE P-18:0_18:1 | 4.96E-01 | 4.52E-10 | | TG 36:3\|TG 8:0_10:0_18:3 | 7.30E+00 | 2.01E-04 |
| PE P-36:2 PE P-18:0_18:2 | 3.66E-01 | 1.23E-13 | | TG 42:0\|TG 12:0_14:0_16:0 | 3.27E-01 | 3.52E-02 |
| PE P-38:2 PE P-20:0_18:2 | 3.38E-01 | 4.76E-14 | | TG 42:3\|TG 8:0_16:1_18:2 | 1.73E+00 | 4.94E-04 |
| PE P-38:4 PE P-18:0_20:4 | 5.71E-01 | 9.45E-08 | | TG 43:0\|TG 12:0_15:0_16:0 | 5.62E-01 | 1.76E-03 |
| PE P-38:5 PE P-18:1_20:4 | 4.53E-01 | 1.90E-15 | | TG 44:0\|TG 10:0_16:0_18:0 | 2.98E-01 | 1.77E-06 |
| PE P-38:6 PE P-16:0_22:6 | 6.05E-01 | 6.29E-09 | | TG 44:1\|TG 10:0_16:0_18:1 | 4.26E-01 | 3.12E-03 |
| PE P-40:5 PE P-18:0_22:5 | 6.27E-01 | 3.13E-06 | | TG 46:0\|TG 12:0_16:0_18:0 | 5.23E-01 | 5.62E-06 |
| PE P-40:5 PE P-20:0_20:5 | 6.62E-01 | 7.62E-05 | | TG 46:0\|TG 14:0_16:0_16:0 | 4.84E-01 | 5.18E-05 |
| PE P-40:6 PE P-18:0_22:6 | 5.64E-01 | 1.39E-08 | | TG 46:1\|TG 14:0_16:0_16:1 | 4.43E-01 | 1.30E-04 |
| PE P-40:7 PE P-18:1_22:6 | 6.03E-01 | 7.36E-07 | | TG 46:2\|TG 12:0_16:1_18:1 | 5.13E-01 | 4.07E-03 |
| PI 32:1 | 6.21E-01 | 1.06E-02 | | TG 48:3\|TG 14:0_16:1_18:2 | 5.95E-01 | 4.73E-03 |
| PI 36:1 | 6.51E-01 | 1.03E-02 | | TG 51:1\|TG 16:0_17:0_18:1 | 1.60E+00 | 9.86E-04 |
| PI 36:3 | 3.90E-01 | 1.44E-03 | | TG 51:2\|TG 16:0_17:1_18:1 | 1.62E+00 | 3.80E-04 |
| PI 38:3 | 6.47E-01 | 7.19E-03 | | TG 51:2\|TG 17:0_16:1_18:1 | 1.66E+00 | 4.76E-08 |
| PI 40:4 | 3.72E-01 | 1.97E-04 | | TG 51:3\|TG 15:0_18:1_18:2 | 1.54E+00 | 1.82E-04 |
| SM 28:1 2O SM 18:1 2O/10:0 | 4.87E-01 | 2.54E-04 | | TG 52:2\|TG 16:0_18:1_18:1 | 1.69E+00 | 9.27E-10 |
| SM 30:1 2O SM 16:1 2O/14:0 | 4.25E-01 | 3.30E-04 | | TG 52:3\|TG 16:0_18:1_18:2 | 1.65E+00 | 8.75E-10 |
| SM 31:1 2O SM 17:1 2O/14:0 | 2.69E-01 | 4.25E-04 | | TG 52:4\|TG 16:1_18:1_18:2 | 1.54E+00 | 4.22E-04 |
| SM 32:0 2O | 4.73E-01 | 4.13E-03 | | TG 52:6\|TG 16:1_18:2_18:3 | 1.66E+00 | 4.44E-08 |
| SM 32:1 2O | 5.92E-01 | 1.38E-02 | | TG 53:2\|TG 16:0_18:1_19:1 | 1.94E+00 | 5.41E-13 |
| SM 32:1 2O SM 16:1 2O/16:0 | 5.95E-01 | 1.47E-02 | | TG 53:3\|TG 17:0_18:1_18:2 | 1.78E+00 | 3.31E-06 |
| SM 32:1 3O | 3.80E-01 | 2.29E-03 | | TG 53:4\|TG 17:1_18:1_18:2 | 1.50E+00 | 9.68E-04 |
| SM 32:5 2O | 2.41E+00 | 1.21E-02 | | TG 54:2\|TG 16:0_18:1_20:1 | 1.75E+00 | 1.06E-10 |
| SM 33:1 2O SM 17:1 2O/16:0 | 6.63E-01 | 4.63E-02 | | TG 54:2\|TG 18:0_18:1_18:1 | 1.67E+00 | 1.39E-04 |
| SM 33:2 2O SM 17:2 2O/16:0 | 4.08E-01 | 2.93E-03 | | TG 54:3\|TG 18:0_18:1_18:2 | 1.63E+00 | 2.39E-05 |
| SM 34:0 2O | 1.87E+00 | 4.84E-05 | | TG 54:4\|TG 16:0_18:1_20:3 | 1.55E+00 | 1.09E-08 |

| | | | | | | |
|---|---|---|---|---|---|---|
| TG 54:4\|TG 18:1_18:1_18:2 | 1.58E+00 | 1.48E-04 | | SM 34:0 3O | 3.93E-01 | 4.05E-05 |
| TG 54:5\|TG 16:0_18:1_20:4 | 1.66E+00 | 6.34E-08 | | SM 34:1 2O | 2.05E+00 | 1.32E-06 |
| TG 54:5\|TG 18:1_18:2_18:2 | 1.57E+00 | 1.45E-02 | | SM 34:7 3O | 2.60E+00 | 3.57E-08 |
| TG 54:6\|TG 16:0_18:2_20:4 | 1.67E+00 | 4.09E-05 | | SM 36:1 3O | 1.88E+00 | 3.46E-02 |
| TG 54:6\|TG 18:1_18:2_18:3 | 1.78E+00 | 2.17E-02 | | SM 36:2 2O | 2.72E+00 | 4.46E-05 |
| TG 54:7\|TG 16:1_18:2_20:4 | 1.86E+00 | 2.71E-03 | | SM 36:3 2O SM 18:1 2O/18:2 | 6.08E-01 | 1.03E-02 |
| TG 55:1\|TG 16:0_21:0_18:1 | 1.62E+00 | 8.20E-05 | | SM 37:2 2O SM 18:1 2O/19:1 | 6.59E-01 | 2.44E-02 |
| TG 55:3\|TG 19:0_18:1_18:2 | 1.95E+00 | 2.76E-03 | | SM 38:1 2O SM 16:1 2O/22:0 | 5.09E-01 | 4.94E-03 |
| TG 55:4\|TG 18:1_19:1_18:2 | 1.93E+00 | 1.56E-08 | | SM 38:1 3O | 1.75E+00 | 1.83E-02 |
| TG 55:5\|TG 19:1_18:2_18:2 | 1.58E+00 | 5.71E-05 | | SM 38:2 2O | 1.73E+00 | 3.82E-03 |
| TG 55:6\|TG 17:0_18:2_20:4 | 1.72E+00 | 6.27E-03 | | SM 38:2 2O SM 18:2 2O/20:0 | 6.42E-01 | 1.24E-02 |
| TG 56:3\|TG 20:0_18:1_18:2 | 1.85E+00 | 5.62E-10 | | SM 39:1 2O SM 17:1 2O/22:0 | 4.09E-01 | 8.87E-04 |
| TG 56:4\|TG 18:0_18:1_20:3 | 2.23E+00 | 9.56E-12 | | SM 39:2 2O SM 18:2 2O/21:0 | 5.63E-01 | 6.83E-03 |
| TG 56:5\|TG 18:0_18:1_20:4 | 2.09E+00 | 2.00E-09 | | SM 40:1 2O SM 18:1 2O/22:0 | 5.12E-01 | 5.10E-03 |
| TG 56:6\|TG 16:0_18:1_22:5 | 1.92E+00 | 7.83E-08 | | SM 40:2 2O SM 18:2 2O/22:0 | 5.44E-01 | 6.28E-03 |
| TG 56:6\|TG 18:0_18:2_20:4 | 1.81E+00 | 2.14E-10 | | SM 41:1 2O SM 18:1 2O/23:0 | 4.88E-01 | 1.62E-03 |
| TG 56:7\|TG 16:0_18:1_22:6 | 1.89E+00 | 4.93E-05 | | SM 41:2 2O SM 17:1 2O/24:1 | 5.59E-01 | 7.89E-03 |
| TG 56:7\|TG 18:1_18:2_20:4 | 1.70E+00 | 8.49E-03 | | SM 41:2;3O | 4.76E-01 | 1.57E-04 |
| TG 56:8\|TG 16:0_18:2_22:6 | 1.96E+00 | 1.00E-03 | | SM 41:3;3O | 4.68E-01 | 1.40E-04 |
| TG 57:0\|TG 16:0_17:0_24:0 | 1.65E+00 | 3.71E-06 | | SM 41:8;2O | 4.54E-01 | 1.28E-05 |
| TG 57:2\|TG 16:0_23:0_18:2 | 1.83E+00 | 2.08E-06 | | SM 42:4;2O | 2.31E+00 | 1.72E-04 |
| TG 57:8\|TG 17:1_18:1_22:6 | 1.86E+00 | 8.19E-03 | | SM 44:9;3O | 1.62E+00 | 8.66E-03 |
| TG 58:10\|TG 16:0_20:4_22:6 | 1.75E+00 | 3.03E-02 | | TG 36:3\|TG 8:0_10:0_18:3 | 7.30E+00 | 2.01E-04 |
| TG 58:6\|TG 16:0_18:1_24:5 | 2.15E+00 | 1.78E-12 | | TG 42:0\|TG 12:0_14:0_16:0 | 3.27E-01 | 3.52E-02 |
| TG 58:6\|TG 18:0_18:1_22:5 | 1.85E+00 | 1.17E-06 | | TG 42:3\|TG 8:0_16:1_18:2 | 1.73E+00 | 4.94E-04 |
| TG 58:7\|TG 18:0_18:1_22:6 | 1.53E+00 | 1.50E-02 | | TG 43:0\|TG 12:0_15:0_16:0 | 5.62E-01 | 1.76E-03 |
| TG 58:8\|TG 18:1_18:2_22:5 | 2.12E+00 | 6.61E-06 | | TG 44:0\|TG 10:0_16:0_18:0 | 2.98E-01 | 1.77E-06 |
| TG 58:9\|TG 18:1_18:2_22:6 | 1.87E+00 | 1.11E-03 | | TG 44:1\|TG 10:0_16:0_18:1 | 4.26E-01 | 3.12E-03 |
| TG 59:4TG 23:0_18:2_18:2 | 1.79E+00 | 3.55E-02 | | TG 46:0\|TG 12:0_16:0_18:0 | 5.23E-01 | 5.62E-06 |
| TG 60:10\|TG 18:0_20:4_22:6 | 1.55E+00 | 4.98E-02 | | TG 46:0\|TG 14:0_16:0_16:0 | 4.84E-01 | 5.18E-05 |
| TG 60:4\|TG 18:1_24:1_18:2 | 1.62E+00 | 3.45E-02 | | TG 46:1\|TG 14:0_16:0_16:1 | 4.43E-01 | 1.30E-04 |
| TG 60:7\|TG 18:1_18:2_24:4 | 1.50E+00 | 2.06E-03 | | TG 46:2\|TG 12:0_16:1_18:1 | 5.13E-01 | 4.07E-03 |
| PE O-38:6\|PE O-18:2_20:4 | 5.10E-01 | 9.89E-16 | | TG 48:3\|TG 14:0_16:1_18:2 | 5.95E-01 | 4.73E-03 |
| PE O-34:3\|PE O-16:1_18:2 | 3.95E-01 | 4.63E-15 | | TG 51:1\|TG 16:0_17:0_18:1 | 1.60E+00 | 9.86E-04 |
| PE O-36:4\|PE O-18:2_18:2 | 3.99E-01 | 7.02E-15 | | TG 51:2\|TG 16:0_17:1_18:1 | 1.62E+00 | 3.80E-04 |
| PC O-34:3\|PC O-16:1_18:2 | 4.95E-01 | 2.15E-13 | | TG 51:2\|TG 17:0_16:1_18:1 | 1.66E+00 | 4.76E-08 |
| FA 20:4 | 8.40E+00 | 5.77E-13 | | TG 51:3\|TG 15:0_18:1_18:2 | 1.54E+00 | 1.82E-04 |
| LPC 18:2 | 4.69E-01 | 2.57E-12 | | TG 52:2\|TG 16:0_18:1_18:1 | 1.69E+00 | 9.27E-10 |
| PE O-36:5\|PE O-16:1_20:4 | 5.83E-01 | 3.83E-12 | | TG 52:3\|TG 16:0_18:1_18:2 | 1.65E+00 | 8.75E-10 |
| FA 18:1 | 4.46E+00 | 7.28E-12 | | TG 52:4\|TG 16:1_18:1_18:2 | 1.54E+00 | 4.22E-04 |
| PE O-36:3\|PE O-18:1_18:2 | 4.45E-01 | 1.90E-11 | | TG 52:6\|TG 16:1_18:2_18:3 | 1.66E+00 | 4.44E-08 |
| PE O-38:5\|PE O-18:1_20:4 | 6.12E-01 | 7.02E-09 | | TG 53:2\|TG 16:0_18:1_19:1 | 1.94E+00 | 5.41E-13 |
| SM 41:1;2O\|SM 18:1;2O/23:0 | 6.39E-01 | 3.56E-08 | | TG 53:3\|TG 17:0_18:1_18:2 | 1.78E+00 | 3.31E-06 |
| PE O-38:5\|PE O-16:1_22:4 | 6.24E-01 | 1.33E-07 | | TG 53:4\|TG 17:1_18:1_18:2 | 1.50E+00 | 9.68E-04 |
| LPC 16:0 | 1.72E+00 | 1.40E-07 | | TG 54:2\|TG 16:0_18:1_20:1 | 1.75E+00 | 1.06E-10 |
| LPE 18:0 | 1.90E+00 | 1.63E-07 | | TG 54:2\|TG 18:0_18:1_18:1 | 1.67E+00 | 1.39E-04 |
| FA 22:6 | 4.08E+00 | 1.74E-07 | | TG 54:3\|TG 18:0_18:1_18:2 | 1.63E+00 | 2.39E-05 |
| LPE O-18:2 | 2.46E+00 | 3.37E-07 | | TG 54:4\|TG 16:0_18:1_20:3 | 1.55E+00 | 1.09E-08 |

| | | |
|---|---|---|
| PE 40:6\|PE 18:0_22:6 | 2.37E+00 | 3.75E-07 |
| PE 38:6\|PE 16:0_22:6 | 2.32E+00 | 5.92E-07 |
| FA 18:2 | 4.70E+00 | 8.58E-07 |
| LPE 16:0 | 1.80E+00 | 1.15E-06 |
| PE 38:6\|PE 18:2_20:4 | 2.37E+00 | 1.65E-06 |
| PE 38:4\|PE 18:0_20:4 | 1.71E+00 | 4.88E-06 |
| PE 34:1\|PE 16:0_18:1 | 2.38E+00 | 1.55E-05 |
| PE 36:4\|PE 16:0_20:4 | 1.87E+00 | 1.60E-05 |
| PI 38:3\|PI 180:_20:3 | 6.38E-01 | 2.55E-05 |
| LPE O-16:1 | 1.91E+00 | 2.98E-05 |
| LPE 22:6 | 2.58E+00 | 9.11E-05 |
| LPC 17:0 | 1.60E+00 | 1.62E-04 |
| PI 36:3\|PI 18:1_18:2 | 5.25E-01 | 1.93E-04 |
| PC 36:5\|PC 16:0_20:5 | 6.54E-01 | 3.46E-04 |
| LPC 22:5 | 1.75E+00 | 4.95E-04 |
| LPC 22:6 | 1.87E+00 | 5.26E-04 |
| LPE O-18:1 | 1.68E+00 | 1.09E-03 |
| LPE 22:5 | 2.63E+00 | 1.12E-03 |
| PE 34:2\|PE 16:0_18:2 | 1.54E+00 | 3.47E-03 |
| FA 44:5 | 2.54E+00 | 5.80E-03 |
| LPE 18:2 | 6.44E-01 | 8.32E-03 |
| PI 40:5\|PI 18:0_22:5 | 1.50E+00 | 1.05E-02 |
| LPE 22:4 | 2.45E+00 | 1.37E-02 |
| LPE 20:4 | 1.64E+00 | 1.47E-02 |
| ST 28:1;OS | 1.56E+00 | 2.09E-02 |

**Table 3**: RSD of the standard spiked in the QC

| | CV% | |
|---|---|---|
| Lipids | POS | NEG |
| DAG 15:0-18:1(d7) | 19.2 | - |
| LPC 15:0-18:1(d7) | 2.7 | 8.0 |
| LPE 15:0-18:1(d7) | 3.2 | 8.3 |
| PC 15:0-18:1(d7) | 5.3 | 6.3 |
| PE 15:0-18:1(d7) | 2.9 | 6.3 |
| TAG 15:0-18:1(d7)-15:0 | 3.2 | - |
| MAG 18:1(d7) | 13.4 | - |
| SM d18:1-18:1(d9) | 3.8 | 9.8 |
| Cholesterol (d7) | 5.1 | - |
| CUDA | 3.8 | 8.2 |

**Table 4**: The 27 modulated lipids from the preliminary lipidomic study of PBMCs samples with fold change and *p*-value

| Lipids | FC | *p*-value |
|---|---|---|
| PC O-46:4 | 3.82E-01 | 5.99E-04 |
| NAE 14:1 | 4.21E-01 | 1.49E-03 |
| PC O-44:4 | 4.75E-01 | 2.55E-04 |
| PE P-38:6\|PE P-16:0_22:6 | 4.93E-01 | 4.02E-02 |
| LPE O-3:0 | 4.96E-01 | 5.28E-07 |
| NAE 22:1 | 5.36E-01 | 4.40E-02 |
| PE 40:5\|PE 18:0_22:5 | 5.38E-01 | 2.11E-02 |
| NAE 13:1 | 5.48E-01 | 1.79E-02 |
| PC 36:3\|PC 18:1_18:2 | 5.53E-01 | 3.92E-02 |
| PE O-40:9 | 5.65E-01 | 3.92E-02 |
| FA 18:1;2O | 5.69E-01 | 2.22E-02 |
| FA 20:1;2O | 5.76E-01 | 1.79E-02 |
| FA 22:0;2O | 5.79E-01 | 1.73E-02 |
| PE O-38:8 | 5.82E-01 | 3.59E-02 |
| PC 40:6\|PC 18:0_22:6 | 6.27E-01 | 3.24E-02 |
| PC 38:4\|PC 18:0_20:4 | 6.67E-01 | 2.79E-02 |
| PE 36:2\|PE 18:0_18:2 | 6.87E-01 | 6.60E-03 |
| PC 34:2\|PC 16:0_18:2 | 7.35E-01 | 4.82E-02 |
| PI 38:4 | 7.47E-01 | 7.06E-03 |
| TG 52:2\|TG 16:0_18:1_18:1 | 1.83E+00 | 2.81E-02 |
| TG 50:2\|TG 16:0_16:1_18:1 | 2.24E+00 | 3.46E-02 |
| TG 56:3\|TG 18:1_18:1_20:1 | 2.49E+00 | 4.23E-02 |
| LPE 20:3 | 2.61E+00 | 4.96E-02 |
| PC O-36:2 | 2.98E+00 | 2.60E-02 |
| NAE 16:1 | 3.12E+00 | 2.94E-02 |
| Cer 38:0;2O\|Cer 18:0;2O/20:0 | 4.00E+00 | 1.48E-02 |
| TG 58:7\|TG 18:1_18:2_22:4 | 8.94E+00 | 4.05E-02 |

## *Bibliography*


1. Hui, D.S.; I Azhar, E.; Madani, T.A.; Ntoumi, F.; Kock, R.; Dar, O.; Ippolito, G.; Mchugh, T.D.; Memish, Z.A.; Drosten, C.; et al. The Continuing 2019-NCoV Epidemic Threat of Novel Coronaviruses to Global Health — The Latest 2019 Novel Coronavirus Outbreak in Wuhan, China. *International Journal of Infectious Diseases* **2020**, *91*, 264–266, doi:10.1016/j.ijid.2020.01.009.
2. Wang, H.; Wang, Z.; Dong, Y.; Chang, R.; Xu, C.; Yu, X.; Zhang, S.; Tsamlag, L.; Shang, M.; Huang, J.; et al. Phase-Adjusted Estimation of the Number of Coronavirus Disease 2019 Cases in Wuhan, China. *Cell Discov* **2020**, *6*, 10, doi:10.1038/s41421-020-0148-0.
3. Zheng, Y.-Y.; Ma, Y.-T.; Zhang, J.-Y.; Xie, X. COVID-19 and the Cardiovascular System. *Nat Rev Cardiol* **2020**, *17*, 259–260, doi:10.1038/s41569-020-0360-5.
4. Ghinai, I.; McPherson, T.D.; Hunter, J.C.; Kirking, H.L.; Christiansen, D.; Joshi, K.; Rubin, R.; Morales-Estrada, S.; Black, S.R.; Pacilli, M.; et al. First Known Person-to-Person Transmission of Severe Acute Respiratory Syndrome Coronavirus 2 (SARS-CoV-2) in the USA. *The Lancet* **2020**, *395*, 1137–1144, doi:10.1016/S0140-6736(20)30607-3.
5. Guan, W.; Ni, Z.; Hu, Y.; Liang, W.; Ou, C.; He, J.; Liu, L.; Shan, H.; Lei, C.; Hui, D.S.C.; et al. Clinical Characteristics of Coronavirus Disease 2019 in China. *N Engl J Med* **2020**, *382*, 1708–1720, doi:10.1056/NEJMoa2002032.
6. Bost, P.; Giladi, A.; Liu, Y.; Bendjelal, Y.; Xu, G.; David, E.; Blecher-Gonen, R.; Cohen, M.; Medaglia, C.; Li, H.; et al. Host-Viral Infection Maps Reveal Signatures of Severe COVID-19 Patients. *Cell* **2020**, *181*, 1475-1488.e12, doi:10.1016/j.cell.2020.05.006.
7. Eisfeld, A.J.; Halfmann, P.J.; Wendler, J.P.; Kyle, J.E.; Burnum-Johnson, K.E.; Peralta, Z.; Maemura, T.; Walters, K.B.; Watanabe, T.; Fukuyama, S.; et al. Multi-Platform 'Omics Analysis of Human Ebola Virus Disease Pathogenesis. *Cell Host & Microbe* **2017**, *22*, 817-829.e8, doi:10.1016/j.chom.2017.10.011.
8. Kyle, J.E.; Burnum-Johnson, K.E.; Wendler, J.P.; Eisfeld, A.J.; Halfmann, P.J.; Watanabe, T.; Sahr, F.; Smith, R.D.; Kawaoka, Y.; Waters, K.M.; et al. Plasma Lipidome Reveals Critical Illness and

Recovery from Human Ebola Virus Disease. *Proc Natl Acad Sci USA* **2019**, *116*, 3919–3928, doi:10.1073/pnas.1815356116.

9. the Canadian Critical Care Translational Biology Group (CCCTBG); Banoei, M.M.; Vogel, H.J.; Weljie, A.M.; Kumar, A.; Yende, S.; Angus, D.C.; Winston, B.W. Plasma Metabolomics for the Diagnosis and Prognosis of H1N1 Influenza Pneumonia. *Crit Care* **2017**, *21*, 97, doi:10.1186/s13054-017-1672-7.
10. Wu, Q.; Zhou, L.; Sun, X.; Yan, Z.; Hu, C.; Wu, J.; Xu, L.; Li, X.; Liu, H.; Yin, P.; et al. Altered Lipid Metabolism in Recovered SARS Patients Twelve Years after Infection. *Sci Rep* **2017**, *7*, 9110, doi:10.1038/s41598-017-09536-z.
11. Wu, D.; Shu, T.; Yang, X.; Song, J.-X.; Zhang, M.; Yao, C.; Liu, W.; Huang, M.; Yu, Y.; Yang, Q.; et al. Plasma Metabolomic and Lipidomic Alterations Associated with COVID-19. *National Science Review* **2020**, *7*, 1157–1168, doi:10.1093/nsr/nwaa086.
12. Shen, B.; Yi, X.; Sun, Y.; Bi, X.; Du, J.; Zhang, C.; Quan, S.; Zhang, F.; Sun, R.; Qian, L.; et al. Proteomic and Metabolomic Characterization of COVID-19 Patient Sera. *Cell* **2020**, *182*, 59-72.e15, doi:10.1016/j.cell.2020.05.032.
13. Song, J.-W.; Lam, S.M.; Fan, X.; Cao, W.-J.; Wang, S.-Y.; Tian, H.; Chua, G.H.; Zhang, C.; Meng, F.-P.; Xu, Z.; et al. Omics-Driven Systems Interrogation of Metabolic Dysregulation in COVID-19 Pathogenesis. *Cell Metabolism* **2020**, *32*, 188-202.e5, doi:10.1016/j.cmet.2020.06.016.
14. Zhang, L.; Jackson, C.B.; Mou, H.; Ojha, A.; Rangarajan, E.S.; Izard, T.; Farzan, M.; Choe, H. *The D614G Mutation in the SARS-CoV-2 Spike Protein Reduces S1 Shedding and Increases Infectivity*; Microbiology, 2020;
15. Struwe, W.; Emmott, E.; Bailey, M.; Sharon, M.; Sinz, A.; Corrales, F.J.; Thalassinos, K.; Braybrook, J.; Mills, C.; Barran, P. The COVID-19 MS Coalition—Accelerating Diagnostics, Prognostics, and Treatment. *The Lancet* **2020**, *395*, 1761–1762, doi:10.1016/S0140-6736(20)31211-3.
16. Tsugawa, H.; Cajka, T.; Kind, T.; Ma, Y.; Higgins, B.; Ikeda, K.; Kanazawa, M.; VanderGheynst, J.; Fiehn, O.; Arita, M. MS-DIAL: Data-Independent MS/MS Deconvolution for Comprehensive Metabolome Analysis. *Nat Methods* **2015**, *12*, 523–526, doi:10.1038/nmeth.3393.

17. Murakami, M.; Nakatani, Y.; Atsumi, G.; Inoue, K.; Kudo, I. Regulatory Functions of Phospholipase A2. *Crit Rev Immunol* **2017**, *37*, 121–179, doi:10.1615/CritRevImmunol.v37.i2-6.20.
18. Lee, E.-Y.; Kim, S.; Kim, M.H. Aminoacyl-TRNA Synthetases, Therapeutic Targets for Infectious Diseases. *Biochemical Pharmacology* **2018**, *154*, 424–434, doi:10.1016/j.bcp.2018.06.009.
19. Thomas, T.; Stefanoni, D.; Reisz, J.A.; Nemkov, T.; Bertolone, L.; Francis, R.O.; Hudson, K.E.; Zimring, J.C.; Hansen, K.C.; Hod, E.A.; et al. COVID-19 Infection Alters Kynurenine and Fatty Acid Metabolism, Correlating with IL-6 Levels and Renal Status. *JCI Insight* **2020**, *5*, e140327, doi:10.1172/jci.insight.140327.
20. Lithander, F.E.; Neumann, S.; Tenison, E.; Lloyd, K.; Welsh, T.J.; Rodrigues, J.C.L.; Higgins, J.P.T.; Scourfield, L.; Christensen, H.; Haunton, V.J.; et al. COVID-19 in Older People: A Rapid Clinical Review. *Age and Ageing* **2020**, *49*, 501–515, doi:10.1093/ageing/afaa093.
21. Yan, B.; Chu, H.; Yang, D.; Sze, K.-H.; Lai, P.-M.; Yuan, S.; Shuai, H.; Wang, Y.; Kao, R.Y.-T.; Chan, J.F.-W.; et al. Characterization of the Lipidomic Profile of Human Coronavirus-Infected Cells: Implications for Lipid Metabolism Remodeling upon Coronavirus Replication. *Viruses* **2019**, *11*, 73, doi:10.3390/v11010073.
22. Das, U.N. Can Bioactive Lipids Inactivate Coronavirus (COVID-19)? *Archives of Medical Research* **2020**, *51*, 282–286, doi:10.1016/j.arcmed.2020.03.004.
23. Coperchini, F.; Chiovato, L.; Croce, L.; Magri, F.; Rotondi, M. The Cytokine Storm in COVID-19: An Overview of the Involvement of the Chemokine/Chemokine-Receptor System. *Cytokine & Growth Factor Reviews* **2020**, *53*, 25–32, doi:10.1016/j.cytogfr.2020.05.003.
24. Das, U.N. Arachidonic Acid and Other Unsaturated Fatty Acids and Some of Their Metabolites Function as Endogenous Antimicrobial Molecules: A Review. *Journal of Advanced Research* **2018**, *11*, 57–66, doi:10.1016/j.jare.2018.01.001.
25. EUCLIDS consortium; Wang, X.; Nijman, R.; Camuzeaux, S.; Sands, C.; Jackson, H.; Kaforou, M.; Emonts, M.; Herberg, J.A.; Maconochie, I.; et al. Plasma Lipid Profiles Discriminate Bacterial from Viral

Infection in Febrile Children. *Sci Rep* **2019**, *9*, 17714, doi:10.1038/s41598-019-53721-1.

26. Arshad, H.; Alfonso, J.C.L.; Franke, R.; Michaelis, K.; Araujo, L.; Habib, A.; Zboromyrska, Y.; Lücke, E.; Strungaru, E.; Akmatov, M.K.; et al. Decreased Plasma Phospholipid Concentrations and Increased Acid Sphingomyelinase Activity Are Accurate Biomarkers for Community-Acquired Pneumonia. *J Transl Med* **2019**, *17*, 365, doi:10.1186/s12967-019-2112-z.
27. Queiroz, A.; Pinto, I.F.D.; Lima, M.; Giovanetti, M.; de Jesus, J.G.; Xavier, J.; Barreto, F.K.; Canuto, G.A.B.; do Amaral, H.R.; de Filippis, A.M.B.; et al. Lipidomic Analysis Reveals Serum Alteration of Plasmalogens in Patients Infected With ZIKA Virus. *Front. Microbiol.* **2019**, *10*, 753, doi:10.3389/fmicb.2019.00753.
28. Fuchs, B.; Schiller, J. Lysophospholipids: Their Generation, Physiological Role and Detection. Are They Important Disease Markers? *MRMC* **2009**, *9*, 368–378, doi:10.2174/1389557510909030368.
29. Stoll, L.L.; Oskarsson, H.J.; Spector, A.A. Interaction of Lysophosphatidylcholine with Aortic Endothelial Cells. *American Journal of Physiology-Heart and Circulatory Physiology* **1992**, *262*, H1853–H1860, doi:10.1152/ajpheart.1992.262.6.H1853.
30. Zou, Y.; Kim, C.H.; Chung, J.H.; Kim, J.Y.; Chung, S.W.; Kim, M.K.; Im, D.S.; Lee, J.; Yu, B.P.; Chung, H.Y. Upregulation of Endothelial Adhesion Molecules by Lysophosphatidylcholine: Involvement of G Protein-Coupled Receptor GPR4. *FEBS Journal* **2007**, *274*, 2573–2584, doi:10.1111/j.1742-4658.2007.05792.x.
31. Li, X.; Wang, L.; Fang, P.; Sun, Y.; Jiang, X.; Wang, H.; Yang, X.-F. Lysophospholipids Induce Innate Immune Transdifferentiation of Endothelial Cells, Resulting in Prolonged Endothelial Activation. *Journal of Biological Chemistry* **2018**, *293*, 11033–11045, doi:10.1074/jbc.RA118.002752.
32. Radu, C.G.; Yang, L.V.; Riedinger, M.; Au, M.; Witte, O.N. T Cell Chemotaxis to Lysophosphatidylcholine through the G2A Receptor. *Proceedings of the National Academy of Sciences* **2004**, *101*, 245–250, doi:10.1073/pnas.2536801100.
33. Jin, Y.; Damaj, B.B.; Maghazachi, A.A. Human Resting CD16-, CD16+ and IL-2-, IL-12-, IL-15- or IFN-α-Activated Natural Killer Cells

Differentially Respond to Sphingosylphosphorylcholine, Lysophosphatidylcholine and Platelet-Activating Factor. *Eur. J. Immunol.* **2005**, *35*, 2699–2708, doi:10.1002/eji.200526129.

34. Asaoka, Y.; Oka, M.; Yoshida, K.; Sasaki, Y.; Nishizuka, Y. Role of Lysophosphatidylcholine in T-Lymphocyte Activation: Involvement of Phospholipase A2 in Signal Transduction through Protein Kinase C. *Proceedings of the National Academy of Sciences* **1992**, *89*, 6447–6451, doi:10.1073/pnas.89.14.6447.
35. Hara, Y.; Kusumi, Y.; Mitsumata, M.; Li, X.-K.; Fujino, M. Lysophosphatidylcholine Upregulates LOX-1, Chemokine Receptors, and Activation-Related Transcription Factors in Human T-Cell Line Jurkat. *J Thromb Thrombolysis* **2008**, *26*, 113–118, doi:10.1007/s11239-007-0158-x.
36. Han, K.H.; Hong, K.H.; Ko, J.; Rhee, K.S.; Hong, M.K.; Kim, J.J.; Kim, Y.H.; Park, S.J. Lysophosphatidylcholine Up-Regulates CXCR4 Chemokine Receptor Expression in Human CD4 T Cells. *Journal of Leukocyte Biology* **2004**, *76*, 195–202, doi:10.1189/jlb.1103563.
37. Qin, X.; Qiu, C.; Zhao, L. Lysophosphatidylcholine Perpetuates Macrophage Polarization toward Classically Activated Phenotype in Inflammation. *Cellular Immunology* **2014**, *289*, 185–190, doi:10.1016/j.cellimm.2014.04.010.
38. Lin, P.; Welch, E.J.; Gao, X.-P.; Malik, A.B.; Ye, R.D. Lysophosphatidylcholine Modulates Neutrophil Oxidant Production through Elevation of Cyclic AMP. *J Immunol* **2005**, *174*, 2981–2989, doi:10.4049/jimmunol.174.5.2981.
39. Sato, H.; Taketomi, Y.; Murakami, M. Metabolic Regulation by Secreted Phospholipase A2. *Inflamm Regener* **2016**, *36*, 7, doi:10.1186/s41232-016-0012-7.
40. Müller, C.; Hardt, M.; Schwudke, D.; Neuman, B.W.; Pleschka, S.; Ziebuhr, J. Inhibition of Cytosolic Phospholipase A $_2$ α Impairs an Early Step of Coronavirus Replication in Cell Culture. *J Virol* **2018**, *92*, doi:10.1128/JVI.01463-17.
41. Shan, J.; Qian, W.; Shen, C.; Lin, L.; Xie, T.; Peng, L.; Xu, J.; Yang, R.; Ji, J.; Zhao, X. High-Resolution Lipidomics Reveals Dysregulation of Lipid Metabolism in Respiratory Syncytial Virus Pneumonia Mice. *RSC Adv.* **2018**, *8*, 29368–29377, doi:10.1039/C8RA05640D.

42. Otsubo, C.; Bharathi, S.; Uppala, R.; Ilkayeva, O.R.; Wang, D.; McHugh, K.; Zou, Y.; Wang, J.; Alcorn, J.F.; Zuo, Y.Y.; et al. Long-Chain Acylcarnitines Reduce Lung Function by Inhibiting Pulmonary Surfactant. *Journal of Biological Chemistry* **2015**, *290*, 23897–23904, doi:10.1074/jbc.M115.655837.
43. Burstein, S.A.; Peng, J.; Friese, P.; Wolf, R.F.; Harrison, P.; Downs, T.; Hamilton, K.; Comp, P.; Dale, G.L. Cytokine–Induced Alteration of Platelet and Hemostatic Function. *Stem Cells* **1996**, *14*, 154–162, doi:10.1002/stem.5530140720.
44. Audi, A.; Soudani, N.; Dbaibo, G.; Zaraket, H. Depletion of Host and Viral Sphingomyelin Impairs Influenza Virus Infection. *Front. Microbiol.* **2020**, *11*, 612, doi:10.3389/fmicb.2020.00612.
45. Pontelli, M.C.; Castro, I.A.; Martins, R.B.; Veras, F.P.; Serra, L.L.; Nascimento, D.C.; Cardoso, R.S.; Rosales, R.; Lima, T.M.; Souza, J.P.; et al. *Infection of Human Lymphomononuclear Cells by SARS-CoV-2*; Microbiology, 2020;
46. Kind, T.; Liu, K.-H.; Lee, D.Y.; DeFelice, B.; Meissen, J.K.; Fiehn, O. LipidBlast in Silico Tandem Mass Spectrometry Database for Lipid Identification. *Nat Methods* **2013**, *10*, 755–758, doi:10.1038/nmeth.2551.
47. Li, Z.; Agellon, L.B.; Allen, T.M.; Umeda, M.; Jewell, L.; Mason, A.; Vance, D.E. The Ratio of Phosphatidylcholine to Phosphatidylethanolamine Influences Membrane Integrity and Steatohepatitis. *Cell Metabolism* **2006**, *3*, 321–331, doi:10.1016/j.cmet.2006.03.007.
48. Li, H.; Xu, Q.-Y.; Xie, Y.; Luo, J.-J.; Cao, H.-X.; Pan, Q. Effects of Chronic HBV Infection on Lipid Metabolism in Non-Alcoholic Fatty Liver Disease: A Lipidomic Analysis. *Annals of Hepatology* **2021**, *24*, 100316, doi:10.1016/j.aohep.2021.100316.
49. Caterino, M.; Gelzo, M.; Sol, S.; Fedele, R.; Annunziata, A.; Calabrese, C.; Fiorentino, G.; D'Abbraccio, M.; Dell'Isola, C.; Fusco, F.M.; et al. Dysregulation of Lipid Metabolism and Pathological Inflammation in Patients with COVID-19. *Sci Rep* **2021**, *11*, 2941, doi:10.1038/s41598-021-82426-7.

50. Aktepe, T.E.; Pham, H.; Mackenzie, J.M. Differential Utilisation of Ceramide during Replication of the Flaviviruses West Nile and Dengue Virus. *Virology* **2015**, *484*, 241–250, doi:10.1016/j.virol.2015.06.015.
51. Haughey, N.J.; Tovar-y-Romo, L.B.; Bandaru, V.V.R. Roles for Biological Membranes in Regulating Human Immunodeficiency Virus Replication and Progress in the Development of HIV Therapeutics That Target Lipid Metabolism. *J Neuroimmune Pharmacol* **2011**, *6*, 284–295, doi:10.1007/s11481-011-9274-7.
52. Abu-Farha, M.; Thanaraj, T.A.; Qaddoumi, M.G.; Hashem, A.; Abubaker, J.; Al-Mulla, F. The Role of Lipid Metabolism in COVID-19 Virus Infection and as a Drug Target. *IJMS* **2020**, *21*, 3544, doi:10.3390/ijms21103544.
53. Koumanov, K.S.; Momchilova, A.B.; Quinn, P.J.; Wolf, C. Ceramides Increase the Activity of the Secretory Phospholipase A2 and Alter Its Fatty Acid Specificity. *Biochemical Journal* **2002**, *363*, 45–51, doi:10.1042/bj3630045.
54. Numata, M.; Kandasamy, P.; Nagashima, Y.; Fickes, R.; Murphy, R.C.; Voelker, D.R. Phosphatidylinositol Inhibits Respiratory Syncytial Virus Infection. *Journal of Lipid Research* **2015**, *56*, 578–587, doi:10.1194/jlr.M055723.
55. Cajka, T.; Davis, R.; Austin, K.J.; Newman, J.W.; German, J.B.; Fiehn, O.; Smilowitz, J.T. Using a Lipidomics Approach for Nutritional Phenotyping in Response to a Test Meal Containing Gamma-Linolenic Acid. *Metabolomics* **2016**, *12*, 127, doi:10.1007/s11306-016-1075-9.

# *Chapter 3: Lipidomic study of different G forces on cells and mice*

## *General introduction to the chapter*

This chapter reports two studies performed on the alteration of the lipidome caused by two different types of gravity: microgravity and hypergravity. These two conditions are present during space mission, spaceflight and parabolic flight. The repercussions of a long exposure to different gravity were studied by scientists all over the world and evidences of several biological modification were found.

In figure 1 it is reported a summary of the two studies; in details: the effect of simulated microgravity (SMG) was evaluated *in vitro*, on human pancreatic ductal adenocarcinoma cell lines (PaCa-44 cells) thanks to the use of a *random positioning machine*. The cells were kept in SMG condition for a total of 9 days and the analysis at different time points (24h, 7 days and 9 days) pointed out that microgravity induces cell transformation over time, towards the acquisition of cancer stem cell-like features, leading to a more aggressive and metastatic phenotype.

The effect of simulated hypergravity (SHG) was instead evaluated *in vivo* on a murine model, using the mice drawer system in order to simulate a gravity force of 3G for 1 month. Plasma samples were collected at the end of the

experiment and lipidomic analysis showed lipids modulation in different classes.

This study is part of the project ESA-CORA-GBF (European Space Agency-Continously Open Research Announcemen- Ground Based Facilities); as regard animals, the protocols were reviewed and approved by the Internal Ethical Committee of the University of Genoa/S.Martino Hospital.

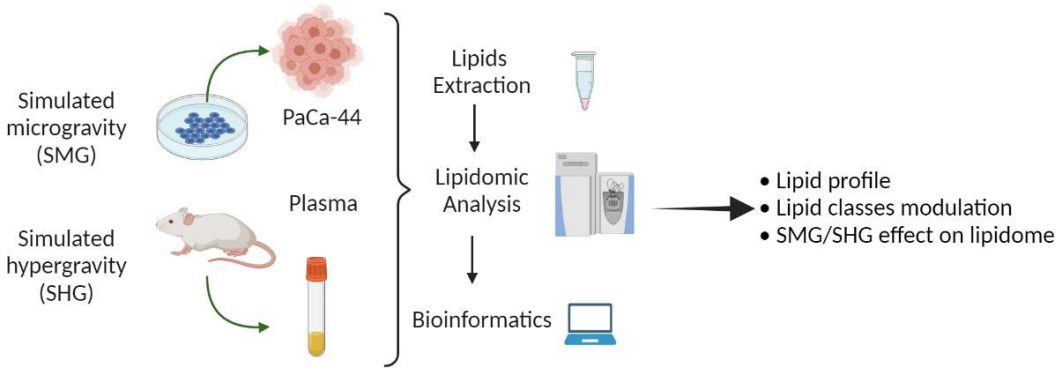


**Figure 1**: workflow of the two studies inspecting the role of gravity on cells PaCa-44 (top) and in mice (bottom). The lipidomic approach was applied to evaluate the effect of impairment of the gravity force on the two different biological matrices.

For both the studies lipidomics was supported by other omics sciences, like transcriptomics and proteomics analyses.

# *Lipidomics investigation on PaCa-44 cells in simulated microgravity condition over time highlighted a cell transformation and acquisition of cancer stem cell-like features*

## *Introduction*

There is an increasing interest on the possible effects of different G forces on living beings, especially in a time where space and, more recently, space travels, are more accessible than ever.

During spaceflights there is a condition of microgravity (μg) that impacts on various biological systems: bone loss, muscle atrophy, cardiovascular deconditioning and space motion sickness, are just some of the effects that astronauts in orbit have shown [1].

Microgravity has effects also on cells: changes in differentiation and growth had been observed [2].

Unfortunately, the data from literature are contradictory and there is no cohesion and standardization on the methods used to generate and maintain the condition of microgravity. Obviously, the best way to study the biological modification is to have direct access to the international space station (ISS), but the costs do not make it affordable to everyone. To avoid this limitation particular instrumentations has been developed: the random positioning machine (RPM) and more specific and custom instrumentations allow to exert different G forces both on *in vivo* and *in vitro* models.

It has already been observed that μg induces a great number of changes in different cell types, including cancer and stem cells [3]. Either if the experiments are conducted in orbit or on Earth with the simulating devices, some similar modifications were observed in the cells, like modification of

cytoskeleton [4], alterations in the composition of the extracellular matrix [5], differentiation [6], changes in growth behavior [2] and reduction of the activity of the cells [7].

Regarding cellular panorama, a large number of publications are focused on cancer cells in μg and their behavior [8–10], but less attention is given to cancer stem cells (CSCs) [7].

CSCs have characteristics belonging to both normal stem cells and cancer cells. The most important one is their ability to give birth to all cell types found in a particular cancer sample. This type of cells is present in a great variety of tumors such as colon, lung, melanoma, pancreas and prostate. CSCs are different from the other tumor cells and are characterized by great plasticity, capability to enter into quiescence and survive to microenvironment changes adapting metabolism, energy machinery and proliferation. Furthermore, this type of cells are the main orchestrators of tumor establishment, metastatic progression and relapse. For these reasons, CSCs could be used as a cancer target, but, to date, further investigations are needed in order to clarify the tumorigenic characteristic and the ability to resist cancer treatment [11].

Thanks to the RPM tool it was possible to perform a study on pancreatic ductal adenocarcinoma cells (PDAC) at different time points in a condition of simulated microgravity (SMG).

PDAC is one of the most severe malignancies, representing the 5$^{th}$ cause of death from cancer in the western world. Only 8% of patients survive after 5 years from the diagnosis, because of a too late diagnosis and/or the cancer resistance to the treatments. Resistance to conventional anti-cancer treatments is imputable to CSCs [12].

Lipidomics was applied together with proteomics and transcriptomics in order to study the effect of μg at 24h (T1 SMG), 7 days (T7 SMG) and 9 days (T9

SMG). As control group (CTR) cells kept in normal adhesion were used (figure 2).

## *Materials and Methods*

Materials and methods of this study are the same as previously reported in Chapter 2 page 51.

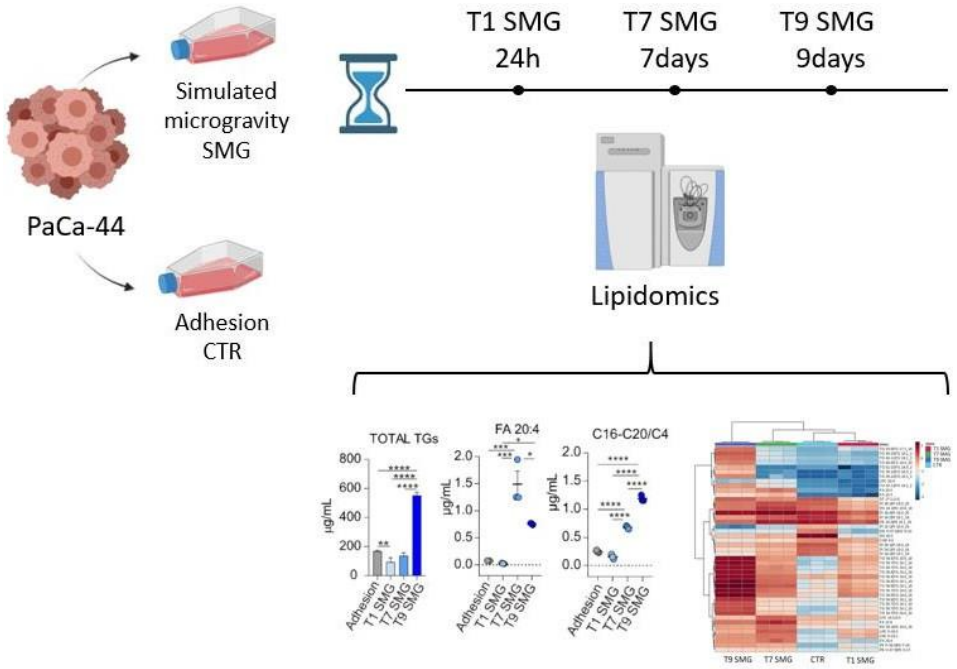


**Figure 2**: workflow of the study. Lipidomics was applied to investigate the effects of simulated microgravity (SMG) on human pancreatic ductal adenocarcinoma (PaCa-44 cell line) over time: 24h (T1 SMG), 7 days (T7 SMG) and 9 days (T9 SMG), using a control group of cells in normal adhesion condition (CTR).

## *Results*

A total of 447 lipids belonging to 18 different lipid classes were identified in PaCa-44 cells: bismonoacylglycerophosphate (BMP); acylcarnitine (CAR); cholesteryl ester (CE); ceramide (Cer); diacylglycerol (DG); free fatty acid (FA); glycosylceramides (HexCer); lysophophatidylcholine (LPC); lysophosphatidylethanolamine (LPE); lysophosphatidylglycerol (LPG);

lysophosphatidylinositol (LPI); N-acyl ethanolamines (NAE); phosphatidylcholine (PC); phosphatidylethanolamine (PE); phosphatidylglycerol (PG); phosphatidylinositol (PI); sphingomyelin (SM); triacylglycerol (TG).

The hierarchical clustering heatmap (figure 3A) highlighted the separation of the four groups of cells, suggesting a phenotypic lipidome alteration caused by the simulated microgravity. In figure 3B the number of lipids identified in each class are reported in details.

TG resulted the most abundant lipid class, with 138 identified lipids. This lipid class is characterized by an average of total carbon chain of 54 and a predominance of C18:1 in the acyl chains, like TG 18:1_18:1_18:1. MGs were not identified, while few DGs were detected. The absence of MGs and the low number of DGs is probably due to the fact that they are intermediate products of the catabolism and synthesis of TGs [13].

Figure 3C reports the total concentrations of lipid classes that show a trend over time in SMG. The total concentrations are reported as µg/mL and were calculated by summing the normalized areas of the single lipids for each class. After 7 days a clear increase of total BMPs, Cers, FAs, LPCs, LPEs, and PGs occurred and after the $7^{th}$ day all these classes showed decreased levels; the TG class showed an increase at the $9^{th}$ day. The only lipid class that have a different trend is the CAR one: it shows a decrease in the abundance of lipids over the time.

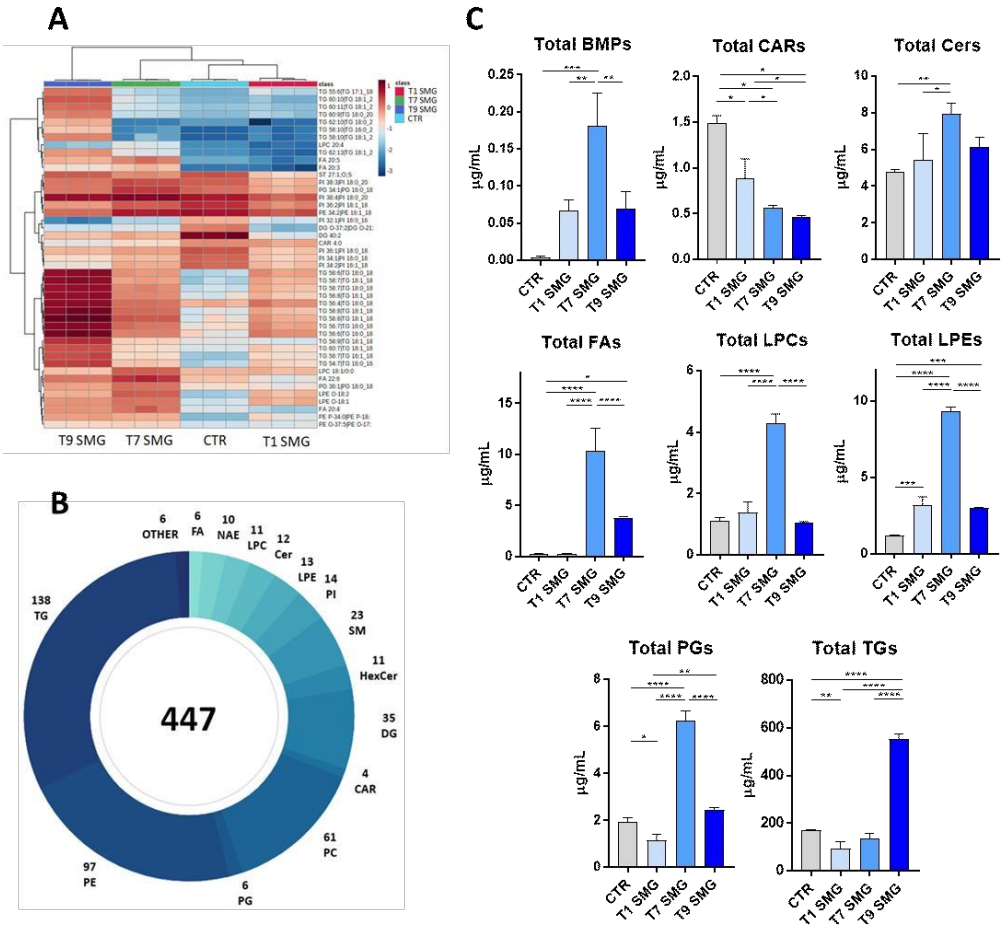


**Figure 3**: lipidomic alteration during simulated microgravity. Hierarchical clustering heatmap of the 4 groups (**A**), donut chart of the number of identified lipids per class (**B**). Total lipid concentration for BMPs, CARs, Cers, FAs, LPCs, LPEs, PGs and TGs (**C**).
*p*-value < 0.05 = *; *p*-value < 0.01 = **; *p*-value < 0.001 = ***; *p*-value < 0.0001 = ****)
Legend: BMP bismonoacylglycerophosphate; CAR acylcarnitine; CE cholesteryl ester; Cer ceramide; DG diacylglycerol; FA free fatty acids; HexCer glycosylceramides; LPC lysophophatidylcholine; LPE lysophosphatidylethanolamine; LPG lysophosphatidylglycerol; LPI lysophosphatidylinositol; NAE N-acyl ethanolamines; PC phosphatidylcholine; PE phosphatidylethanolamine; PG phosphatidylglycerol; PI phosphatidylinositol; SM sphingomyelin; TG triacylglycerol.

Among the modulated lipids, fatty acids resulted increase after 7 days under simulated microgravity condition. Interestingly, all modulated FAs (FA 20:3,

FA 20:4, FA 20:5, FA22:5 and FA 22:6) but one (FA 18:1), have polyunsaturated chains (figure 4A). The same trend is shared with some PCs and PEs, like PC 18:0_20:4, PC 16:0_18:0, PE O-18:1_20:4 and PC 18:1_20:4 (figure 4B). Furthermore, these glycerophospholipids are composed by arachidonic acid (C20:4), stearic acid (C18:0), palmitic acid (C16:0) and oleic acid (C18:1).

11 LPCs were identified, with an average of 19 carbons and 1 unsaturation; the LPC with the shorter carbon chain is the LPC 16:0 and the one with the longer carbon chain is LPC 28:1. There are two LPCs with the presence of an alkyl ether substituent: LPC O-18:1 and LPC O-16:1. The following LPCs species reflect the trend of the entire class, suggesting that there is not a single lipids that have a higher impact on the total concentration: LPC 16:1; LPC 20:4; LPC 18:1; LPC 18:2; LPC 20:1; LPC 20:3; LPC 28:1; LPC O-18:1 and LPC 16:1 (figure 5A). LPE class was also identified with 13 lipids, sharing the same characteristic of the LPC class. Notably, there were more species with an alkyl ether substituent (LPE O-16:1; LPE O-18:1; LPE O-18:2; LPE O-24:2 and LPE O-3:0). Also for this class most lipids shared the trend of the total class: LPE 16:1; LPE 18:0; LPE 18:1; LPE 18:2; LPE 20:4; LPE 22:6 LPE O-16:1; LPE O-18:1; LPE O-18:2 (figure 5B).

As regard the CAR class, only four lipids were identified, one with a short chain (CAR 4:0) and three with medium/long chains (CAR 16:0; CAR 16:1; CAR 18:1).

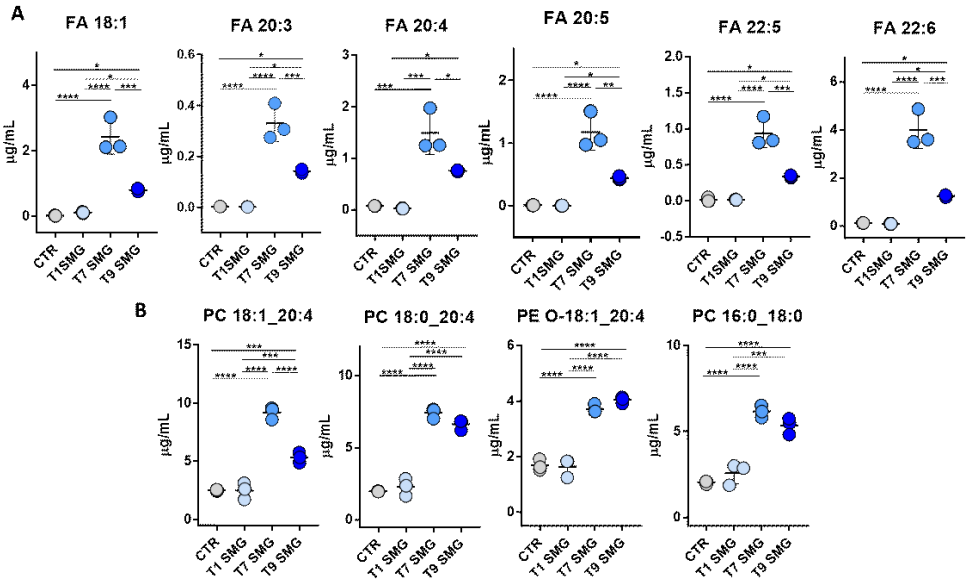


**Figure 4:** box plot of the abundances of FA 18:1, FA 20:3, FA 20:4, FA 20:5, FA 22:5, FA 22:6 (**A**). Box plot of the abundances of PC 18:0_20:4; PC 16:0_18:0; PE O-18:1_20:4; PC 18:1_20:4 (**B**).

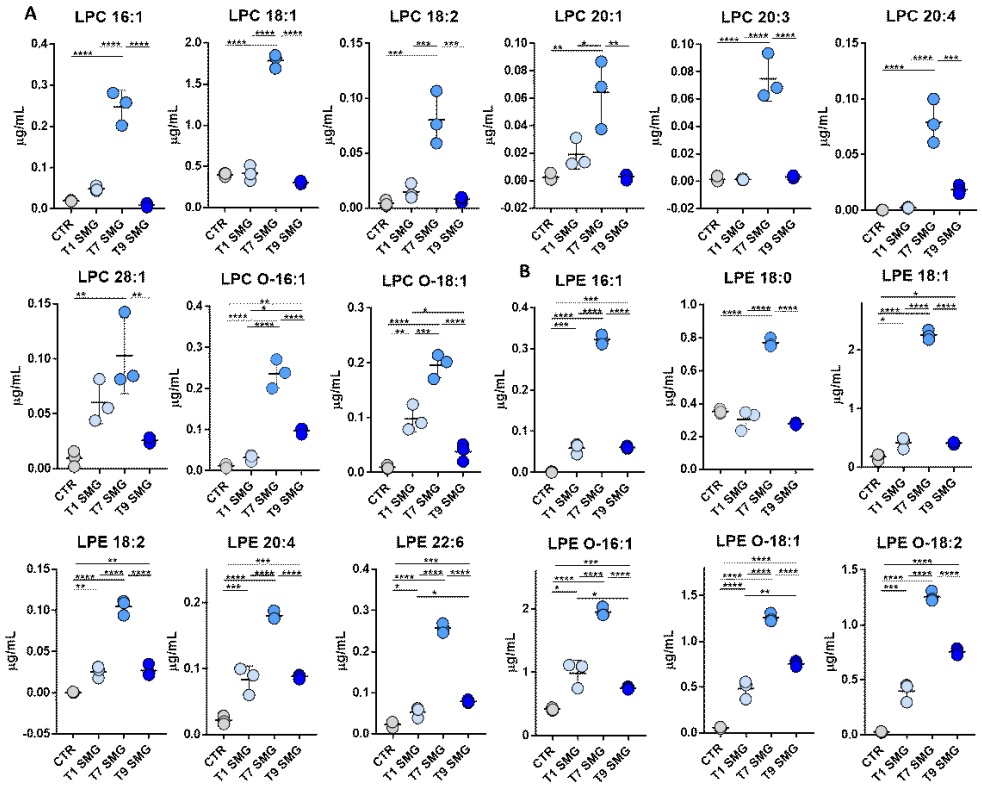


**Figure 5**: box plot of the abundances of LPC 16:1; LPC 20:4; LPC 18:1; LPC 18:2; LPC 20:1; LPC 20:3; LPC 28:1; LPC O-18:1 and LPC 16:1 (**A**). Box plot of the abundances of LPE 16:1; LPE 18:0; LPE 18:1; LPE 18:2; LPE 20:4; LPE 22:6 LPE O-16:1; LPE O-18:1 and LPE O-18:2 (**B**).

## *Lipidome alteration in PDAC cells between T1 SMG, T7 SMG and T9 SMG*

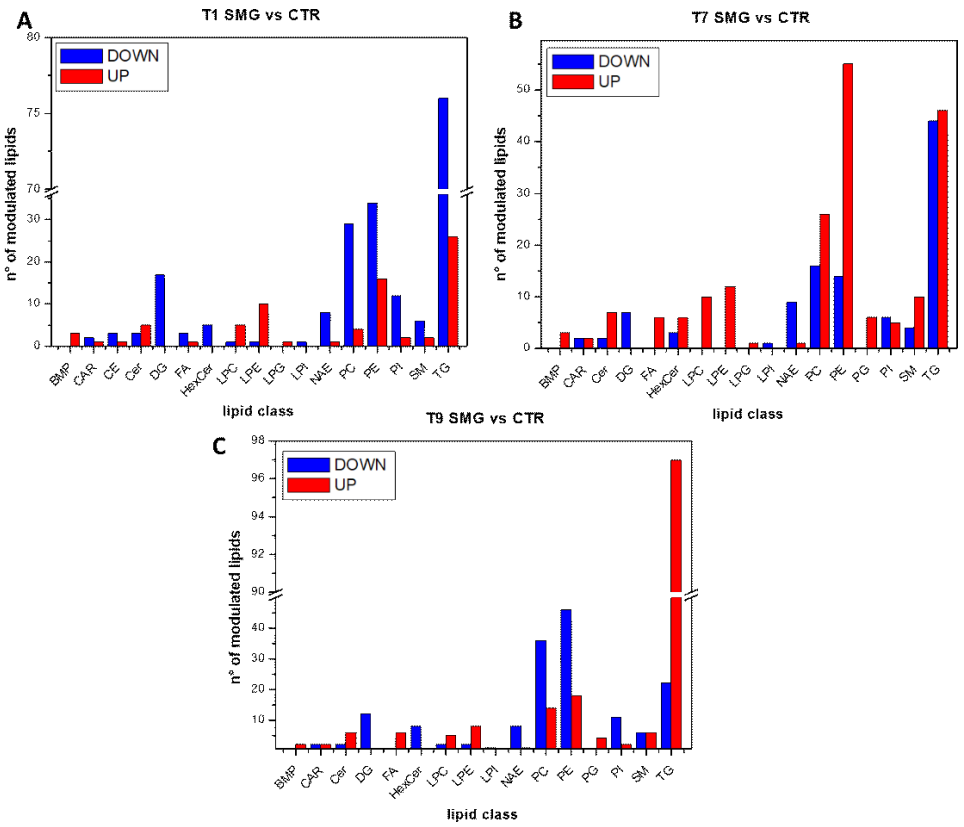


**Figure 6**: histograms with number of modulated lipids per class and donut charts of the percentage of modulated lipids per class: T1 SMG vs CTR (**A**), T7 SMG vs CTR (**B**), T9 SMG vs CTR (**C**). Legend: blue down-modulated and red up modulated lipids. FC > 1.3, *p*-value ≤ 0.05 thresholds.

Figure 6A, B and C report the histograms with the number of modulated lipids for each class in the comparison between the groups: T1 SMG vs CTR, T7 SMG vs CTR, T9 SMG vs CTR, respectively. For all the comparisons, we found a great number of modulated lipids, in detail: T1 SMG vs CTR 80 down-regulated and 195 up-regulated; T7 SMG vs CTR 197 down-regulated and 108 up-regulated; T9 SMG vs CTR 177 down-regulated and 108 up-regulated. The modulated lipids belong to all the lipid classes identified.

In particular, from the histograms, it is worth to note that there is a similar behavior in the classes involved in the modulation. As previously observed from the total lipids, at the 7$^{th}$ day there is an increase in glycerophospholipids (LPC, LPE, PC, PE, and PG) (figure 6B); while at 9$^{th}$ day it is confirmed the up-modulation of TG and the decrease of the other glicerophospholipids classes (figure 6C), which have the same trend after 24h (figure 6A).

These results suggest that there is a clear modification of lipids metabolism that bring to important changes in lipids after 7 days under microgravity condition, then, after this time, the lipids seems to return to the initial state.

This particular trend seems to be confirmed also by the comparison T1 SMG vs T7 SMG (figure 7A) where we can see that all the lipids are down modulated, especially PC and PE class, with 35 and 67 lipids respectively. While the comparison T1 SMG vs T9 SMG (figure 7B) did not show a marked trend, just the DG and TG classes have a great number of down modulated lipids. As regards the PC and PE ones there is no evidence of a clear trend (8 and 12 lipids down and up modulated respectively in PC class; 13 and 16 down and up modulated respectively in PE class).

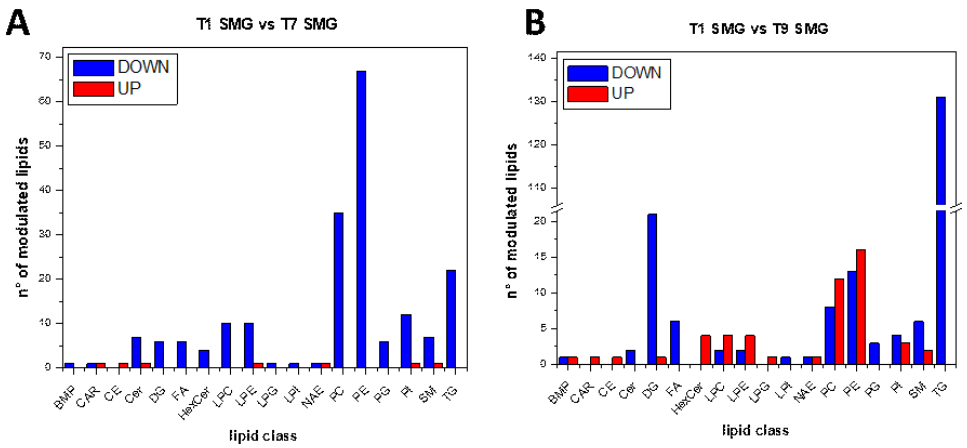


**Figure 7**: histograms with the number of modulated lipids per class: T1 SMG vs T7 SMG (**A**), T1 SMG vs T9 SMG (**B**). Legend: blue down-modulated and red up modulated lipids. FC > 1.3, *p*-value ≤ 0.05 thresholds.

### *Proteome and trascriptome alteration in PaCa-44 cells induced by SMG*

Lipidomic results were also supported by transcriptomic and proteomic analysis that showed a clear time dependent effect of microgravity on PDCA cells. SMG induces stemness enrichment: after 9 days the specific stemness-related genes Nanog, Sox2 and Oct4 were found increased with respect to the cells in adhesion. Proteomics confirmed these findings with the up modulation at 9 days of IL-8 signaling, involved in stemness, neo-angionenesis and EMT process regulation. Furthermore, one of the pathway most modulated by SMG exposure is the "Regulation of actin-based motility by Rho", that is involved in the cytoskeleton reorganization inducing actin migration toward the external plasma membrane.

## ***Discussion***

The effects of simulated microgravity were investigated over time on human pancreatic adenocarcinoma cells line (PaCa-44). Lipidomic, proteomic and transcriptomic analysis pointed out different effects of SMG on PaCa-44 cells, such as alteration in migration and cytoskeletal organization, leading to morphological changes in tumor cells inducing the acquisition of a mesenchymal phenotype, supporting the spreading of cancer cells and the acquisition of stemness characteristic.

Lipidomics added some clarification to those findings, suggesting a role of lipids in cell metabolism.

The importance of lipid metabolism in cancer stem cells is well known: it is essential for the stem properties and to satisfy their biomass and energy demands, which ultimately lead to growth and their typical aggressiveness. Cancer stem cells are also characterized by an elevated β-oxidation to support their survival during extreme conditions. Among modulated lipids, fatty acids

resulted increased after 7 days under microgravity condition. Fatty acids could be used as substrates to produce TGs by esterification with diacylglycerols, or they can be simply stored in the form of TG to later generate energy through β-oxidation. Thus, triglycerides are packed into lipid droplets, which have been shown to accumulate under hypoxic condition and are associated with higher tumor aggressiveness [13]. At 9 days, the increment of TG together with the reduction of LPC, LPE and FA suggests the synthesis of novel triglycerides, phosphatidylcholine and phosphatidylethanolamine (PC and PE), probably to sustain the request of membrane lipids. In particular, we observed an increase of PC 18:1_20:4; PC 18:0_20:4, PC O-18:1_20:4 and PE 16:0_18:0, supporting the hypothesis of a remodeling of the cellular membrane.

The high degree of unsaturation makes these metabolites reactive and susceptible to oxygenation and hydrogenation reactions, suggesting a metabolic flexibility that allows cells to adapt their metabolism to survive in hostile conditions, typical of CSCs [14]. Furthermore, the polyunsaturated fatty acids are rapidly released by cell membranes in response to stress or altered homeostasis, making them available for oxidative metabolism by COX, LOX and P450 enzymes [14].

Free fatty acids can also couple with CoA to form acyl CoA moieties that are then transferred to carnitine to generate acyl carnitine, which subsequently enters the mitochondrial matrix via the carnitine shuttle [15]. In order to understand if there is an impairment of the β-oxidation over time, we focused our attention on the acylcarnitine class. The acylcarnitine to L-carnitine ratio is recognized as a marker of carnitine deficiency and associated to mitochondrial β-oxidation [16]. In addition, the trend of this ratio is also maintained between long-intermediate-chain acylcarnitines (C16-20) compared to short-chain ones (C4) (figure 8). Our data shows an increased

(C16-20)/(C4) ratio over the time, suggesting an impairment of the β-oxidation [17].

Furthermore, proteomic and transcriptomic results showed an up-regulation of several proteins involved in autophagy biological pathway. Metabolic studies have reported that in pancreatic cancer cells possessing CSCs characteristics, there is an increased autophagy and lysosome activity, suggesting that metabolic alterations and active autophagy are critical features of cancer stem cells [18].

Our results showed a clear alteration of the ceramide levels during the days in microgravity and it was showed that this lipid class has been implicated in the autophagy induction [19].

Even if the role of ceramide in the autophagy process is still unclear, it was suggested that chain length-specific ceramides may differentially regulate autophagy [19].

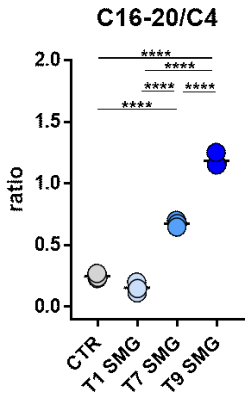


**Figure 8**: trend over time of the ratio long-intermediate-chain acylcarnitines (C16-C20) to short-chain ones (C4).

Understanding the effects of different G forces on tumor cells is the first step toward developing new anti-cancer treatments.

Using a lipidomics approach, together with proteomics and transcriptomics, to study the impact of SMG to PDCA cells (PaCa-44) over the time (24h, 7 and

9 days), allow us to elucidate the biological alteration occurring in cancer cells due to the condition of microgravity.

In the first 24 hours, the cells gather energy surplus (ATP) in order to survive SMG exposure, by activating fatty acids β-oxidation in the perissosome. This mechanism is suggested by the increase of acyl-Coa dehydrogenase very long (ACADV) from proteomics results and supported by lipidomics: in fact, we have found a decrease of polyunsaturated FAs.

The prolonged exposure (7 days) to SMG increased the synthesis of new phospholipids (as indicated by the increase of total LPC, LPE, and in particular some species of PC and PE) and FA. These classes are essential to sustain the formation of novel membrane lipids.

It has been demonstrated that the axis PI3K/mTOR/PKC induces calcium-dependent phospholipase A2 (cPLA2) involved in the release of arachidonic acid, oleic acid (FA 18:1) and other bioactive lipids (such as eicosanoids) [20], that trigger the aggressive phenotype of CSCs [21,22].

Through the production of PC and PE from LPC and FA, after 9 days the cells undergo significant membrane remodeling. At this time point we observed a reduction in total LPC and LPE as well as FA and, on the contrary, an increase in some species of PC and PE (composed by arachidonate and oleate, involved in the mobilization enhancement).

These findings are particularly significant because they suggest, for the first time, the cell transition toward a more stem and aggressive phenotype generated by SMG exposure over time. Because this cell rearrangement may impact tumor cells' drug sensitivity, we will test pancreatic cancer cells' response to anti-neoplastic treatments under simulated microgravity in the future.

# *Proteomic and lipidomic alterations in mice exposed to hypergravity*

## *Introduction*

From the origin of life on Earth, gravity has never changed. This constant mechanical force (G) has strongly impacted on the evolution of all living beings.

Since 3rd November 1957, when the dog Laika was launched into space by Russian scientists, the comprehension of the effect of different G forces on animals, particularly on mammals, became one of the most important priorities of researchers. In the last few years, thanks to the technological innovation, the interest on space flights has strongly grown: today, also normal people can hope to have the possibility to travel in space.

In orbit, the absence of gravity creates a microgravity environment, while take-off and landing of spaceflights and parabolic flights generate a condition of hypergravity. Despite it is well-known that an altered gravity is a stress factor that influences the physiological systems, studies on different gravitational forces are limited due to the cost and the poor availability of spaceflight missions. For these reasons, several ground-based models to simulate hypergravity conditions have been developed. All these models act mechanically and can simulate some of the chronic stress factors concerning spaceflight experiments, such as exposure to a novel environment, cephalic fluid distribution shifts, changes in limbs loads, and orthostatic intolerance [23].

Several studies have investigated the effect of different gravity forces on cells, bones, and muscular tissues [24–27]. Muscle mass, composition, and contractility, as well as bone density, can be negatively affected by hypergravity, with long-term consequences even after the return to normal

gravity [28]. Moreover, hypergravity affects myoblast proliferation and differentiation, PC12 neuron-like cell differentiation *in vitro* [29], and cyclooxygenase-2 expression in the heart vessels *in vivo* [30]. Chronic exposure to hypergravity conditions induces dysregulation of immune functions [31] and furthermore, it also decreases learning ability [32] and increases anxiety and stress response [31,33], effects potentially detrimental to cytoskeletal and organelle structures, together with energy metabolism in general. Even the liver, which is characterized by a high energy metabolism, just because of its sponge-like nature, may be more vulnerable to hemodynamic changes such as physical or compressional stress induced by spaceflights.

Although hypergravity seems to greatly impacts the biology of living beings, little is known about circulating lipids and proteins and its effect on living beings' biochemical pathways. Additionally, some studies focused on the effect of space radiation on the splenic metabolome, identifying metabolites enriched in purine metabolism, tricarboxylic acid cycle, fatty acids, acylcarnitines, and amino acids [34].

An untargeted metabolomic screening of blood plasma and a targeted analysis of the urinary metabolome were included in the well-known NASA twin study, which investigated the impact of the spaceflight environment on an astronaut on a year-long mission and his Earth-bound twin. The levels of metabolites linked to genotoxicity and inflammation, as well as amino acids, were considerably altered in plasma and urine of the astronaut. This exhaustive study therefore reported the effect of spaceflight, and in general of a microgravity condition on a human [35].

As regard proteomics, targeted [36] and untargeted [37] analyses have been both performed in order to characterize the plasma of astronauts in orbit, focusing more on microgravity [38] rather than on hypergravity condition.

Moreover, a comprehensive investigation on the proteome changes due to chronic hypergravity was carried out in *Drosophila melanogaster* adults [39] using high-resolution mass spectrometry.

The aim of the present study was to understand how a gravity impairment caused by hypergravity may impact on circulating proteins and lipids in a mouse model. For this reason, five mice were subjected to simulated hypergravity (SHG) for one month and then compared to control animals kept in normal conditions (TC). Proteomics and lipidomics analysis were performed on plasma samples and the biochemical changes were analyzed using bioinformatic tools. Our results showed a modulation of lipids belonging to different classes and proteins implicated in several biological processes, shedding new light on the effect of SHG on mammals, opening interesting perspectives on the necessity to deepen the study of the effect of this altered condition on mammals, as a potential to develop a hypergravity medicine, similar to the isobaric one.

## *Materials and Methods*

Materials and methods of this study are the same as previously reported in Chapter 2 page 51. At the end of Chapter 3, in the section “Materials and Methods”, instead, are reported the details for the proteomic methods.

## *Results*

Figure 9 reports the details of the present study: 5 mice were subjected to simulated hypergravity (SHG) for one month, while 6 mice were maintained in normal condition (TC). All the animals were fed the same way. At the end of the experiment, blood was collected, and plasma was prepared and stocked at -80°C until the lipidomic and proteomic analysis. High resolution mass spectrometry coupled to liquid chromatography was then used to detect

alterations in the plasma lipidome and proteome. Finally, a bioinformatic analysis was used to mine the biological effect of SHG on mice.

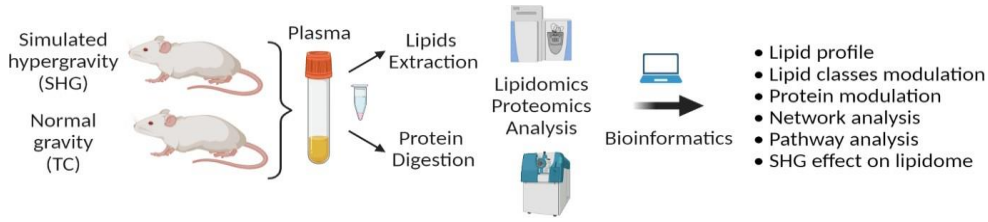


**Figure 9:** experimental design of the study. Plasma from mice subjected to SHG for one month was compared to plasma from mice maintained in normal conditions. Plasma lipidomics and proteomics followed by bioinformatic analysis were used to map the biochemical alterations caused by hypergravity.

## *Lipids are strongly altered by simulated hypergravity*

The lipidomic analysis of the plasma samples clearly showed how hypergravity impacted the circulating lipidome in a mouse model. A total of 443 lipids belonging to 19 different lipid classes were identified, including: 9 acylcarnitines (CAR), 9 cholesteryl esters (CE), 8 ceramides (Cer), 28 diacylglycerols (DG), 9 free fatty acids (FA), 4 glycosylceramides (HexCer), 25 lysophophatidylcholines (LPC), 13 lysophosphatidylethanolamines (LPE), one lysophosphatidylinositol (LPI), 3 monoacylglycerols (MG), 10 N-acyl ethanolamines (NAE), 90 phosphatidylcholines (PC), 45 phosphatidylethanolamines (PE), 30 phosphatidylinositols (PI), 5 esterified deoxycholic acids (SE), 4 sulphonolipids (SL), 21 sphingomyelins (SM), 4 sterol lipids and 124 triacylglycerols (TG).

The hierarchical clustering heatmap (figure 10A) highlighted the presence of two distinct groups of samples based on the treatment, in red the mice subjected to SHG while in green the mice kept in normal condition. In addition, also the partial least square discriminant analysis (figure 10B) showed the presence of a lipidomics signature associated to hypergravity; the most predictive or discriminant features, that are potentially useful in helping

sample classification, were also determined through the VIP (variable of importance in projection) score. The VIP score summarized the most prominent molecules contributing to the observed phenotypic variations in the SHG (figure 10C).

The monovariate statistical analysis reported the modulation of 156 lipids from 14 different lipid classes, with the TG class characterized by the largest number of modulated lipids (n = 97): 96 lipids were down-regulated while only one increased its level after SHG. The second most modulated lipid class was the PC one, with 39 altered lipids, 37 of which were down-modulated. Figure 10D reports the abundance percentage of down-modulated lipids for each class, while figure 10E reports the number of up (red) and down (blue) modulated lipids per class: the analysis confirmed a strong modulation of TG, ST, LPE and Cer, with 91%, 97%, 88% and 84% of total lipids modulated, which were almost all decreased after SHG. Glycerophospholipids (LPC, LPE, PC, PE and PI) resulted the most impacted classes by SHG, with a global decrease of their concentrations.

The only up-modulated class was the CAR one, constituted by the acyl esters of carnitine, which was characterized by the up-regulation of 6 lipids, namely CAR 14:1, CAR 14:2, CAR 16:0, CAR 18:1, CAR 18:2, and CAR 20:4 (figure 10E), also confirmed by the enrichment analysis (figure 10F).

Interestingly, hypergravity caused the modulation of two sterol lipids namely ST 27:1;O;S (cholesterol sulfate) and ST 28:1;O;S which are two important sterol sulfates.

The down-modulated TGs were characterized by a long carbon chain (average of 54 carbon atoms) and, as suggested by the enrichment analysis, the most relevant are composed by unsaturated species: an average of 4 unsaturations were present on the acyl chains, with oleic and linoleic acids the most abundant chains. PC class was mainly composed by the same acyl chains of

TG, while PEs reported also the presence of arachidonic acid chains (PE 18:0_20:4, PE 18:1_20:4 and PE 16:0_20:4).

All the ceramides, except one (Cer 18:2;2O/24:1), were constituted by one oleic acid chain such as Cer 18:1;2O/24:0 or Cer 18:1;2O/24:1. Noteworthy, all ceramides were down-modulated after SHG. Another modulated sphingolipid class was the sphingomyelin, even if only few species (n = 2) decreased their levels, representing 5% of the total SM abundance.

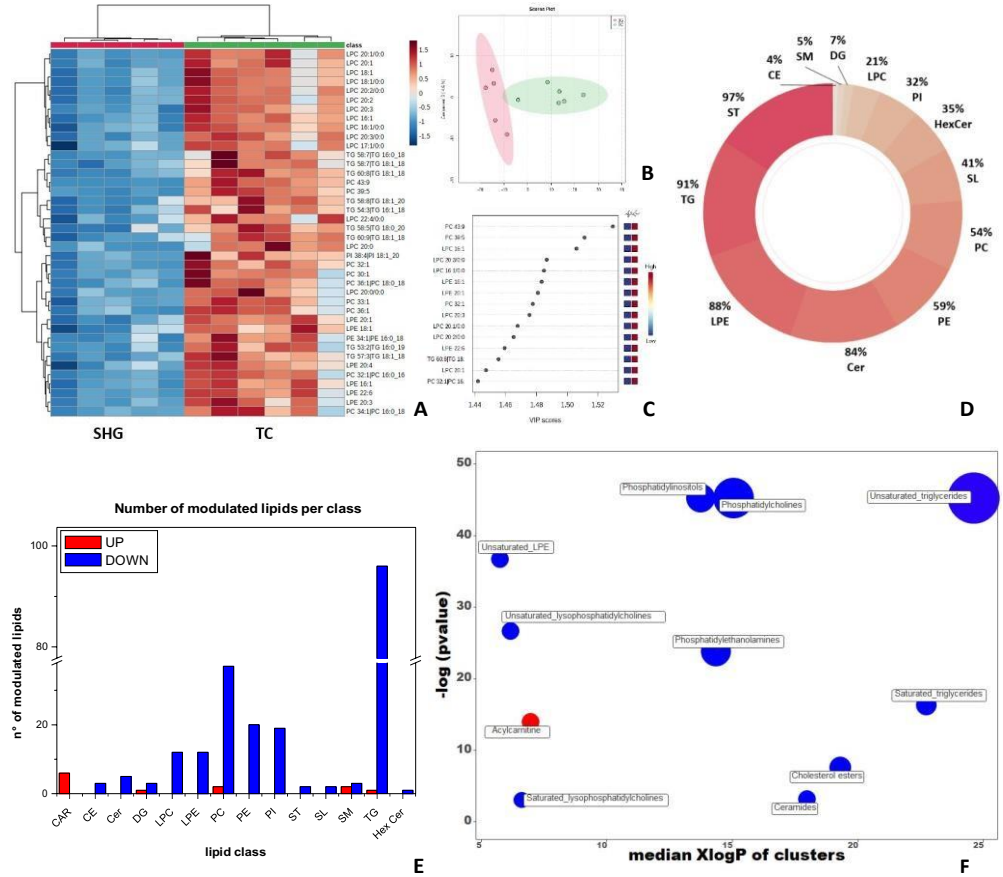


**Figure 10**: effect of simulated hypergravity on plasma lipidome. Hierarchical clustering heatmap (**A**) of the lipidomic profiling of mice subjected to SHG (red) and mice kept in normal condition (green); partial least square discriminant analysis (**B**); VIP score of most important lipids (**C**); abundance percentage of down-modulated lipids for each class (**D**); number of up (red) and down (blu) modulated lipids per class (**E**); enrichment analysis calculated by Kolmogorov–Smirnov test. (red:

increased, blue: decreased), each bubble represents a cluster of lipids with similar structure (**F**).

The MetaMapp visualization reported in figure 11 clearly shows the impact of SHG on the plasma lipidome of the mouse model: red nodes represent lipids with increased concentration, blue nodes represent lipids with decreased concentration, while light grey nodes represent lipids that were not modulated. The most increased lipid was CAR 18:2 (FC = 3.67), while the most decreased was the TG 15:1_16:1_18:2 (FC = 0.05). No fatty acids were found to be somehow regulated.

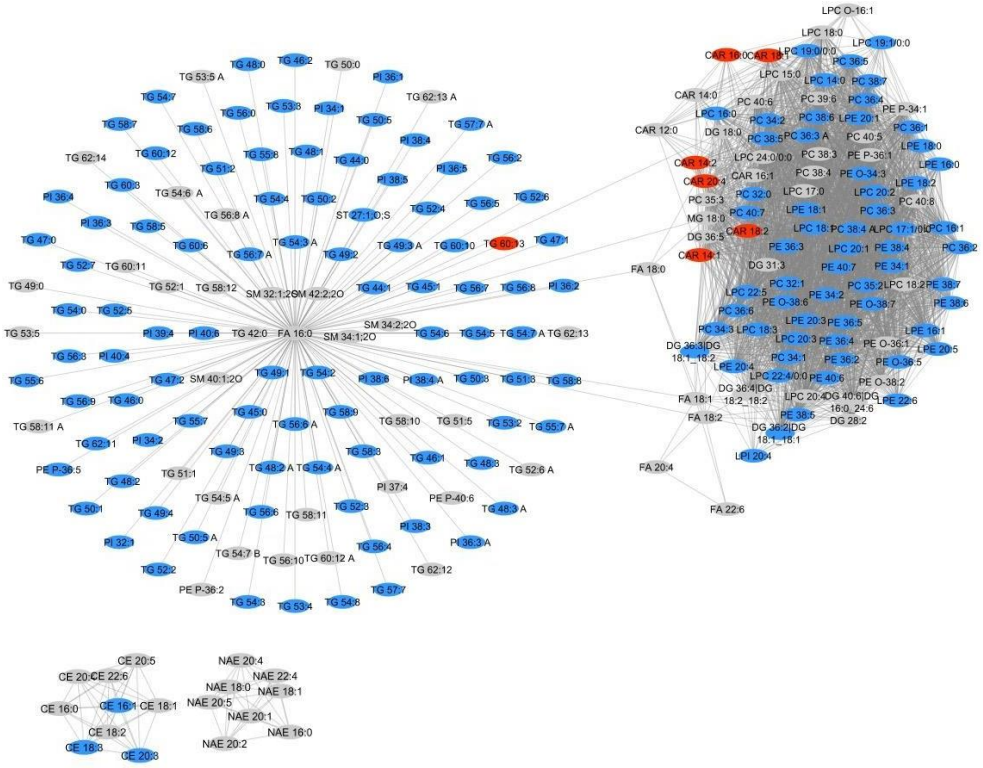


**Figure 11**: MetaMapp visualization of the lipidomic changes in mice subjected to SHG. Lipids with increased concentration are depicted using red nodes, lipids with decreased concentration are represented by blue nodes, while the ones that present no change are depicted in light grey. The central group are neutral lipids, sphingomyelin, phosphatidylinositol and palmitic acid. Lipids grouped on the left are cholesteryl ester

and N-acyl ethanolamine, while on the right are reported glycerolipids, diacylglycerol and monoacylglycerol.

## *Coagulation, cholesterol metabolism and immune response proteins are influenced by SHG*

Untargeted proteomic analysis was performed on plasma from SHG and TC mice to investigate the effect of hypergravity on the circulating proteome. In order to improve the quantification of low abundant proteins, all the samples were depleted of the 14 most abundant proteins and then digested and analyzed with SWATH-MS (Sequential window acquisition of all theoretical mass spectra) [40]. A total of 295 proteins were identified, 203 of which were quantified in a reproducible manner. Fold change analysis of SHG mice versus control group revealed the presence of 28 modulated proteins (*p-value* $\leq 0.05$ and fold change > 1.3) as reported in figure 12A.

To assess the overall impact of simulated hypergravity, protein abundances were analyzed using multivariate statistical analysis. Principal component analysis (figure 12B) but also hierarchical clustering heatmap analysis (figure 12C) clearly separated the samples according to the groups, indicating the presence of a proteomic signature associated to the effect of SHG.

The statistical analysis showed that hypergravity caused the up-regulation of 9 proteins, in detail: CFAD_MOUSE (FC = 7.61), EST1C_MOUSE (FC = 2.067), CBG_MOUSE (FC = 1.98), ANGT_MOUSE (FC = 1.68), GPX3_MOUSE (FC = 1.58), MUG1_MOUSE (FC = 1.57), CO3_MOUSE (FC = 1.51), ITIH2_MOUSE (FC = 1.50), CERU_MOUSE (FC = 1.48). On the other hand, 19 proteins resulted under-expressed as reported in table 1 (figure 13A).

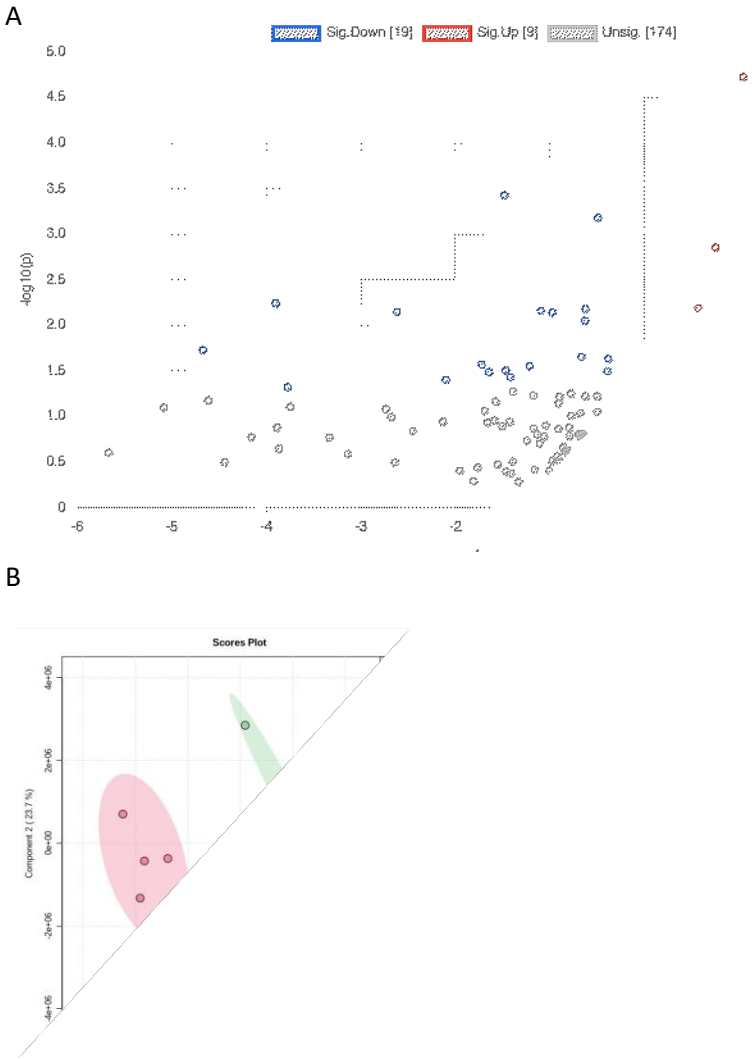


**Figure 12**: effect of simulated hypergravity on plasma proteome. Volcano plot of the modulated proteins (*FC* > 1.3 and *p*-value ≤ 0.05) (**A**); principal component analysis (PCA) of the two groups (red SHG group and green TC group) (**B**); Hierarchical heatmap (**C**).

To obtain a global overview of the hypergravity impact on mice, the modulated proteins were analyzed with bioinformatics tools. STRING [41] software and ingenuity pathway analysis (IPA) [42] were employed to identify the main pathways, biological processes and molecular functions associated

with SHG. STRING analysis showed that hypergravity condition affects proteins that are related to the complement and coagulation cascades (figure 13B; red proteins: C9, C8a, C8g, CLU, CFD, C3, FGA, Serpina1a) and the cholesterol metabolism (figure 13B; purple proteins: APOE; APOA4; APOC1). Regarding KEGG pathway and biological process, defense response (green proteins: AGT; APOA4; CFD; CLU; C3; C9; C8a; C8g; EGFR; FA4; SAA4; Serpina1a) and humoral immune response resulted the most important functions involved (yellow proteins: C3; C9; C8a; C8g; CFD; FGA).

Furthermore, ingenuity pathway analysis (IPA) (figure 13C) reported the modulation of the following main pathways: LXR/RXR activation, FXR/RXR activation, acute phase response signaling, complement system, IL-12 signaling and production in macrophages, atherosclerosis signaling and production of nitric oxide and reactive oxygen species in macrophages. Some of these pathways were predicted inhibited: LXR/RXR pathway (AGT, APOA4, APOE, C3, C9, CLU, FGA, HPX, SERPINA1) with a *p*-value of 2.57E-14 and FXR/RXR pathway (AGT, APOA4, APOE, C3, C9, CLU, FGA, HPX, SERPINA1) with a *p*-value of 4.18E-14. As already observed by STRING analysis, most of the proteins associated to the modulated pathways are involved in inflammation, immune response, and coagulation.

**Figure 13**: over-expressed and under-expressed proteins in SHG mice (Log FC > 0.114 or Log FC < -0.114; *p*-value ≤ 0.05) (**A**); STRING network analysis of the regulated proteins (**B**). Legends: complement coagulation cascades pathway (red proteins) and cholesterol metabolism (purple proteins), defense response (green proteins) and humoral immune response (yellow); significantly altered pathways predicted by ingenuity pathway analysis for the comparison SHG vs TC mice; blue: predicted inactivated pathway (**C**).

**Table 1**: list of increased and decreased proteins in SHG mice with fold change and *p*-value

| Proteins | FC | *p*-value |
|---|---|---|
| PGM1_MOUSE | 5.00E-02 | 1.56E-02 |
| SNX33_MOUSE | 6.71E-02 | 5.75E-03 |
| PPGB_MOUSE | 7.33E-02 | 4.78E-02 |
| FAT2_MOUSE | 1.63E-01 | 7.15E-03 |
| MUP3_MOUSE | 2.34E-01 | 3.98E-02 |
| CO9_MOUSE | 3.04E-01 | 2.70E-02 |
| APOC1_MOUSE | 3.20E-01 | 3.26E-02 |
| APOE_MOUSE | 3.59E-01 | 3.80E-04 |
| SAA4_MOUSE | 3.62E-01 | 3.14E-02 |
| CO8G_MOUSE | 3.75E-01 | 3.72E-02 |
| CO8A_MOUSE | 4.31E-01 | 2.81E-02 |
| LIFR_MOUSE | 4.68E-01 | 6.94E-03 |
| A1AT1_MOUSE | 5.09E-01 | 7.24E-03 |
| FIBA_MOUSE | 6.31E-01 | 2.23E-02 |
| EGFR_MOUSE | 6.48E-01 | 8.92E-03 |
| CPN2_MOUSE | 6.51E-01 | 6.64E-03 |
| CLUS_MOUSE | 7.12E-01 | 6.60E-04 |
| APOA4_MOUSE | 7.63E-01 | 3.21E-02 |
| HEMO_MOUSE | 7.67E-01 | 2.33E-02 |
| CERU_MOUSE | 1.48E+00 | 6.45E-03 |
| ITIH2_MOUSE | 1.51E+00 | 1.61E-02 |
| CO3_MOUSE | 1.51E+00 | 4.25E-02 |
| MUG1_MOUSE | 1.57E+00 | 3.07E-02 |
| GPX3_MOUSE | 1.59E+00 | 1.47E-02 |
| ANGT_MOUSE | 1.69E+00 | 1.40E-03 |
| CBG_MOUSE | 1.98E+00 | 3.66E-02 |
| EST1C_MOUSE | 2.07E+00 | 1.90E-05 |
| CFAD_MOUSE | 7.61E+00 | 3.86E-02 |

## *Discussion*

Hypergravity, and in general a variation of the gravity force for a prolonged time, is a stressful condition for animals. Cells, bones and muscular tissue analysis have shown important modification in the phenotype and in biological functions [27,43,44]. Furthermore, it may modify the circadian cycle [45], but it may also have an impact on the serotonin receptors in the brain of mice [46].

Although several researches investigated the effect of hypergravity, a comprehensive analysis of the plasma lipidome and proteome not only is still lacking, but it could also shed new light on how this condition impact on the feeling good of animals.

In the present study, the aim was to fill this gap by performing a profile analysis of the plasma proteome and lipidome of 11 mice, 6 of them exposed for 1 month to SHG and 5 maintained in normal condition. We then measured the proteins and lipids alterations caused by SHG to figure out how hypergravity impacted on mice.

The first striking results is that SHG promoted a global down-modulation of glycerophospholipids (LPC, LPE, PC, PE and PI), and TG. These lipids are the core structure of lipoproteins: phospholipids PCs and PEs are the constituents of the plasmatic membrane that enclose TGs, cholesterol, and cholesteryl ester. A depletion of these lipids has been already identified as the cause of the lipid raft disruption that lead to a remodeling of the plasma membrane [47]. Lipoproteins are also made by apolipoproteins (APOA4, APOE, and APOC1). The proteomics analysis reported a down-modulation of these proteins after SHG, thus supporting an alteration of the lipids transportation that involves lipoproteins.

The origin of the circulating lipoproteins is still unclear. The lipid transport system in plasma involves two pathways: an exogenous route for the transport

of cholesterol and triglycerides absorbed from dietary fats in the intestine, and an endogenous system through which cholesterol and triglycerides reach plasma from the liver and other non-intestinal tissues [25]. Thus, the investigation of cholesterol levels would add more biological information on the specific processes involved.

In agreement with previous data on lipoproteins and glycerophospholipids, we found a decrease of cholesterol in SHG, even if the modulation was not statistically different between the two groups (figure 14). A decrease of cholesterol sulfate (ST 27:1;O;S) was also detected. In human plasma, cholesterol sulfate, which is the most abundant sterol sulfate, has a stabilizing function on the membrane, supports platelet adhesion and it is involved in signal transduction. It has been already observed that the condition of stress caused by hypergravity can promote a change in the levels of molecules associated with the energy metabolism, such as cholesterol, CE and TG [48]. Furthermore, the bioinformatic analysis suggested a potential link between liver activity and hypergravity through the alteration of LXR/RXR and FXR/RXR pathways. It has been already demonstrated that hypergravity has an effect on the internal organs of animals [28], and the liver resulted the more affected one due to its spongy structure. Changes in LXR/RXR and FXR/RXR pathways can be a result of the down-regulation of proteins and lipid classes found in the plasma after the prolonged exposition to SHG condition. The RXR is a nuclear hormone receptor belonging to the retinoid receptor family. These kind of nuclear receptors are a class of ligand-activated transcription factors that play important roles in physiology [49]. They regularly interact with other retinoid receptors, such as the LXR (liver X receptor) and the FXR (farnesoid X receptor). In particular, the farnesoid one promotes cholesterol homeostasis, triacylglycerol metabolism, and inflammation suppression [50]. LXRs also control several enzymes involved in the remodeling of lipoproteins

[51]. In addition, LXRs are recognized as critical regulators of lipids homeostasis at cellular and systemic levels, including sterols, fatty acids, and phospholipids. It is worth to note that at the molecular level, FXR controls the TG metabolism by regulating hepatic de novo lipogenesis [52].

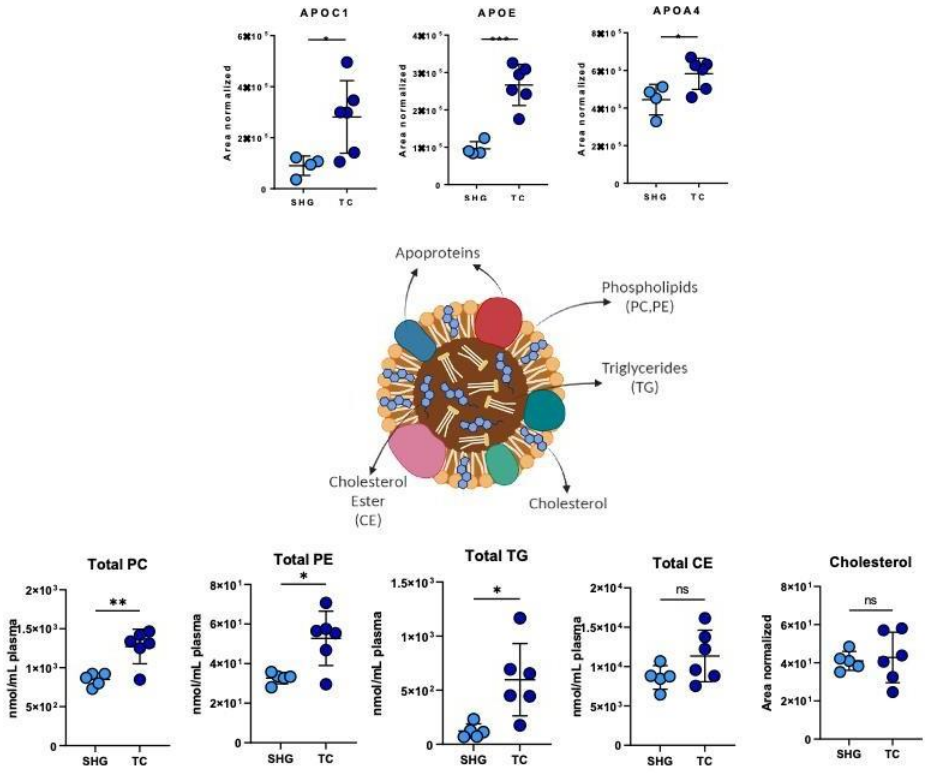


**Figure 14**: impact of simulated hypergravity on lipid transport system in plasma. Total lipid classes (PC, PE, TG), Cholesterol and CE reported as nmol/mL plasma; modulated proteins APOE, APOC1 and APOA4 reported as normalized area. *p*-value < 0.1 = * *p*-value < 0.01 = **; *p*-value < 0.001 = ***.

Furthermore, a study of lipid fraction deriving from mouse thyroid tissue [53], reported a down-modulation of cholesterol and PCs such as PC 18:1_18:0 and PC 16:0_18:1. These data suggested that hypergravity may directly impact on lipids rafts, thus remodeling the cell membrane structure.

Lipid rafts are made up not only of lipids, but also of proteins that house multiple receptors and regulatory molecules, acting as a platform for signal

transduction [54]. It has been reported [55] that in several cell types there is a rapid change of the cytoskeleton occurring as a reaction to gravitational modification, leading to a modification of the lipids raft and changes in surface receptors. This remodeling could have consequences on the immune response, and further investigations at the cellular level are needed. But interestingly, our results reported a down-modulation of AGT, APOA4, CFD, CLU, C3, C9, C8a, C8g, EGFR, FA4, SAA4, Serpina1a and FGA, leading to a potential inhibition of the defense and humoral immune response. A modulation of the innate response was already observed in larvae and adult subjects of Drosophila during a space flight [56]. In particular, it was found that parabolic flights can affect the entire human immune system, by lowering the number of distinct leukocytes [57]. Under gravitational stress, the number of basophils and eosinophils dropped, and the number of naive and memory T and B cells decreased. Consequently, it is possible that gravitational stress can have clinically relevant impacts on the control of immune responses.

In conclusion, our data demonstrated that hypergravity impacted on the modulation of several lipids and proteins implicated in important pathways and biological processes. The most relevant observation was the modulation of membrane lipids and their role in the transport of lipids by lipoproteins, suggesting an impairment of the normal activity of the liver induced by hypergravity, involving also the LXR/RXR and FXR/RXR pathways. In addition, the study suggested a potential involvement of protein receptors through the remodeling of plasmatic membrane.

## *Conclusion of chapter 3*

In this chapter, an *in vitro* and *in vivo* studies were performed in order to understand the effects of microgravity on cells behaviors and of hypergravity on circulating lipids and proteins of mice. This two particular condition are present during space missions, spaceflight and parabolic flights.

In the first study, the use of lipidomics, together with proteomics and transcriptomics, lead us to understand the biological alteration occurring in cancer cells due to the condition of microgravity on PDCA cells (PaCa-44) over time (24h, 7, and 9 days).

From both type of data (increase of acyl-Coa dehydrogenase very long (ACADV) from proteomics results and decrease of polyunsaturated FAs from lipidomic ones) it was suggested that there is a β-oxidation involvement in the perissosome in the first 24 hours, this because the cells had to survive SMG exposure. Furthermore, it was suggested the formation of novel membrane lipids by the increased levels of some phospholipids species (LPC, LPE, PC, and PE) and some FAs (FA 20:3, FA 20:4, FA 20:5, FA 22:5, FA 22:6 and FA 18:1).

After 7 days it was observed a reduction of total LPC and LPE as well as FA and, on the contrary, an increase in some species of PC and PE (composed by arachidonate and oleate, involved in the mobilization enhancement). These findings are particularly significant because they show, for the first time, the cell transition toward a more stem and aggressive phenotype generated by SMG exposure over time. Because this cell rearrangement may impact tumor cells' medication sensitivity, we will be testing pancreatic cancer cells' response to anti-neoplastic treatments under simulated microgravity in the future.

The second study showed the use of lipidomics and proteomics to investigate the lipidome and proteome alteration due to simulated hypergravity in mice. Our data demonstrated that hypergravity impacted on the modulation of several lipids and proteins implicated in important pathways and biological processes. The most relevant observation was the modulation of membrane lipids and their role in the transport of lipids by lipoproteins, suggesting an impairment of the normal activity of the liver induced by hypergravity, involving also the LXR/RXR and FXR/RXR pathway. In addition, the study suggested a potential involvement of protein receptors through the remodeling of plasmatic membrane.

# *Materials and Methods*

## *Mice Drawer System (MDS)*

Simulated hypergravity was performed using the mice drawer system (MDS) [58]. The mice were exposed to a 3G environment by means of the Large Diameter Centrifuge (LDC) for one month. Vivarium control mice were also considered in the experiment. One technical short stop for water/food refill and filter change was performed.

## *Plasma preparation for Proteomic Analysis*

For the extraction of proteins 12 µL of serum were used, that were previously depleted of high-abundance proteins using the Seppro IgY14 spin column kit (Sigma-Aldrich Inc., St. Louis, MO, USA), according to the manufacturer's procedure. The samples were transferred into an Amicon Ultra-0.5 mL 3-kDa centrifugal filter (Millipore, Billerica, MA, USA) following the manufacturer's procedure to collect high molecular weight proteins. The samples were then subjected to denaturation with TFE, to reduction with DTT 200 mM, to alkylation with IAM 200mM and to complete protein digestion with 2 µg of Trypsin/Lys-C (Promega, Madison, WI, USA). The peptide digests were desalted on the Discovery® DSC-18 solid phase extraction (SPE) 96-well plate (25 mg/well) (Sigma-Aldrich Inc., St. Louis, MO, USA). The SPE plate was preconditioned with 1 mL of acetonitrile and 2 mL of water. After loading the sample, the SPE was washed with 1 mL of water. For eluting the proteins 800 µL of a mixture of acetonitrile/water (80:20) was used [61]. After the desalting process, the sample was evaporated and reconstituted with 20 µL of water acidified with 0.05% formic acid. In each sample was spiked 2 µL of stable-isotope-labeled peptide standard, DPEVRPTSAVAA, Val-13C515N1 at V10, precursor monitored 609.8215+, 610.8242++ and

611.32553+++, with a retention time of 9.2 min and mass accuracy of 3.5 ppm, (Cellmano Biotech Limited, Anhui, China) used for instrument quality control.

### *LC-MS/MS proteins analysis*

Serum proteins were analyzed with the micro-LC Eksigent Technologies (Eksigent, Dublin, USA) system coupled with a 5600+ TripleTOF system (AB Sciex, Concord, Canada) equipped with DuoSpray Ion Source and CDS (Calibrant Delivery System). For the reverse phase chromatography a Halo C18 column (0.5 × 100 mm, 2.7 µm; Eksigent Technologies Dublin, USA) was used. The column was maintained at 40 °C. The mobile phase A was water and B was acetonitrile, both modified with 0.1% (v/v) formic acid, the flow-rate was 15.0 µL/min. The gradient increased from 2% to 40% of solvent B in 30 min. Injection volume was 4.0 µL. A

data-dependent acquisition (DDA) was used for identified proteins: mass range of 100–1500 Da (TOF scan with an accumulation time of 0.25 s), followed by an MS/MS product ion scan from 200 to 1250 Da (accumulation time of 5.0 ms) with the abundance threshold set at 30 cps (35 candidate ions can be monitored during every cycle). Only ESI positive mode was used for the proteomic analysis. The ion source parameters were set as follows: curtain gas (N2) 25 psig, nebulizer gas GAS1 25 psig, and GAS2 20 psig, ion spray voltage floating (ISVF) 5000 V, source temperature 450 °C and declustering potential 25 V.

As regard the label-free quantification, a cyclic data-independent analysis (DIA) was used. A 25-Da window was chosen: the mass spectrometer was operated so that a 50-ms survey scan (TOF-MS) was performed and subsequent MS/MS experiments were performed on all precursors. MS/MS experiments were carried out in a cyclical manner using an accumulation time

of 40 ms per 25-Da swath (36 swaths in total) for a total cycle time of 1.5408 s. The ions were fragmented in the collision cell using the rolling collision energy. The MS data were acquired with Analyst TF 1.7 (AB SCIEX, Concord, Canada). Two DDA and three DIA acquisitions were performed.
Peptides and corresponding proteins were identified using DDA followed by database search while the quantification was obtained by integrating the area under the chromatographic peak for each ion fragment of identified peptides by using the DIA file [62].

## *Protein database search*

Protein Pilot software v. 4.2 (SCIEX, Concord, Canada) and Mascot v. 2.4 (Matrix Science Inc., Boston, USA) was used in order to identified proteins from the DDA files. For both software, Trypsin was specified as the digestion enzyme. 2 missed cleavages were used for Mascot, setting the instrument to ESI-QUAD-TOF and specified the following modifications for the assay: carbamidomethyl cysteine as fixed modification and oxidized methionine as variable modification. An assay tolerance of 50 ppm was specified for peptide mass tolerance, and 0.1 Da for MS/MS tolerance. Peptide charges to be detected were set to 2 +, 3 + and 4 +, and the assay was set on monoisotopic mass [63]. The UniProt Swiss-Prot reviewed database containing mouse proteins (version 2015.07.07, containing 42,131 sequence entries) was used and a target-decoy database search was performed. False Discovery Rate was fixed at 1%.

## *Protein quantification*

To perform protein quantification, the extracted ion chromatogram of the unique ions for a given peptide was integrated. SwathXtend was employed to build an integrated assay library with the DDA acquisitions, with a protein FDR threshold of 1% [22].

PeakView 2.0 and MarkerView 1.2. (ABSCIEX, Concord, Canada) were employed to perform quantification. From the SWATH files the six peptides per protein with the highest MS1 intensity and the six transitions per peptide were extracted. Peptides in common were excluded as well as peptides with modifications. Peptides with FDR lower than 1.0% were exported in MarkerView for the *t*-test.

### *Bioinformatics and statistics software*

STRING software (http://string-db.org) [41] was used in order to find or predict possible protein interactions between the modulated proteins. Cytoscape 3.1.0 plug-ins ClueGO v 2.0.8 were also used for functional annotation clustering and network analysis of proteins [64].

## *Bibliography*


1. Iwase, S.; Nishimura, N.; Tanaka, K.; Mano, T. Effects of Microgravity on Human Physiology. In *Beyond LEO - Human Health Issues for Deep Space Exploration [Working Title]*; IntechOpen, 2020.
2. Grimm, D.; Egli, M.; Krüger, M.; Riwaldt, S.; Corydon, T.J.; Kopp, S.; Wehland, M.; Wise, P.; Infanger, M.; Mann, V.; et al. Tissue Engineering Under Microgravity Conditions–Use of Stem Cells and Specialized Cells. *Stem Cells and Development* **2018**, *27*, 787–804, doi:10.1089/scd.2017.0242.
3. Grimm, D.; Wehland, M.; Corydon, T.J.; Richter, P.; Prasad, B.; Bauer, J.; Egli, M.; Kopp, S.; Lebert, M.; Krüger, M. The Effects of Microgravity on Differentiation and Cell Growth in Stem Cells and Cancer Stem Cells. *STEM CELLS Transl Med* **2020**, *9*, 882–894, doi:10.1002/sctm.20-0084.
4. Thiel, C.S.; Tauber, S.; Seebacher, C.; Schropp, M.; Uhl, R.; Lauber, B.; Polzer, J.; Neelam, S.; Zhang, Y.; Ullrich, O. Real-Time 3D High-Resolution Microscopy of Human Cells on the International Space Station. *IJMS* **2019**, *20*, 2033, doi:10.3390/ijms20082033.
5. Growth of Endothelial Cells in Space and in Simulated Microgravity – a Comparison on the Secretory Level. *Cell Physiol Biochem* **2019**, *52*, 1039–1060, doi:10.33594/000000071.
6. Ma, X.; Pietsch, J.; Wehland, M.; Schulz, H.; Saar, K.; Hübner, N.; Bauer, J.; Braun, M.; Schwarzwälder, A.; Segerer, J.; et al. Differential Gene Expression Profile and Altered Cytokine Secretion of Thyroid Cancer Cells in Space. *FASEB j.* **2014**, *28*, 813–835, doi:10.1096/fj.13-243287.
7. Topal, U.; Zamur, C. Microgravity, Stem Cells, and Cancer: A New Hope for Cancer Treatment. *Stem Cells International* **2021**, *2021*, 1–9, doi:10.1155/2021/5566872.
8. Jhala, D.; Kale, R.; Singh, R. Microgravity Alters Cancer Growth and Progression. *CCDT* **2014**, *14*, 394–406, doi:10.2174/1568009614666140407113633.
9. Prasanth, D.; Suresh, S.; Prathivadhi-Bhayankaram, S.; Mimlitz, M.; Zetocha, N.; Lee, B.; Ekpenyong, A. Microgravity Modulates Effects of

Chemotherapeutic Drugs on Cancer Cell Migration. *Life* **2020**, *10*, 162, doi:10.3390/life10090162.

10. Ahn, C.B.; Lee, J.-H.; Han, D.G.; Kang, H.-W.; Lee, S.-H.; Lee, J.-I.; Son, K.H.; Lee, J.W. Simulated Microgravity with Floating Environment Promotes Migration of Non-Small Cell Lung Cancers. *Sci Rep* **2019**, *9*, 14553, doi:10.1038/s41598-019-50736-6.
11. Yu, Z.; Pestell, T.G.; Lisanti, M.P.; Pestell, R.G. Cancer Stem Cells. *The International Journal of Biochemistry & Cell Biology* **2012**, *44*, 2144–2151, doi:10.1016/j.biocel.2012.08.022.
12. Phi, L.T.H.; Sari, I.N.; Yang, Y.-G.; Lee, S.-H.; Jun, N.; Kim, K.S.; Lee, Y.K.; Kwon, H.Y. Cancer Stem Cells (CSCs) in Drug Resistance and Their Therapeutic Implications in Cancer Treatment. *Stem Cells International* **2018**, *2018*, 1–16, doi:10.1155/2018/5416923.
13. Jones, D.T.; Valli, A.; Haider, S.; Zhang, Q.; Smethurst, E.A.; Schug, Z.T.; Peck, B.; Aboagye, E.O.; Critchlow, S.E.; Schulze, A.; et al. 3D Growth of Cancer Cells Elicits Sensitivity to Kinase Inhibitors but Not Lipid Metabolism Modifiers. *Mol Cancer Ther* **2019**, *18*, 376–388, doi:10.1158/1535-7163.MCT-17-0857.
14. Yanes, O.; Clark, J.; Wong, D.M.; Patti, G.J.; Sánchez-Ruiz, A.; Benton, H.P.; Trauger, S.A.; Desponts, C.; Ding, S.; Siuzdak, G. Metabolic Oxidation Regulates Embryonic Stem Cell Differentiation. *Nat Chem Biol* **2010**, *6*, 411–417, doi:10.1038/nchembio.364.
15. Visweswaran, M.; Arfuso, F.; Warrier, S.; Dharmarajan, A. Aberrant Lipid Metabolism as an Emerging Therapeutic Strategy to Target Cancer Stem Cells: Lipid Metabolism in CSCs. *Stem Cells* **2020**, *38*, 6–14, doi:10.1002/stem.3101.
16. Yoshihisa, A.; Watanabe, S.; Yokokawa, T.; Misaka, T.; Sato, T.; Suzuki, S.; Oikawa, M.; Kobayashi, A.; Takeishi, Y. Associations between Acylcarnitine to Free Carnitine Ratio and Adverse Prognosis in Heart Failure Patients with Reduced or Preserved Ejection Fraction: Heart Failure and Carnitine. *ESC Heart Failure* **2017**, *4*, 360–364, doi:10.1002/ehf2.12176.
17. Afshinnia, F.; Rajendiran, T.M.; Soni, T.; Byun, J.; Wernisch, S.; Sas, K.M.; Hawkins, J.; Bellovich, K.; Gipson, D.; Michailidis, G.; et al. Impaired $\beta$ -Oxidation and Altered Complex Lipid Fatty Acid

Partitioning with Advancing CKD. *JASN* **2018**, *29*, 295–306, doi:10.1681/ASN.2017030350.

18. Viale, A.; Pettazzoni, P.; Lyssiotis, C.A.; Ying, H.; Sánchez, N.; Marchesini, M.; Carugo, A.; Green, T.; Seth, S.; Giuliani, V.; et al. Oncogene Ablation-Resistant Pancreatic Cancer Cells Depend on Mitochondrial Function. *Nature* **2014**, *514*, 628–632, doi:10.1038/nature13611.
19. Young, M.M.; Kester, M.; Wang, H.-G. Sphingolipids: Regulators of Crosstalk between Apoptosis and Autophagy. *Journal of Lipid Research* **2013**, *54*, 5–19, doi:10.1194/jlr.R031278.
20. Koundouros, N.; Karali, E.; Tripp, A.; Valle, A.; Inglese, P.; Perry, N.J.S.; Magee, D.J.; Anjomani Virmouni, S.; Elder, G.A.; Tyson, A.L.; et al. Metabolic Fingerprinting Links Oncogenic PIK3CA with Enhanced Arachidonic Acid-Derived Eicosanoids. *Cell* **2020**, *181*, 1596-1611.e27, doi:10.1016/j.cell.2020.05.053.
21. Bennett, D.T.; Deng, X.-S.; Yu, J.A.; Bell, M.T.; Mauchley, D.C.; Meng, X.; Reece, T.B.; Fullerton, D.A.; Weyant, M.J. Cancer Stem Cell Phenotype Is Supported by Secretory Phospholipase A2 in Human Lung Cancer Cells. *The Annals of Thoracic Surgery* **2014**, *98*, 439–446, doi:10.1016/j.athoracsur.2014.04.044.
22. Bellamkonda, K.; Chandrashekar, N.K.; Osman, J.; Selvanesan, B.C.; Savari, S.; Sjölander, A. The Eicosanoids Leukotriene D4 and Prostaglandin E2 Promote the Tumorigenicity of Colon Cancer-Initiating Cells in a Xenograft Mouse Model. *BMC Cancer* **2016**, *16*, 425, doi:10.1186/s12885-016-2466-z.
23. Cogoli, A. The Effect of Hypogravity and Hypergravity on Cells of the Immune System. *J Leukoc Biol* **1993**, *54*, 259–268, doi:10.1002/jlb.54.3.259.
24. Ciofani, G.; Ricotti, L.; Rigosa, J.; Menciassi, A.; Mattoli, V.; Monici, M. Hypergravity Effects on Myoblast Proliferation and Differentiation. *Journal of Bioscience and Bioengineering* **2012**, *113*, 258–261, doi:10.1016/j.jbiosc.2011.09.025.
25. Gaubin, Y.; Croute, F.; Pianezzi, B.; Prevost, M.C.; Soleilhavoup, J.P. Effects of Hypergravity on Adherent Human Cells. *Microgravity Sci Technol* **1991**, *3*, 246–250.

26. Tascher, G.; Brioche, T.; Maes, P.; Chopard, A.; O'Gorman, D.; Gauquelin-Koch, G.; Blanc, S.; Bertile, F. Proteome-Wide Adaptations of Mouse Skeletal Muscles during a Full Month in Space. *J. Proteome Res.* **2017**, *16*, 2623–2638, doi:10.1021/acs.jproteome.7b00201.
27. Ohira, T.; Ino, Y.; Nakai, Y.; Morita, H.; Kimura, A.; Kurata, Y.; Kagawa, H.; Kimura, M.; Egashira, K.; Moriya, S.; et al. Proteomic Analysis Revealed Different Responses to Hypergravity of Soleus and Extensor Digitorum Longus Muscles in Mice. *Journal of Proteomics* **2020**, *217*, 103686, doi:10.1016/j.jprot.2020.103686.
28. Lee, S.G.; Lee, C.G.; Wu, H.M.; Oh, C.S.; Chung, S.W.; Kim, S.G. A Load of Mice to Hypergravity Causes AMPKα Repression with Liver Injury, Which Is Overcome by Preconditioning Loads via Nrf2. *Sci Rep* **2015**, *5*, 15643, doi:10.1038/srep15643.
29. Genchi, G.G.; Cialdai, F.; Monici, M.; Mazzolai, B.; Mattoli, V.; Ciofani, G. Hypergravity Stimulation Enhances PC12 Neuron-Like Cell Differentiation. *BioMed Research International* **2015**, *2015*, 1–10, doi:10.1155/2015/748121.
30. Oshima, M.; Oshima, H.; Taketo, M.M. Hypergravity Induces Expression of Cyclooxygenase-2 in the Heart Vessels. *Biochemical and Biophysical Research Communications* **2005**, *330*, 928–933, doi:10.1016/j.bbrc.2005.03.060.
31. Guéguinou, N.; Bojados, M.; Jamon, M.; Derradji, H.; Baatout, S.; Tschirhart, E.; Frippiat, J.-P.; Legrand-Frossi, C. Stress Response and Humoral Immune System Alterations Related to Chronic Hypergravity in Mice. *Psychoneuroendocrinology* **2012**, *37*, 137–147, doi:10.1016/j.psyneuen.2011.05.015.
32. Mitani, K.; Horii, A.; Kubo, T. Impaired Spatial Learning after Hypergravity Exposure in Rats. *Cognitive Brain Research* **2004**, *22*, 94–100, doi:10.1016/j.cogbrainres.2004.08.002.
33. Santucci, D.; Francia, N.; Aloe, L.; Alleva, E. Neurobehavioural Responses to Hypergravity Environment in the CD-1 Mouse. *J Gravit Physiol* **2002**, *9*, P39-40.
34. Laiakis, E.C.; Shuryak, I.; Deziel, A.; Wang, Y.-W.; Barnette, B.L.; Yu, Y.; Ullrich, R.L.; Fornace, A.J.; Emmett, M.R. Effects of Low Dose Space Radiation Exposures on the Splenic Metabolome. *IJMS* **2021**, *22*, 3070, doi:10.3390/ijms22063070.

35. Garrett-Bakelman, F.E.; Darshi, M.; Green, S.J.; Gur, R.C.; Lin, L.; Macias, B.R.; McKenna, M.J.; Meydan, C.; Mishra, T.; Nasrini, J.; et al. The NASA Twins Study: A Multidimensional Analysis of a Year-Long Human Spaceflight. *Science* **2019**, *364*, eaau8650, doi:10.1126/science.aau8650.
36. Larina, I.M.; Percy, A.J.; Yang, J.; Borchers, C.H.; Nosovsky, A.M.; Grigoriev, A.I.; Nikolaev, E.N. Protein Expression Changes Caused by Spaceflight as Measured for 18 Russian Cosmonauts. *Sci Rep* **2017**, *7*, 8142, doi:10.1038/s41598-017-08432-w.
37. Brzhozovskiy, A.G.; Kononikhin, A.S.; Pastushkova, L.Ch.; Kashirina, D.N.; Indeykina, M.I.; Popov, I.A.; Custaud, M.-A.; Larina, I.M.; Nikolaev, E.N. The Effects of Spaceflight Factors on the Human Plasma Proteome, Including Both Real Space Missions and Ground-Based Experiments. *IJMS* **2019**, *20*, 3194, doi:10.3390/ijms20133194.
38. Strauch, S.M.; Grimm, D.; Corydon, T.J.; Krüger, M.; Bauer, J.; Lebert, M.; Wise, P.; Infanger, M.; Richter, P. Current Knowledge about the Impact of Microgravity on the Proteome. *Expert Review of Proteomics* **2019**, *16*, 5–16, doi:10.1080/14789450.2019.1550362.
39. Hosamani, R.; Leib, R.; Bhardwaj, S.R.; Adams, C.M.; Bhattacharya, S. Elucidating the "Gravome": Quantitative Proteomic Profiling of the Response to Chronic Hypergravity in *Drosophila*. *J. Proteome Res.* **2016**, *15*, 4165–4175, doi:10.1021/acs.jproteome.6b00030.
40. Ludwig, C.; Gillet, L.; Rosenberger, G.; Amon, S.; Collins, B.C.; Aebersold, R. Data-independent Acquisition-based SWATH - MS for Quantitative Proteomics: A Tutorial. *Mol Syst Biol* **2018**, *14*, doi:10.15252/msb.20178126.
41. Szklarczyk, D.; Gable, A.L.; Lyon, D.; Junge, A.; Wyder, S.; Huerta-Cepas, J.; Simonovic, M.; Doncheva, N.T.; Morris, J.H.; Bork, P.; et al. STRING V11: Protein–Protein Association Networks with Increased Coverage, Supporting Functional Discovery in Genome-Wide Experimental Datasets. *Nucleic Acids Research* **2019**, *47*, D607–D613, doi:10.1093/nar/gky1131.
42. Krämer, A.; Green, J.; Pollard, J.; Tugendreich, S. Causal Analysis Approaches in Ingenuity Pathway Analysis. *Bioinformatics* **2014**, *30*, 523–530, doi:10.1093/bioinformatics/btt703.

43. Tominari, T.; Ichimaru, R.; Taniguchi, K.; Yumoto, A.; Shirakawa, M.; Matsumoto, C.; Watanabe, K.; Hirata, M.; Itoh, Y.; Shiba, D.; et al. Hypergravity and Microgravity Exhibited Reversal Effects on the Bone and Muscle Mass in Mice. *Sci Rep* **2019**, *9*, 6614, doi:10.1038/s41598-019-42829-z.
44. Michaletti, A.; Gioia, M.; Tarantino, U.; Zolla, L. Effects of Microgravity on Osteoblast Mitochondria: A Proteomic and Metabolomics Profile. *Sci Rep* **2017**, *7*, 15376, doi:10.1038/s41598-017-15612-1.
45. Casey, T.; Zakrzewska, E.I.; Maple, R.L.; Lintault, L.; Wade, C.E.; Baer, L.A.; Ronca, A.E.; Plaut, K. Hypergravity Disruption of Homeorhetic Adaptations to Lactation in Rat Dams Include Changes in Circadian Clocks. *Biology Open* **2012**, *1*, 570–581, doi:10.1242/bio.2012687.
46. Ishikawa, C.; Li, H.; Ogura, R.; Yoshimura, Y.; Kudo, T.; Shirakawa, M.; Shiba, D.; Takahashi, S.; Morita, H.; Shiga, T. Effects of Gravity Changes on Gene Expression of BDNF and Serotonin Receptors in the Mouse Brain. *PLoS ONE* **2017**, *12*, e0177833, doi:10.1371/journal.pone.0177833.
47. Nerstedt, A.; Johansson, A.; Andersson, C.X.; Cansby, E.; Smith, U.; Mahlapuu, M. AMP-Activated Protein Kinase Inhibits IL-6-Stimulated Inflammatory Response in Human Liver Cells by Suppressing Phosphorylation of Signal Transducer and Activator of Transcription 3 (STAT3). *Diabetologia* **2010**, *53*, 2406–2416, doi:10.1007/s00125-010-1856-z.
48. Hershock, D.; Vogel, W.H. The Effects of Immobilization Stress on Serum Triglycerides, Nonesterified Fatty Acids, and Total Cholesterol in Male Rats after Dietary Modifications. *Life Sciences* **1989**, *45*, 157–165, doi:10.1016/0024-3205(89)90290-7.
49. Evans, R.M.; Mangelsdorf, D.J. Nuclear Receptors, RXR, and the Big Bang. *Cell* **2014**, *157*, 255–266, doi:10.1016/j.cell.2014.03.012.
50. van Diepen, J.A.; Berbée, J.F.P.; Havekes, L.M.; Rensen, P.C.N. Interactions between Inflammation and Lipid Metabolism: Relevance for Efficacy of Anti-Inflammatory Drugs in the Treatment of Atherosclerosis. *Atherosclerosis* **2013**, *228*, 306–315, doi:10.1016/j.atherosclerosis.2013.02.028.

51. Zelcer, N. Liver X Receptors as Integrators of Metabolic and Inflammatory Signaling. *Journal of Clinical Investigation* **2006**, *116*, 607–614, doi:10.1172/JCI27883.
52. Jiao, Y.; Lu, Y.; Li, X. Farnesoid X Receptor: A Master Regulator of Hepatic Triglyceride and Glucose Homeostasis. *Acta Pharmacol Sin* **2015**, *36*, 44–50, doi:10.1038/aps.2014.116.
53. Albi, E.; Curcio, F.; Lazzarini, A.; Floridi, A.; Cataldi, S.; Lazzarini, R.; Loreti, E.; Ferri, I.; Ambesi-Impiombato, F.S. A Firmer Understanding of the Effect of Hypergravity on Thyroid Tissue: Cholesterol and Thyrotropin Receptor. *PLoS ONE* **2014**, *9*, e98250, doi:10.1371/journal.pone.0098250.
54. Varshney, P.; Yadav, V.; Saini, N. Lipid Rafts in Immune Signalling: Current Progress and Future Perspective. *Immunology* **2016**, *149*, 13–24, doi:10.1111/imm.12617.
55. Hughes-Fulford, M. Function of the Cytoskeleton in Gravisensing during Spaceflight. *Advances in Space Research* **2003**, *32*, 1585–1593, doi:10.1016/S0273-1177(03)90399-1.
56. Marcu, O.; Lera, M.P.; Sanchez, M.E.; Levic, E.; Higgins, L.A.; Shmygelska, A.; Fahlen, T.F.; Nichol, H.; Bhattacharya, S. Innate Immune Responses of Drosophila Melanogaster Are Altered by Spaceflight. *PLoS ONE* **2011**, *6*, e15361, doi:10.1371/journal.pone.0015361.
57. Stervbo, U.; Roch, T.; Kornprobst, T.; Sawitzki, B.; Grütz, G.; Wilhelm, A.; Lacombe, F.; Allou, K.; Kaymer, M.; Pacheco, A.; et al. Gravitational Stress during Parabolic Flights Reduces the Number of Circulating Innate and Adaptive Leukocyte Subsets in Human Blood. *PLoS ONE* **2018**, *13*, e0206272, doi:10.1371/journal.pone.0206272.
58. Cancedda, R.; Liu, Y.; Ruggiu, A.; Tavella, S.; Biticchi, R.; Santucci, D.; Schwartz, S.; Ciparelli, P.; Falcetti, G.; Tenconi, C.; et al. The Mice Drawer System (MDS) Experiment and the Space Endurance Record-Breaking Mice. *PLoS ONE* **2012**, *7*, e32243, doi:10.1371/journal.pone.0032243.
59. Cajka, T.; Davis, R.; Austin, K.J.; Newman, J.W.; German, J.B.; Fiehn, O.; Smilowitz, J.T. Using a Lipidomics Approach for Nutritional Phenotyping in Response to a Test Meal Containing Gamma-Linolenic Acid. *Metabolomics* **2016**, *12*, 127, doi:10.1007/s11306-016-1075-9.

60. Tsugawa, H.; Cajka, T.; Kind, T.; Ma, Y.; Higgins, B.; Ikeda, K.; Kanazawa, M.; VanderGheynst, J.; Fiehn, O.; Arita, M. MS-DIAL: Data-Independent MS/MS Deconvolution for Comprehensive Metabolome Analysis. *Nat Methods* **2015**, *12*, 523–526, doi:10.1038/nmeth.3393.
61. Guo, X.; Kristal, B.S. The Use of Underloaded C18 Solid-Phase Extraction Plates Increases Reproducibility of Analysis of Tryptic Peptides from Unfractionated Human Plasma. *Analytical Biochemistry* **2012**, *426*, 86–90, doi:10.1016/j.ab.2012.04.003.
62. Martinotti, S.; Patrone, M.; Manfredi, M.; Gosetti, F.; Pedrazzi, M.; Marengo, E.; Ranzato, E. HMGB1 Osteo-Modulatory Action on Osteosarcoma SaOS-2 Cell Line: An Integrated Study From Biochemical and -Omics Approaches: O MICS A PPROACHES FOR HMGB1 O STEO -M ODULATION. *J. Cell. Biochem.* **2016**, *117*, 2559–2569, doi:10.1002/jcb.25549.
63. Cvijetic, S.; Bortolotto, V.; Manfredi, M.; Ranzato, E.; Marengo, E.; Salem, R.; Canonico, P.L.; Grilli, M. Cell Autonomous and Noncell-Autonomous Role of NF-KB P50 in Astrocyte-Mediated Fate Specification of Adult Neural Progenitor Cells: Adult Neural Progenitor-Astrocyte Cross-Talk. *Glia* **2017**, *65*, 169–181, doi:10.1002/glia.23085.
64. Su, G.; Morris, J.H.; Demchak, B.; Bader, G.D. Biological Network Exploration with Cytoscape 3. *Current Protocols in Bioinformatics* **2014**, *47*, doi:10.1002/0471250953.bi0813s47.

# *Chapter 4: Lipids alterations in patients affected by prostate cancer*

## *General introduction to the chapter*

In the current chapter, is reported a case-study in which it was applied a combined discovery-validation approach in order to find possible lipids able to discriminate between two groups of patients, one affected by prostate cancer (PCa) and another by chronic prostate inflammation or prostatitis, that was used as control (Ctr). The approach used is schematized in figure 1: an untargeted analysis was used in the discovery phase, where a small number of patients was enrolled (15 patients for each group). The discovery phase was used to identifying the most promising lipids able to discriminate between the two groups. In the validation phase, focusing only on the promising lipids, a larger cohort of patients (50 Ctr and 90 PCa) was enrolled: as regard the PCa group we enrolled patients with different Gleason score, ranging from 6 to 9. The main goal was to identify a combination of lipids that could be used as a more robust biomarkers for the diagnosis of prostate cancer and the severity of the disease.

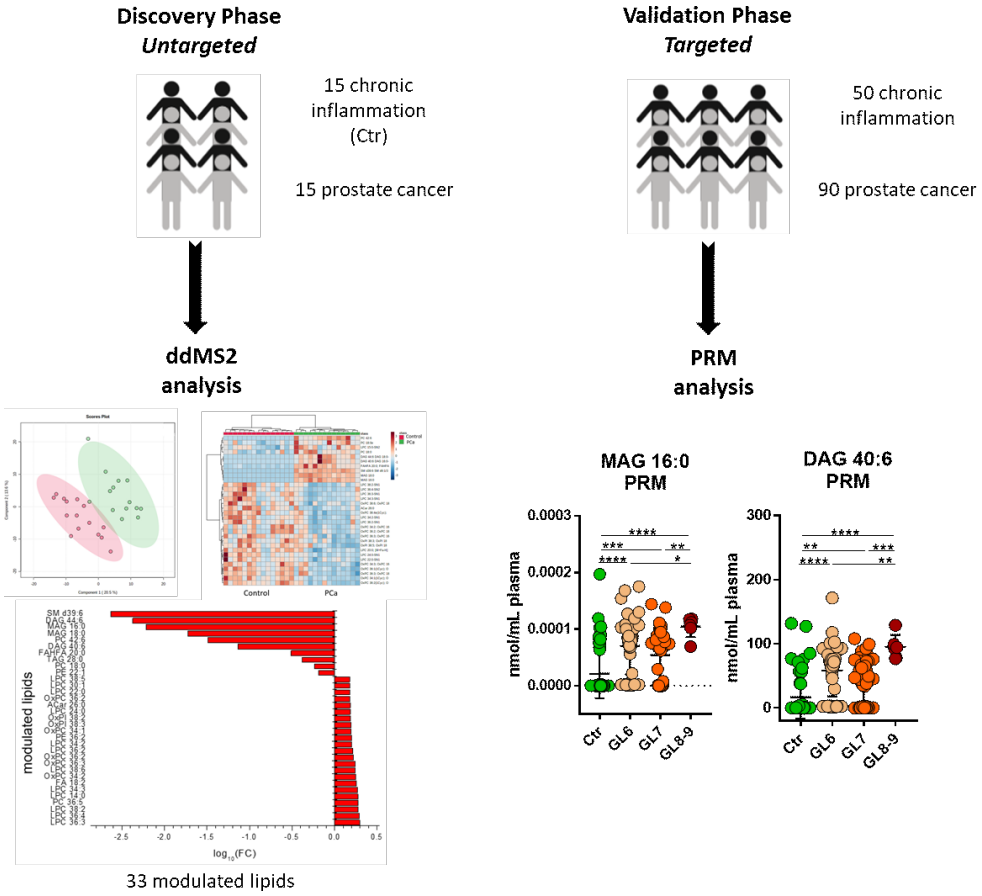


**Figure 1:** overview of the study. A first discovery phase in which an untargeted method of acquisition (ddMS2) was used (left), and validation phase where a targeted method (PRM) was used (right).

## *Introduction*

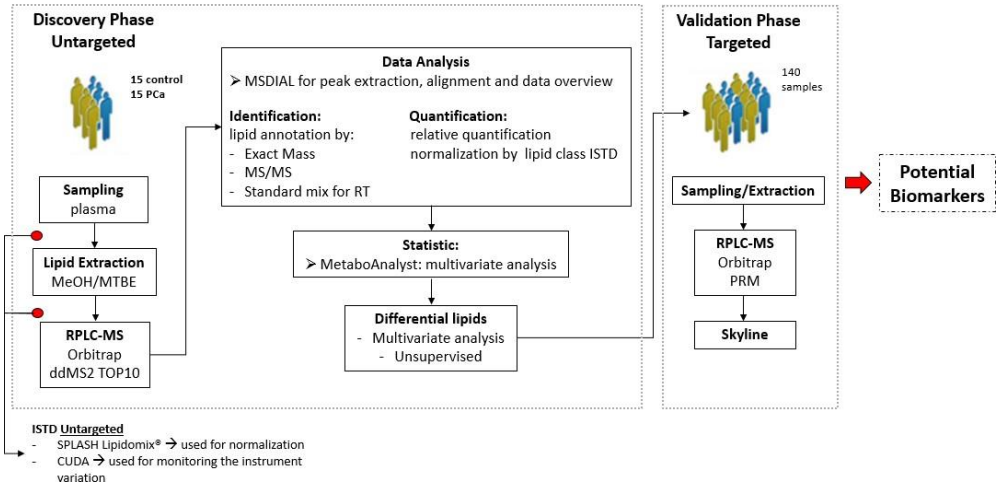


**Figure 2:** workflow of the study. In the discovery phase a small number of patients were enrolled, lipids were extracted and then analyzed by an Orbtrap Q-Exactive Plus, using an untargeted method (ddMS2). Performing statistical analysis we were able to identify the best promising lipids able to discriminate the two groups (control and prostate cancer). In the validation phase we enlarged our cohort and performed a targeted analysis (PRM) by an Orbitrap Q-Exactive Plus, focusing on the best discriminant lipids found in the discovery phase.

Despite the significant advances achieved in the diagnosis and treatment of cancer, prostate cancer (PCa) is the second most frequent cancer diagnosis made in men and the fifth leading cause of death worldwide [1].

Early diagnosis and aggressive treatment is the only option to cure PCa, and biomarkers play an important and decisive role in the early diagnosis. Today, the screening for PCa involves the digital rectal examination (DRE) and the prostate specific antigen (PSA) blood test.

Unfortunately, these tests are not enough accurate. In fact, PSA test is not very specific for prostate cancer: this antigen is abundantly produced by prostatic epithelium and it is secreted by the epithelium of periurethral glands. In addition, PSA can be secreted by both benign and cancer cells of prostate [2].

Furthermore, there is the possibility of an over-diagnosis of PCa in circumstances where there is limited potential for disease progression [3].

Advanced "Omics" technologies have identified altered genome, transcriptome and proteome related to PCa [4–6]. These studies have provided a number of potential genomic and proteomic biomarkers for diagnostic purposes. However, none of these markers were translated into routine diagnostic and/or prognostic applications.

Together with these omics science, lipidomics could be useful in order to find suitable lipids able to discriminate subjects affected by chronic inflammation (such as prostatitis) from PCa patients, avoiding unnecessary biopsies. In fact, a recent study [7] has found a significant positive relationship between prostatitis and prostate cancer. Prostatitis can be described as the swelling and inflammation of the prostate gland: this condition can have several causes and sometimes its identification is very difficult. Depending on the cause, prostatitis can come on gradually or suddenly. It might improve quickly, either on its own or with treatment. Some types of prostatitis last for months or keep recurring (chronic prostatitis). For these reasons, a misleading false-positive PCa diagnosis is not that unlikely.

Lipids consist of a large and diverse family of structurally distinct biomolecules that are hydrophobic or amphiphilic and play diverse and important roles in biological systems, including composing the membrane bilayer, storing energy, producing signal transduction, providing functional implementations of membrane proteins and their interactions [8]. Blood plasma is rich in lipids and related metabolites, and its composition reflects different aspects of both metabolism and general human physiology in health and disease [9].

In recent years many studies have focused on this particular omic science to profile the lipid plasma content in order to obtain further information and

biomarkers for some pathologies and diseases (i.e. mitochondrial disease [10] and coronary artery disease [11]).

In the present study, plasma lipids from patients were examined with UHPLC-HRMS to perform a global lipid profiling and identifying molecules useful to avoid unnecessary invasive treatment (biopsy) for patients with chronic inflammation. Additionally, it was investigated the possibility to discriminate PCa patients by their Gleason score. A combined approach, as reported in the workflow in figure 2, was employed. In the first step a total of 30 plasma samples were analyzed, divided into 15 patients diagnosed with PCa (Gleason score of 7), and 15 patients with chronic inflammation used as our control group (Ctr). Using unsupervised statistics the most promising lipid biomarkers were identified; these lipids were then validated in the second step of the study, where 140 candidate were enrolled, including also patient with a Gleason score of 6, 7, 8 and 9.

The results showed that DAG 40:6 and MAG 16:0 were the best promising lipids able to separate chronic inflammation patients from the prostate cancer ones, with an area under the curve (AUC) of the relative operating characteristic curve (ROC curve) of 0.817 and 0.793, respectively. Furthermore, when combined with other variables, such as the PSA, the AUC increase to 0.833. Finally, DAG 40:6 and MAG 16:0 could also discriminate the PCa samples based on their Gleason score.

## *Patients*

Characteristics of the study cohort are listed in table 1. For the untargeted lipidomic analysis in the discovery phase 15 patients with prostate cancer and Gleason score of 7 (PCa) and 15 patients with chronic inflammation as control group (Ctr) were included. All the patients included in the study reported a PSA > 10 ng/mL and had underwent diagnostic prostate biopsy according to

current Italian hospital protocols. Then, the cohort was enlarged for the targeted lipidomic analysis in the validation phase with a total of 140 samples: 50 plasma samples for the Ctr group and 90 samples in the PCa group with different Gleason score. The average age of the control group was 67±7.0, and 66±7.0 in the PCa group.

**Table 1**: characteristics of subjects involved in the study.

| | **Discovery Phase** | | **Validation Phase** | |
|---|---|---|---|---|
| Gleason Score | Cancer (PCa) | Chronic Inflammation (Ctr) | Cancer (PCa) | Chronic Inflammation (Ctr) |
| - | - | 15 | - | 50 |
| 6 | - | - | 41 | - |
| 7 | 15 | - | 43 | - |
| 8 | - | - | 5 | - |
| 9 | - | - | 1 | - |

| | Ctr | GS6 | GS7 | GS8-9 |
|---|---|---|---|---|
| Age range (years, mean ±SD) | 67±7.5 | 67±7.0 | 64±7.0 | 69±5.0 |

## *Materials and Methods*

Materials and methods of this study are the same as previously reported in Chapter 2 page 51. At the end of Chapter 4, in the section “Materials and Methods” only the targeted LC-MS/MS method is reported.

## *Results*

### *Untargeted lipidomics: comprehensive profile of plasma lipids*

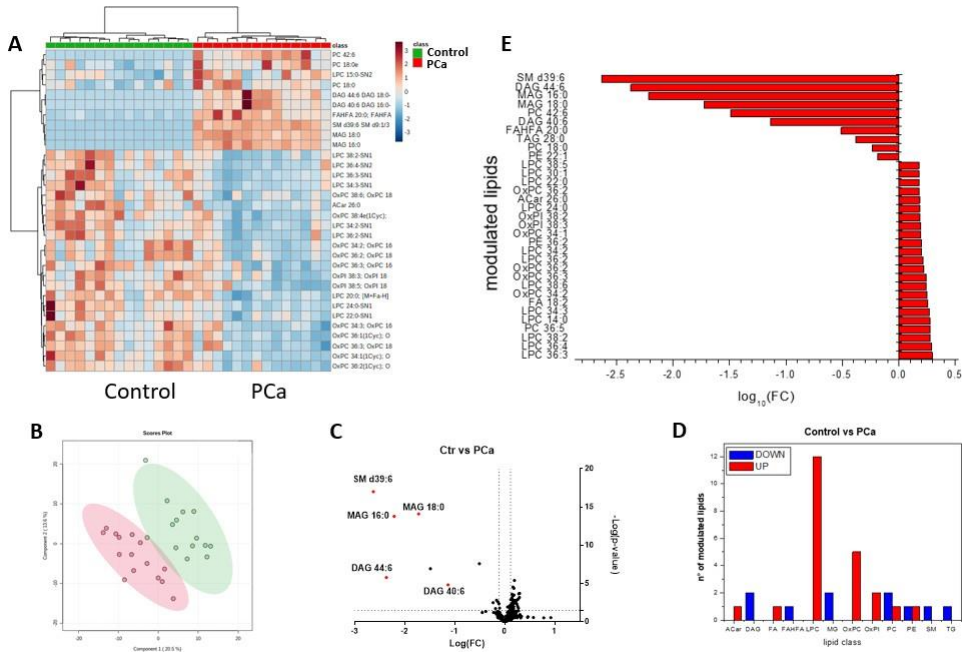


**Figure 3**: results from the untargeted lipidomic analysis of the comparison PCa and healthy groups: (**A**) hierarchical cluster analysis (heatmap) of the two groups; (**B**) PLSDA analysis (legends: green control group, red PCa group); (**C**) volcano plot FC $\geq 1.5$ and $p$-value $\leq 0.05$ where are highlighted the most modulated lipids; (**D**) histograms of number of modulated lipids per class in the comparison Control vs PCa; (**E**) $\log_{10}$(FC) of modulated lipids.

From the analysis of the 30 plasma samples a total of 420 lipids were detected, belonging to 17 different lipid classes: acylcarnitine (ACar), bismonoacylglycerophosphate (BMP), cholesteryl ester (CE), diacylglycerol (DG), free fatty acid (FA), fatty acid ester of hydroxyl fatty acid (FAHFA), lysophophatidylcholine (LPC), lysophosphatidylethanolamine (LPE), lysophosphatidylinositol (LPI), monoacylglycerol (MG), oxidized phosphatidylcholine (OxPC), oxidized phosphatidylinositol (OxPI),

phosphatidylcholine (PC), phosphatidylethanolamine (PE), phosphatidylinositol (PI), sphingomyelin (SM), triacylglycerol (TG). Figures 3A and B report the hierarchical heatmap and the partial least square discriminant analysis (PLSDA) from which it is possible to observe a clear separation of the two groups, indicating that the lipidome is useful in order to separate chronic inflammation from prostate cancer patients.

Through MetaboAnalyst software we performed a univariate analysis of the quantified lipids. Using a fold change $\geq 1.5$, and a $p$-value $\leq 0.05$, 33 modulated lipids were identified (figure 3C). In figure 3D it is reported the number of up and down modulated lipids per class while in figure 3E the complete list of modulated lipids and their $\log_{10}$(FC) value are reported. The most abundant modulated class is the LPC one, with 12 lipids up-modulated in the chronic inflammation group. Despite the abundance of this type of lipids, no one was in the top five modulated lipids. Another class up-regulated is the OxPC class with 5 lipids.

The modulated lysophophatidylcholines are characterized by long acyl chain (from 14 to 38 carbon atoms) and a great number of insaturations (0 to 6 double bonds). LPCs are “cone-shaped”, with a polar head and a non-polar carbon tail and therefore IT possess detergent-like properties. The geometry of the LPC structure is also determined by the degree of saturation of the acyl chain. Combined, the saturation and length of the acyl chain is detrimental to its biophysical properties as well as its activity [12]. Oxidized glycerophospholipids (OxPC and OxPI) are composed by carbon chains with 34-38 atoms and 1 to 3 double bonds. Together with ACar (ACar 26:0) and FA (FA 18:2), LPC, OxPC and OxPI classes are the only ones that have exclusively up-regulated lipids. The other classes (DAG, FAHFA, MG, PC, PE, SM and TG) are composed by down regulated lipids with at most 2 lipids per class.

Figure 4 reports the 5 most promising lipids able to discriminate the chronic inflammation group from the prostate cancer one: SM d39:6 (FC= 0.002 and *p*-value= 9.6x10-18), DAG 44:6 (FC= 0.004 and *p*-value= 1.6x10-6), MAG 16:0 (FC= 0.006 and *p*-value= 1.6x10-14), MAG 18:0 (FC= 0.019 and *p*-value= 7.8x10-15) and DAG 40:6 (FC= 0.073 and *p*-value= 1.2x10-5). These lipids were chosen for the validation by targeted analysis (PRM).

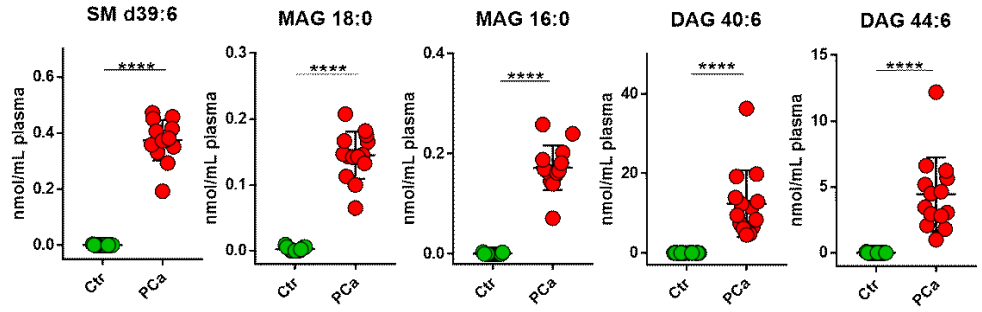


**Figure 4**: box plot of SM d39:6, MAG 18:0, MAG 16:0, DAG 44:6 and DAG 40:6 from the untargeted analysis. **** *p*-value < 0.0001.

## *Targeted lipidomics: validation of potential biomarkers*

For the validation phase, 140 plasma samples were analyzed, subdivided into: 50 controls (chronic inflammation), 41 PCa with Gleason score 6, 43 PCa with Gleason score 7, 5 PCa samples with Gleason score 8 and 1 PCa samples with Gleason score 9 focusing only on the 5 most promising lipids (SM d39:6, DAG 44:6, MAG 16:0, MAG 18:0 and DAG 40:6) by PRM.

As results, DAG 40:6, MAG 16:0, and SM d39:6 resulted statistically different between the two groups, as reported in figure 5A, B and C. In addition, multivariate ROC curves based analysis were performed on these 3 lipids, obtaining the following results: for DAG 40:6 an AUC of 0.814, a sensitivity of 0.87 and a specificity of 0.771, for MAG 16:0 an AUC of 0.793, a sensitivity of 0.793 and a specificity of 0.771, and for SM d39:6 an AUC of 0.768, a sensitivity of 0.717, and a specificity of 0.771 (figure 5F, G and H).

On the contrary MAG 18:0 and DAG 44:6 shown no significant differences between the chronic inflammation and the cancer group (figure 5D and E).

We also performed multivariate ROC curve analysis on the PSA, obtaining an area under the curve of 0.674 (sensitivity: 0.63, specificity: 0.708) that is much smaller than the validated lipids (figure 5M and N), confirming the low specificity of this biomarker.

We also combined these three lipids with PSA levels, in order to increase their discrimination power. Interestingly, we find out that the best area under the curve (AUC 0.833) was given by combining DAG 40:6, MAG 16:0 and PSA, while combing DAG 40:6, MAG 16:0, SM d39:6 and PSA the AUC value was of 0.824 (figure 6A and B). Combining DAG 40:6 and MAG 16:0 it did not showed an improvement (AUC: 0.809), while using MAG 16:0 with PSA we obtained an AUC of 0.832 (figure 6C and D), that is similar to the area under the curve of the combination between DAG 40:6, MAG 16:0 and PSA.

Furthermore, we have also tested whether our biomarkers correlate with the severity of the disease. Interestingly only MAG 16:0 and DAG 40:6 were able to significantly separate the groups, even if no statistically differences were detected between patients with Gleason score 6 and 7 (figure 7).

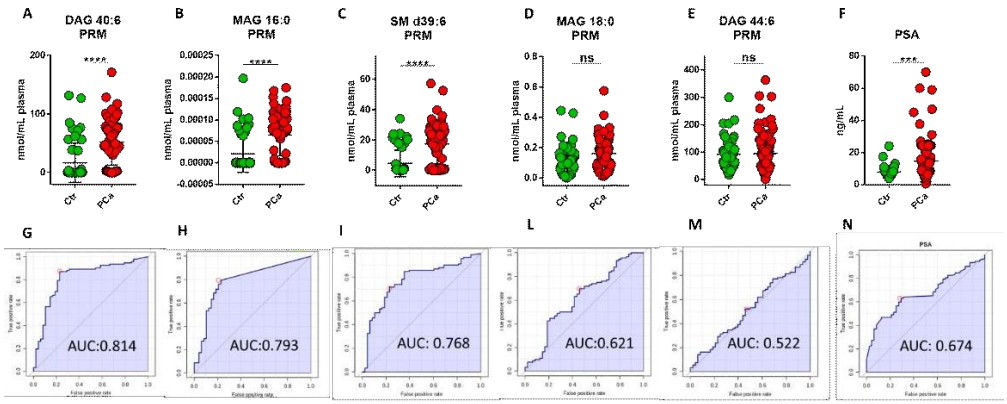


**Figure 5**: box plot and relative ROC curve from targeted analysis by PRM. DAG 40:6 (**A** and **G**); MAG 16:0 (**B** and **H**); SM d39:6 (**C** and **I**); MAG 18:0 (**D** and **L**); DAG 44:6 (**E** and **M**). PSA (**F** and **N**). Legend: * *p*-value < 0.05; ** *p*-value < 0.01; *** *p*-value < 0.001; **** *p*-value < 0.0001.

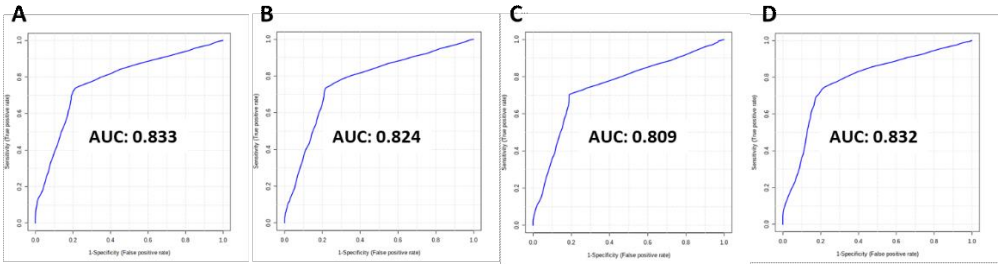


**Figure 6**: ROC curve of DAG 40:6, MAG 16:0 and PSA combined (AUC: 0.833) (**A**); ROC curve of DAG 40:6, MAG 16:0, SM d39:6 and PSA combined (AUC: 0.824) (**B**); DAG 40:6 and MAG 16:0 (AUC 0.809) (**C**); ROC curve of MAG 16:0 and PSA (AUC: 0.832) (**D**).

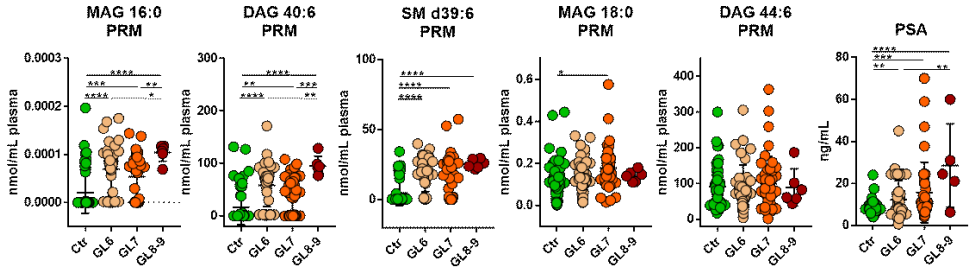


**Figure 7**: box plot from targeted analysis by PRM of MAG 16:0: DAG 40:6; SM d39:6; MAG 18:0; DAG 44:6 and PSA. Legend: * *p*-value < 0.05; ** *p*-value < 0.01; *** *p*-value < 0.001; **** *p*-value < 0.0001. Ctr control group, GL6 Geason score 6; GL7 Gleason score 7; GL8-9 Gleason score 8-9.

## *Discussion*

PCa is the most frequent type of cancer in men and it is the second cause of cancer deaths. The mortality rate of PCa has decreased dramatically with advent of PSA test and DRE diagnostic methods. Unfortunately, the PSA test is not very specific for this type of cancer. Our result, confirmed the diagnostic issues related to the use of PSA, that within our cohort of patients showed an area under the curve of 0.674 (sensitivity: 0.648, specificity: 0.74) (figure 5). In order to increase the discrimination power of the antigen it is possible to combine it with other biomarkers metabolites, proteins and lipids with a higher specificity and sensitivity [3]. Regarding proteins and metabolites there are

plenty of studies that show how it is possible to identify possible biomarkers from serum or plasma samples [13].

In this study we aimed to find possible biomarkers for a more accurate diagnosis of prostate cancer.

The main goal was to discriminate the PCa group from the chronic inflammation one to avoid unnecessary biopsies and to find possible lipids or groups of lipids able to characterize the severity of the cancer.

Our results showed the presence of 33 modulated lipids between the two sample groups: five of them, namely MAG 16:0, MAG 18:0, SM d39:6, DAG 40:6 and DAG 44:6 were also validated on a larger cohort (140 samples), including in the PCa group patients with Gleason score ranging from 6 to 9. After the validation, only 3 out of 5 lipids reported significant difference between the two groups DAG 40:6 (AUC: 0.817), MAG 16:0 (AUC 0.793), and SM d39:6 (AUC: 0.768). Additionally, MAG 16:0 and DAG 40:6 were also correlated with the severity of the disease.

In order to increase the discriminant power of the biomarkers, we combined lipids between each other and PSA: the best area under the ROC curve (AUC 0.833) was obtained by combining DAG 40:6, MAG 16:0 and PSA, even if, MAG 16:0 with PSA showed an AUC of 0.832. These results demonstrated the potential use of lipids as a complementary diagnostic indicator.

Another unique feature of our study is the use of patients affected by chronic prostate inflammation as the control group.

In conclusion, the present work showed that lipidomcis analysi can be used to discriminate prostate cancer to prostate inflammation, obtaining improved diagnostic performances and avoidig unnecessary biopsies.

# *Materials and Methods*

## *UHPLC-HRMS for targeted lipidomic validation*

The samples were analyzed by the same instrument of the untargeted phase, but the chromatographic run was modified. With the results of the untargeted phase the retention time of the lipids detected allowed us to reduce the LC run from 30 min to 10 min. We modified the gradient as follows: 0-2 min from 30% to 43% B, 2-2.1 min from 43% to 55% B, 2.1-5 min from 55% to 100% B, 5-7 keep at 100% of B then let the column riequilibrate at 30% B for 3 min. The flow rate was 0.300 mL/min.

For the validation step, the Orbitrap Q-Exactive Plus was operated in a target mode: parallel reaction monitoring (PRM), that allow us to focus only on the lipids of interest.

The setting of the PRM mode were: resolution 17500 and AGC target 2e5, maximum IT 100 ms, isolation windows 1.2 m/z. The NCE was set to 15, 30, and 45. In table 1 are reported adduct type, m/z and retention time range of the lipids monitored during the run.

**Table 1**: details of the lipids monitored in the validation phase by target analysis (PRM): adduct type, m/z values and retention time expressed as minutes.

| Name | Adduct | m/z | RT (min) |
|---|---|---|---|
| MAG 16:0 | [M+H] | 348.3108 | 4.9 |
| DAG 40:6 | [M+H] | 686.5717 | 4.9 |
| SM d39 | [M+H] | 763.5676 | 6.0 |
| DAG 44:6 | [M+H] | 742.6343 | 5.4 |
| MAG 18:0 | [M+H] | 376.3421 | 5.0 |
| DAG 12:0 | [M+H] | 479.3701 | 6.0 |

## *Bibliography*


1. Rawla, P. Epidemiology of Prostate Cancer. *World J. Oncol.* **2019**, *10*, 63–89, doi:10.14740/wjon1191.
2. Bandu, R.; Mok, H.J.; Kim, K.P. Phospholipids as Cancer Biomarkers: Mass Spectrometry-Based Analysis: PHOSPHOLIPIDS AS CANCER BIOMARKERS. *Mass Spectrom. Rev.* **2018**, *37*, 107–138, doi:10.1002/mas.21510.
3. Zhou, X.; Mao, J.; Ai, J.; Deng, Y.; Roth, M.R.; Pound, C.; Henegar, J.; Welti, R.; Bigler, S.A. Identification of Plasma Lipid Biomarkers for Prostate Cancer by Lipidomics and Bioinformatics. *PLoS ONE* **2012**, *7*, e48889, doi:10.1371/journal.pone.0048889.
4. Ryan, M.J.; Bose, R. Genomic Alteration Burden in Advanced Prostate Cancer and Therapeutic Implications. *Front. Oncol.* **2019**, *9*, 1287, doi:10.3389/fonc.2019.01287.
5. Ren, S.; Wei, G.-H.; Liu, D.; Wang, L.; Hou, Y.; Zhu, S.; Peng, L.; Zhang, Q.; Cheng, Y.; Su, H.; et al. Whole-Genome and Transcriptome Sequencing of Prostate Cancer Identify New Genetic Alterations Driving Disease Progression. *Eur. Urol.* **2018**, *73*, 322–339, doi:10.1016/j.eururo.2017.08.027.
6. Scaravilli, M.; Afyounian, E.; Nykter, M.; Visakorpi, T.; Latonen, L. Integrative Proteomics of Prostate Cancer. *Curr. Opin. Endocr. Metab. Res.* **2020**, *10*, 43–49, doi:10.1016/j.coemr.2020.02.012.
7. Jiang, J.; Li, J.; Yunxia, Z.; Zhu, H.; Liu, J.; Pumill, C. The Role of Prostatitis in Prostate Cancer: Meta-Analysis. *PLoS ONE* **2013**, *8*, e85179, doi:10.1371/journal.pone.0085179.
8. Hu, C.; Li, J.; Xu, G. Mass Spectrometry-Based Lipidomics for Biomarker Research. In *General Methods in Biomarker Research and their Applications*; Preedy, V.R., Patel, V.B., Eds.; Biomarkers in Disease: Methods, Discoveries and Applications; Springer Netherlands: Dordrecht, 2015; pp. 49–74 ISBN 978-94-007-7695-1.
9. Burla, B.; Arita, M.; Arita, M.; Bendt, A.K.; Cazenave-Gassiot, A.; Dennis, E.A.; Ekroos, K.; Han, X.; Ikeda, K.; Liebisch, G.; et al. MS-Based Lipidomics of Human Blood Plasma: A Community-Initiated Position Paper to Develop Accepted Guidelines. *J. Lipid Res.* **2018**, *59*, 2001–2017, doi:10.1194/jlr.S087163.

10. Ren, C.; Liu, J.; Zhou, J.; Liang, H.; Zhu, Y.; Wang, Q.; Leng, Y.; Zhang, Z.; Yuan, Y.; Wang, Z.; et al. Lipidomic Profiling of Plasma Samples from Patients with Mitochondrial Disease. *Biochem. Biophys. Res. Commun.* **2018**, *500*, 124–131, doi:10.1016/j.bbrc.2018.03.160.
11. Djekic, D.; Pinto, R.; Repsilber, D.; Hyotylainen, T.; Henein, M. Serum Untargeted Lipidomic Profiling Reveals Dysfunction of Phospholipid Metabolism in Subclinical Coronary Artery Disease. *Vasc. Health Risk Manag.* **2019**, *Volume 15*, 123–135, doi:10.2147/VHRM.S202344.
12. Knuplez, E.; Marsche, G. An Updated Review of Pro- and Anti-Inflammatory Properties of Plasma Lysophosphatidylcholines in the Vascular System. *Int. J. Mol. Sci.* **2020**, *21*, 4501, doi:10.3390/ijms21124501.
13. Duscharla, D.; Bhumireddy, S.R.; Lakshetti, S.; Pospisil, H.; Murthy, P.V.L.N.; Walther, R.; Sripadi, P.; Ummanni, R. Prostate Cancer Associated Lipid Signatures in Serum Studied by ESI-Tandem Mass Spectrometryas Potential New Biomarkers. *PLOS ONE* **2016**, *11*, e0150253, doi:10.1371/journal.pone.0150253.
14. Cajka, T.; Davis, R.; Austin, K.J.; Newman, J.W.; German, J.B.; Fiehn, O.; Smilowitz, J.T. Using a Lipidomics Approach for Nutritional Phenotyping in Response to a Test Meal Containing Gamma-Linolenic Acid. *Metabolomics* **2016**, *12*, 127, doi:10.1007/s11306-016-1075-9.
15. Tsugawa, H.; Cajka, T.; Kind, T.; Ma, Y.; Higgins, B.; Ikeda, K.; Kanazawa, M.; VanderGheynst, J.; Fiehn, O.; Arita, M. MS-DIAL: Data-Independent MS/MS Deconvolution for Comprehensive Metabolome Analysis. *Nat. Methods* **2015**, *12*, 523–526, doi:10.1038/nmeth.3393.
16. Kind, T.; Liu, K.-H.; Lee, D.Y.; DeFelice, B.; Meissen, J.K.; Fiehn, O. LipidBlast in Silico Tandem Mass Spectrometry Database for Lipid Identification. *Nat. Methods* **2013**, *10*, 755–758, doi:10.1038/nmeth.2551.
17. Chong, J.; Wishart, D.S.; Xia, J. Using MetaboAnalyst 4.0 for Comprehensive and Integrative Metabolomics Data Analysis. *Curr. Protoc. Bioinforma.* **2019**, *68*, doi:10.1002/cpbi.86.

# *Conclusions and future perspectives*

In this doctoral thesis, lipidomic analysis was performed to explore biological mechanisms and biomarkers in three different case-studies. These investigations were carried out from plasma and cells to understand the host response as result of virus infection, environmental condition, and cancer disease. All the studies were carried out through an untargeted approach using a high-resolution mass spectrometry coupled with ultra-high liquid chromatography.

Plasma is the best biological matrices for lipidomic investigation because well represent the phenotype of the host and summarized the potential biological modification occurring during infection. Furthermore, circulating lipids can be used to understand how and which biological pathways are involved during particularly condition of the host. Additionally, the collection of plasma is not invasive and do not required specific equipment. The use of biological fluids lead to perform quick and simple extraction methods, like liquid-liquid extraction. In this thesis a consolidate method was applied, using harmless solvents like MTBE and water.

Notably is the possibility to use mass spectrometry coupled with liquid chromatography. This techniques allows to use small quantities of sample, reducing waste and solvents used.

As regard cell samples the bottleneck for the success of the analysis is the collection of a suitable number of cells. Cells, particularly peripheral blood mononuclear cells, are involved during the immune response and the

investigation of their lipids can help the understanding of the host response, for example, during SARS-CoV-2 infection.

The promising results reported in previous chapters, suggest that the lipidome is reactive to alteration states and that can be involved in interesting biological mechanisms, elucidating some behaviors previously unclear.

As regard virus infection, a deep investigation of plasma from patients affected by the novel SARS-CoV-2 was reported, together with a pilot study on peripheral blood mononuclear cells from plasma to investigate the possible immune response of the host.

The plasma study was performed on a large cohort of patients, composed by 161 subjects, subdivided into COVID-19 (n = 103) and non-COVID-19 (n = 58) groups. The main findings revealed a number of processes and pathways involved in the host response to SARS-CoV-2, such as the activation of $PLA_2$ in patients affected by the virus; as well as several promising biomarkers and therapeutic targets, like the combination of arachidonic acid, oleic acid and two different phosphoethanolamines. Furthermore, it was observed an increase of fatty acids in patients infected by the virus. This finding may be a consequence of the defense mechanism of the host, but, at the same time, the higher levels of FAs may also cause inflammation. Additionally, the analysis from peripheral blood mononuclear cells from plasma, confirmed the findings of the previous work, regarding the involvement of the immune system as response to the viral infection. Furthermore, at cellular level, it was observed the modulation of lipid classes involved in membrane structure, suggesting a membrane remodeling, favored by some lipid classes such as ceramides, enhancing the entry of the virus into host cells.

It will be interesting to perform a large-scale lipidomic analysis also on PBMCs in order to have a representative vision of the host response to viral infection from SARS-CoV-2 at the cellular level.

The effects of the environmental conditions were evaluated through *in vitro* and *in vivo* studies, evaluating the impact of microgravity and hypergravity on circulating lipids and proteins.

In the first study, the use of lipidomics, together with proteomics and transcriptomics, lead us to understand the biological alteration occurring in cancer cells due to the condition of microgravity on PDCA cells (PaCa-44) over time (24h, 7, and 9 days). The results suggested an involvement of β-oxidation in the perissosome during the first 24 hours. Furthermore, the formation of novel membrane lipids by the increased levels of some phospholipids species (LPC, LPE, PC, and PE) and some FAs (FA 20:3, FA 20:4, FA 20:5, FA 22:5, FA 22:6 and FA 18:1) was detected. These findings were observed after 7 days, after this time point almost all the lipid classes involved in the modulation return to the initial levels. This *in vitro* study had shown the cancer cell transition toward a more stem and aggressive phenotype generated by simulated microgravity.

It would be interesting testing pancreatic cancer cells' response to anti-neoplastic treatments under simulated microgravity.

The *in vivo* study was performed on mice to investigate the lipidome and proteome alteration due to simulated hypergravity. The main observation was the modulation of some apolipoproteins (APOA4, APOE, and APOC1) and lipids species (LPC, LPE, PC, PE, PI, and TG). These lipids and proteins are the core structure of lipoproteins: phospholipids PCs and PEs are the constituents of the plasmatic membrane that enclose TGs, cholesterol, and cholesteryl ester. A depletion of these lipids may be the cause of lipid raft disruption that lead to a remodeling of the plasma membrane. The involvement of lipoproteins may suggest an impairment of the normal activity of the liver induced by hypergravity, involving also the LXR/RXR and FXR/RXR pathway.

The last study had been performed on plasma samples belonging to patients affected by prostate cancer and patients affected by chronic prostate inflammation. Both the two groups presented elevated levels of prostate specific antigen (PSA) and for this reason were subjected to biopsy. For this work, a double approach has been applied: a first untargeted UHPLC-HRMS method was involved for the analysis of 30 plasma samples to find the best promising lipid biomarkers, then a second targeted method was applied on 140 samples to validate the lipids found in the first part.

The finding of potential biomarkers able to discriminate plasma samples belonging to cancer patients from the ones affected by chronic inflammation, despite the elevated PSA levels, showed that lipidomics could be used as a powerful tool to improved diagnostic performances and avoiding unnecessary biopsies.

In this thesis it has been shown how lipidomics can be used to better understand the impairment in biological pathways and mechanisms that occur in the host. Furthermore, it was demonstrated that lipids can be used as a powerful diagnostic tool for some pathologies, avoiding unnecessary and invasive treatments.

For the future it would be interesting to complete the previously studies, adding the mentioned analysis and maybe focusing on particular lipid classes or single lipid.

## *Published article*

"Large-scale plasma analysis revealed new mechanisms and biomarkers associated with the host response to SARS-CoV-2". Elettra Barberis, Sara Timo, Elia Amede, Virginia V. Vanella, Chiara Puricelli, Giuseppe Cappellano, Davide Raineri, Micol G. Cittone, Eleonora Rizzi, Anita R. Pedrinelli, Veronica Vassia, Francesco G. Casciaro, Simona Priora, Ilaria Nerici, Alessandra Galbiati, Eyal Hayden, Marco Falasca, Rosanna Vaschetto, Pier Paolo Sainaghi, Umberto Dianzani, Roberta Rolla, Annalisa Chiocchetti, Gianluca Baldanzi, Emilio Marengo, Marcello Manfredi.

## *Submitted article*

“Prolonged exposure to simulated microgravity promotes stemness impairing morphological, metabolic and migratory profile of pancreatic cancer cells: a comprehensive proteomic, lipidomic and transcriptomic analysis” Maria Masini; Valentina Bonetto; Marcello Manfredi; Anna Pastò; Elettra Barberis; Sara Timo; Virginia Vita Vanella; Elisa Robotti; Francesca Masetto; Francesca Andreoli; Sara Tavella; Antonio Sica; Massimo Donadelli; Emilio Marengo

## *Manuscripts under submission*

- “Hypergravity impacts on circulating lipids and proteins in mice”

- “Untargeted and targeted plasma lipidomics to discover lipids alteration in patients affected by prostate cancer”